Czech Technical University in Prague
Faculty of Nuclear Sciences and Physical Engineering

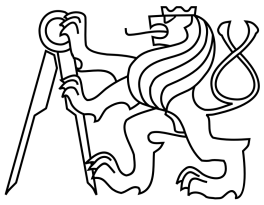

DISSERTATION

Dynamics of percolated quantum walks on graphs

Prague 2020 Jan Mareš

Prohlášení

Prohlašuji, že jsem svou disertační práci vypracoval samostatně a použil jsem pouze podklady uvedené v přiloženém seznamu.

Nemám závažný důvod proti použití tohoto školního díla ve smyslu §60 Zákona č 121/2000 Sb., o právu autorském, o právech souvisejících s právem autorským a o změně některých zákonů (autorský zákon).

V Praze dne .....

.....
Mgr. Ing. Jan Mareš

Declaration

I declare, I wrote my Dissertation independently and exclusively with the use of cited bibliography.

I agree with the usage of this dissertation in the purport of the §60 Act 121/2000 (Copyright Act).

In Prague .....

.....
Mgr. Ing. Jan Mareš

Acknowledgments

I would like to acknowledge the cooperation, advice and guidance provided by my supervisor prof. Igor Jex and my consultant Dr. Jaroslav Novotný during the time of working on my research projects leading to publishable results and during writing the text of manuscripts and also for all the assistance while shaping the core of the presented thesis.

I am also grateful to my wife for allowing me the time needed to work on the dissertation.

Mgr. Ing. Jan Mareš

Bibliografický záznam

Autor:	Mgr. Ing. Jan Mareš Katedra fyziky, Fakulta jaderná a fyzikálně inženýrská, České vysoké učení technické v Praze
Název práce:	**Dynamika perkolovaných kvantových procházek na grafech**
Studijní program:	Aplikace přírodních věd
Studijní obor:	Matematické inženýrství
Školitel:	prof. Ing. Igor Jex, DrSc. Katedra fyziky, Fakulta jaderná a fyzikálně inženýrská, České vysoké učení technické v Praze
Školitel specialista:	Ing. Jaroslav Novotný, Ph.D. Katedra fyziky, Fakulta jaderná a fyzikálně inženýrská České vysoké učení technické v Praze
Akademický rok:	2020
Počet stran:	125
Klíčová slova:	kvantové procházky, perkolace, kvantový transport

Bibliographic Entry

Author:	Mgr. Ing. Jan Mareš Department of Physics, Faculty of Nuclear Sciences and Physical Engineering, Czech Technical University in Prague
Title of Dissertation:	**Dynamics of percolated quantum walks on graphs**
Degree Programme:	Applications of Natural Sciences
Field of Study:	Mathematical Engineering
Supervisor:	prof. Ing. Igor Jex, DrSc. Department of Physics, Faculty of Nuclear Sciences and Physical Engineering, Czech Technical University in Prague
Supervisor specialist:	Ing. Jaroslav Novotný, Ph.D. Department of Physics, Faculty of Nuclear Sciences and Physical Engineering, Czech Technical University in Prague
Academic Year:	2020
Number of Pages:	125
Key words:	quantum walks, percolation, quantum transport

Abstrakt: Kvantové procházky jsou vhodným nástrojem pro zkoumání kvantového transportu na různých grafech včetně případů, kdy je transport narušen vnějšími vlivy. Tato disertační práce se věnuje studiu diskrétních kvantových procházek na grafech s dynamickou perkolací – náhodným uzavíráním a otevíráním hran grafu během časového vývoje procházky. Uvádíme veškeré potřebné teoretické kroky využité k následnému zkoumání kvantového transportu. Konkrétně zavádíme upravenou definici kvantové procházky vhodnou pro procházky s perkolací a také pro zkoumání různých pravidel pro pohyb chodce na grafu (operátor posunu). Dále prezentujeme postup pro zkoumání časově asymptotického vývoje perkolovaných kvantových procházek a aplikujeme jej na procházky s Groverovou mincí. Následně zkoumáme kvantové procházky s Groverovou mincí a cyklickými operátory posunu a odhalujeme spojitost jejich asymptotického vývoje s teoretickou vlastností hranového obarvení grafu. Nakonec se zabýváme kvantovými procházkami s Groverovou mincí a odrazivým operátorem posunu, které vykazují jev asymptotického zachycení chodce v grafu. V rámci transportu pomocí těchto procházek na grafu přímky, grafu žebříku, grafech reprezentujících uhlíkové nanotrubice a grafech Cayleyho stromů identifikujeme několik zajímavých jevů. Důležitým a velmi neintuitivním výsledkem je zjištění, že kvantový transport podél lineární struktury žebříku nebo nanotrubice s absorpčním místem lokalizovaným v jednom z okrajových vrcholů grafu se zefektivňuje prodlužováním těchto struktur.

Abstract: Quantum walks represent a convenient tool for the study of quantum transport on various structures and also in the presence of external disturbances. This dissertation investigates discrete quantum walks on graphs with dynamical percolation – random closing and reopening of edges of the graph during the evolution of the walk. We present all the necessary theoretical steps for the final investigation of quantum transport. Namely, we give a modified definition of a quantum walk suited for walks with percolation and also convenient for classification of various shifting rules of the walker. Further, we present a procedure for investigation of time-asymptotic dynamics of percolated quantum walks and apply it to walks with the Grover coin. We then investigate Grover quantum walks with cyclic shift operators and relate their asymptotic evolution to the theoretical concept of graph edge-coloring. Finally, we study Grover quantum walks with a reflecting shift operator, which exhibit the phenomenon of asymptotic trapping. In transport by these quantum walks on the line graph, the ladder graph, graphs representing carbon nanotubes and graphs of Cayley trees we identify several interesting effects. Particularly, on the linear structures of the ladder and tubes with the absorbing sink localized at a single border vertex of the graph the probability of the walker traversing from one end to the other increases with the length of the structure.

Contents

Introduction

A standard approach in physics is to use simple models to describe real-life systems and study their key properties. One of the models heavily used in the classical domain are random walks. Random walks allow for natural incorporation of the inherent randomness within physical processes into non-trivial models. They can describe pure physical phenomena like Brownian motion as the underlying mechanism of diffusion [1, 2] or processes in polymeric materials [3]. Nevertheless, applications of random walks reach far beyond the field of physics for example by their usage in modeling of financial markets [4] or in ranking web pages by Google [5]. Motivated by the success of classical random walks the concept of quantum walks was introduced [6] to model systems governed by the laws of quantum physics.

Similarly to random walks, quantum walks represent a mathematically non-trivial model, in which various effects have been reported. Those are often related to ballistic spreading of the walker's wave function facilitated by the quantum interference. This is given by the fact that the state of a quantum walker is described by complex-number amplitudes in contrast to real-number non-negative probabilities for the classical walker. While probabilities of the classical walker coming to a given site from others can only add up, quantum amplitudes can interfere both constructively and destructively giving rise to classically impossible behavior. On one hand, the interference can increase the rate of spreading significantly. A quadratic speedup of the quantum walk on the line over the classical random walk was already presented in the founding work [6] and for the very artificial "glued trees" graph a quantum walk can even discover the exit vertex exponentially faster in a black-box search problem [7]. On the other hand, quantum walks can exhibit exponential – Anderson localization [8, 9] or even the effect of complete trapping of the walker in a part of the position space with non-zero probability regardless of the evolution time [10]. Further, there are for example intricate dependencies of the recurrence on characteristics of the walk [11].

One of the possible applications of quantum walks is in the field of quantum computation. They can provide state transfer [12] or perform multiple quantum algorithms. Several algorithms employing quantum walks were proposed giving polynomial speedup in an oracle database search [13] or exponential speedup in search on the "glued trees" graph [7] demonstrating the possibility of even more significant improvements in some particular cases. Quantum walks were even proven to be able to perform universal quantum computations [14, 15] giving hopes to benefit from the exponential speedup of quantum computation provided by Shor's algorithm [16]. Nevertheless, there is a problem with scaling for processing larger inputs. The basal

information unit in quantum computation is called a qubit – a two-level quantum system, which in contrast to the classical bit can be in an arbitrary superposition of the states 0 and 1. The problem is that for a standard quantum walk with a single walker the size of the walker's position space required to perform a quantum computation grows exponentially with the number of qubits involved n [17]. Therefore, this does not represent a scalable architecture for building a large multi-purpose quantum computer. This problem can be faced by considering quantum walks with many walkers. Quantum algorithms are often described in so called gate model, in which gates are basic operations performed on qubits. It was proven that arbitrary g-gate quantum computation on n qubits can be performed by a quantum walk with both the number of walkers and the number of sites in the position space polynomial in both g and n [17].

Another stimulus for studying quantum walks is their experimental realizability in multiple physical systems [18, 19, 20, 21, 22]. Nevertheless, in accordance with the previous paragraph about the computational power of single-walker quantum walks, it was pointed out in [23], that it is very unlikely for single walker standard unitary quantum walks of a size not allowing simulation on classical computers to be realized experimentally in the near future. Therefore, quantum walks with a single walker are more likely to be used as a model for understanding effects in quantum systems rather than actual devices performing computations not feasible by classical computers.

Simulation of other quantum systems is actually another fundamental task for quantum computers. In this task we are given a system with some Hamiltonian and an initial quantum state $|\psi(0)\rangle$ and we are asked to produce the final quantum state $|\psi(t)\rangle$ resulting from $|\psi(0)\rangle$ after a given time t. The first problem with performing such task with classical computers is the mere representation of the quantum states, which requires an amount of memory exponentially growing with the number of qubits of the states. Further, quantum simulators can perform some tasks inaccessible to classical computers for principal reasons. If the initial state is not known and we are only in possession of one copy stored in some quantum system a quantum simulator may be able to produce the state $|\psi(t)\rangle$ even without any knowledge about $|\psi(0)\rangle$. With the classical approach it is not even possible to determine $|\psi(0)\rangle$ to begin with any further calculation. Therefore, the task of quantum simulation is fundamental. Since we believe that the World is ruled by quantum physics, in order to truly understand the Nature the usage of quantum computers seems necessary.

Let us now introduce some more technical aspects of quantum walks. Both random walks and quantum walks can be defined on mathematical structures called graphs – structures composed of discrete vertices with some pairs of vertices connected by edges. (This approach is very common despite the fact that it e.g. can not accommodate the first classical random walk introduced [24].) On this common structure different kinds of quantum walks have been proposed. The two main branches of quantum walks copy the two corresponding branches of classical random walks: time-continuous and discrete walks. The evolution of continuous quantum walks is driven by a Hamiltonian derived from the adjacency matrix of the graph underlying the walk. There is a direct correspondence between the state space of a continuous

random walk and the state space of the corresponding continuous quantum walk – the base states simply correspond to vertices of the graph. In discrete quantum walks the evolution proceeds in steps by repeated application of a unitary evolution operator U. In contrast, when one wants to quantize a discrete random walk (mapping the walker to some superposition of states in the adjacent vertices by every dicrete time step), the state space of such walk needs to be enlarged to ensure unitarity of the evolution [6].[1] There are multiple approaches for doing this resulting in multiple types of discrete quantum walks: coined quantum walks [6] with an additional coin degree of freedom associated with the walker, scattering quantum walks [25] identifying the base states of the walker with directed edges instead of vertices of the graph or Szegedy quantum walks [26] utilized in quantum search problems. These are mutually equivalent, at least on some subset of admissible graphs [27, 28]. In Chapter 1 we present a novel modification of the definition specially suited for the study of percolated quantum walks.

In this work we focus on discrete quantum walks, which have two main ingredients: the underlying graph (with the associated rules for the movement of the walker) and the coin. (Note that the coin is also implicitly present in scattering and Szegedy quantum walks.) The simplest and most studied quantum walks are those on a line – a chain of vertices with the nearest neighbors connected. The line can be infinite, closed into a cycle or just finite with reflecting boundaries. Obviously, quantum walks on various other graphs were studied like the lazy quantum walk [29] (line with the added possibility of not making a step), quantum walks on hypercubes [30], tree graphs [31], spider nets (Cayley trees with concentric cycles) [32], honeycombs [33] and carbon nanotube structures [34] or on the Sierpiński gasket fractal [35]. Also, quantum walks with various coins were studied [36], which can have crucial impact on properties of the walks like trapping [37]. Lastly, it is possible to tweak the way in which the walker moves among vertices – the shift operator. Nevertheless, all admissible shift operators can be achieved by a proper modification of the coin as was shown in [38] and we present that in detail in section 1.5.5 of this work.

Quantum walks are a very useful tool for investigation of various phenomena in quantum systems. This is given by their ability to be naturally modified from very simple models to complex ones by using different graphs and various coins or shifting rules. This can be further extended by considering external disturbances. A number of studies were published investigating disturbances in quantum walks: random modifications of the quantum coin, introduction of random phase shifts in the shift operator or the introduction of intermediate measurements in the walk typically result in transition from quantum ballistic spreading to classical diffusive spreading as the magnitude of the disturbance increases [39]. The next main option is to disrupt the graph of a quantum walk by breaking for instance some of its edges, not allowing the walker to pass from one vertex to another. In this work we investigate, among others, so called dynamical percolation in quantum walks.

In the classical theory, the study of percolation deals with infinite lattices in which

[1] It is possible to just take the continuous time quantum walk and only allow discrete time steps. Nevertheless, such walk lacks the property of locality - the step can move the walker to very distatnt vertices.

edges are randomly assigned to be open with probability p and closed with probability $1-p$. Attention is mainly drawn to a phase transition effect, which occurs at some critical probability p_c. For $p > p_c$ there is non-zero probability of any given vertex in the graph being contained withing an infinite cluster [40]. This relates to the original idea of a piece of material submerged in water and the question about its center staying dry or being soaked in water. In fact, some porous materials can be modeled using the percolation approach [41].

The application in quantum walks takes the meaning of the word "percolation" quite far from its original classical usage. In dynamical percolation it simply refers to randomly dynamically closing and reopening edges in the graph during the evolution of a quantum walk. It was shown that quantum coherence may be partially preserved even in the presence of dynamical percolation and the time-asymptotic evolution may show non-static limit cycles of different quantum states on finite graphs and lead to interesting phenomena [42, 43]. Probably the most outstanding phenomenon is trapping in walks with at least three-dimensional coins [29]. Classification of trapping coins in 2D lattices and further references on the occurrence of trapping in quantum walks can be found in [44]. Degeneracy of the coin eigenvalues in these walks allows for the presence of eigenstates of the dynamics localized only in some subset of vertices of the graph. (The localization is in the strong sense that the amplitudes outside of a given support of the eigenstate are zero.) These states are clearly also present in quantum walks without percolation, but percolation may simplify the asymptotic dynamics sufficiently so that all the trapped states can be identified analytically using the method presented in [45]. In fact, one of the main results presented in this work is that the set of trapped states can be identified in general for a quantum walk with the Grover coin and reflecting (flip-flop [46]) shift operator on any 3-regularized[2] planar graph [38].

The presence of trapping in quantum walks gives rise to non-classical effects regarding transport of an excitation. Not only the speed of transport is relevant for quantum walks, but also the probability of the walker actually ever being transported from one site in the graph to another. In a classical random walk on a connected graph (with all transition probabilities being non-zero), the walker initiated anywhere in the graph will visit any given vertex in the graph with probability approaching to 1 as the number of steps goes to infinity. In contrast, the interference in quantum walks allows for a non-zero time-asymptotic probability of trapping the walker in a subset of vertices. Therefore, it is possible for the walker to evade the target site indefinitely. This quantum transport effect can turn out to be very relevant in some processes in nature as there is evidence for coherent energy transport in photosynthesis systems [47]. The asymptotic transport on graphs of a ladder, Cayley trees and carbon nanotubes is studied in [48, 49]. Presentation of these results and their extension form the main content of Chapter 4 of this dissertation.

The present work has the following structure: In Chapter 1 we give a short introduction to classical random walks and discrete quantum walks. We present our modified definition of a quantum walk published in [38]. This definition is well suited to work

[2]By 3-regularized graphs we mean graphs with vertices of maximal degree 3 with added self-loops in vertices of lower degree. This is described in tedail in the text.

with various shift operators and also to tackle quantum walks with dynamical percolation. We also introduce the sink into quantum walks and define the asymptotic transport probability. In Chapter 2 we describe the general procedure for finding asymptotic evolution of percolated quantum walks originally presented in [42] and [43]. The approach from Chapter 2 is further utilized in Chapter 3 for the special case of percolated quantum walks on 3-regularized graphs with the Grover coin. Here we investigate walks with various shift operators – the reflecting (flip-flop) shift operator with trapped states, cyclic shift operators with an interesting relation between edge-coloring of the graph and non-trivial asymptotic dynamics of the walk, and swapping shift operator used in the lazy quantum walk. Finally, in Chapter 4 we focus on the asymptotic quantum transport by both percolated and non-percolated Grover quantum walks with the reflecting shift operator on multiple example graphs. Among other results we present the counter-intuitive behavior that the asymptotic transport probability can grow with the increasing distance of the initial site and the absorbing sink in the linear structures of both the ladder graph and carbon nanotube structures. In Appendix A we provide some basic concepts, notation, and terminology from the mathematical theory of graphs, which is used through the whole work. Further, examples of graphs used in the main chapters are presented.

Chapter 1

Definitions of quantum walks

In this chapter we first describe the transition from classical random walks to quantum walks. Then we move to its main topic: a modified definition of quantum walks, which primarily extends the possible usage from regular lattices to general graphs with various shift operators. Some ideas already taking form in the Master's thesis [51] were substantially extended (most importantly by considering quantum transport) and published in [38]. Here we present all the concepts in an extended and refined version mainly to make this work self contained and to get all the notation and terminology unified.

1.1 Classical random walks

1.1.1 The walk on a line

The most basic example of a classical random walk is a random walk on a line. There is a walker equipped with a coin who flips the coin at discrete time steps and makes a step either to the left or to the right according to the result of the coin flip.

Every particular realization of a random walk results in a sequence of positions visited by the walker in subsequent steps. We can not predict in advance which one of the walker's possible trajectories will be realized. Nevertheless, if the initial position and the probabilities of steps in each direction are known (e.g. starting at 0 with a fair coin – probability $p = 1/2$ for both directions), it is possible to calculate the position probability distribution for any number of time steps. This uses the notion of classical probability in the frequentist sense: when many realizations of the walk are performed, we expect the obtained frequencies of final positions of the walker to approach the calculated probabilities.

For the walk on a line we obtain the binomial distribution on positions with the same parity as is the parity of the number of steps. As an example, the distribution for a walker with a fair coin after 10 steps is shown in FIG. 1.1.

What is notable and will be contrasted with quantum walks is that the variance of

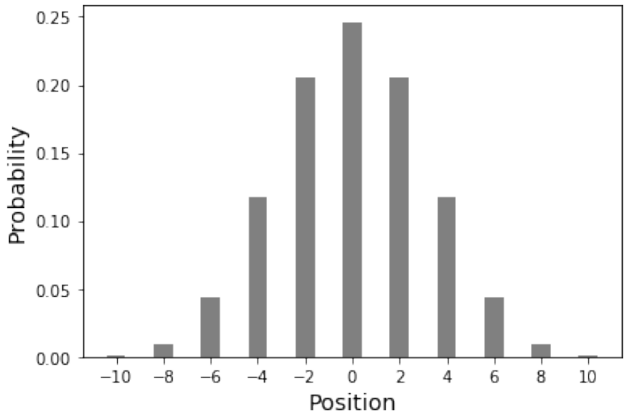

FIG. 1.1. Probability distribution of a classical random walk on a line with a fair coin after ten steps. As the number of steps is even, only even positions have non-zero probabilities.

the distribution is $p(1-p)n$, where p is the probability of a step to the right and n the number of steps. Therefore, the standard deviation, which describes the speed of the walker's spreading on the line, scales as $\sqrt{n}$.

1.1.2 Classical random walk on a graph

All kinds of graphs can be used for the definition of random walks to tackle various related problems. For example random walks on directed graphs are used in the Google page rank algorithm [5]. To allow comparison to quantum walks studied in this work, we define one type of a random walk on undirected graphs. All the necessary concepts from the graphs theory are presented in Appendix A.

Let us have an undirected graph $G(V, E)$, where V is a finite set of vertices and E a finite set of undirected edges connecting some pairs of vertices in V. For simplicity, let the graph be simple and connected. The vertices represent possible positions of the walker. When standing in a vertex v the walker can make one of $d(v)$ possible steps each leading to some neighboring vertex v_i from $\{v_i\}_{i=1}^{d(v)}$. (Here we do not allow the walker to stay in the vertex v.) In general, we can choose an arbitrary distribution of probabilities among possible steps. The obvious nontrivial choice is to set the probability of each step to be $p_i = 1/d(v)$. Again, without knowledge of particular steps the states of the walker can be best described by a probability distribution over vertices. The probability distribution over a finite set of vertices can be represented by a vector

$$\vec{P} = \sum_i p_i \vec{x}_i, \tag{1.1}$$

where p_i is the probability of the walker being at the position x_i ($p_i \geq 0\ \forall i$ and $\sum_i p_i = 1$) and $\vec{x}_i$ is a vector with all elements zeros except one element 1 at the i-th position. The transition probabilities can be cast into a stochastic matrix M

and one step of the walk transforms a distribution $\vec{P}_0$ to

$$\vec{P}_1 = M\vec{P}_0.$$

In this manner, the time evolution of a random walk is given by subsequent applications of M. It is important that all the elements of both the state vectors $\vec{P}_t$ at all times t and of the matrix M are non-negative real numbers and so there are only additions of non-negative numbers in the matrix multiplications. This results in the classical behavior where the probabilities of a walker coming to one vertex from multiple directions can only add up.

1.2 Transition to quantum walks

We may ask, what happens when we replace the classical random walker with a system governed by the laws of quantum physics. For simplicity, in this section we assume the graph underlying the random/quantum walk to have finite numbers of vertices and edges.

1.2.1 Description of the quantum walker

In any given time step a classical random walker is found at some position x_i from the set of positions $\{x_i\}_i$. Here, we do not consider a state given by a probability distribution as in (1.1). A quantum walker can be in a corresponding quantum state which is given by a vector $|x_i\rangle$ [1] from the Hilbert space

$$\mathcal{H} = \text{span}\{|x_i\rangle \, | x_i \in \{x_i\}_i\}.$$

Importantly, the state of a quantum walker is not restricted to the base states $|x_i\rangle$, but can be given by an arbitrary complex linear combination (i.e. quantum superposition) of these states

$$|\psi\rangle = \sum_i \psi_i \, |x_i\rangle \, . \tag{1.2}$$

Such state of a quantum walker is called pure and in general a quantum walker can also be in a mixed state as mentioned below.

There is a clear formal similarity of the expressions (1.1) and (1.2). Nevertheless, they describe fundamentally different situations. While (1.1) already gives a probability distribution on positions at which the classical walker can be found, the situation in quantum case is more complicated. In quantum mechanics the act of observation/measurement itself influences the state of the system and only after a certain final projective measurement at some chosen time point[2] the state $|\psi\rangle$ is projected (collapses) into one of the states $|x_i\rangle$ with the probability distribution given

[1] In this work we use the standard bra-ket notation and we expect the reared to be familiar with this notation. Also, we further do not distinguish between vectors and the corresponding states.

[2] If the state of a quantum walk is measured after every step, this results in a classical random walk.

by probabilities

$$p_i = |\psi_i|^2.$$

In fact, a quantum walker can also be in a so called mixed quantum state – a statistical mixture in which particular pure quantum states appear with various classical probabilities. A mixed quantum state is mathematically described by a density matrix

$$\rho = \sum_k p_k \left|\psi_k\right\rangle \left\langle\psi_k\right| = \sum_{i,j} \rho_{i,j} \left|x_i\right\rangle \left\langle x_j\right|,$$

where p_k is the probability of the state $|\psi_k\rangle$ in the mixture. The probability of finding the walker at position x_i is then

$$p_i = \mathrm{Tr}(\left|x_i\right\rangle \left\langle x_i\right| \rho) = \langle x_i|\rho|x_i\rangle = \rho_{ii},$$

where Tr stands for the trace operation.

The key difference between random and quantum walks lies in the fact that the probabilities p_i in (1.1) are non-negative real numbers while the amplitudes ψ_i in (1.2) can be negative or even complex [55]. The probabilities coming from two directions can only add up. In contrast, the quantum amplitudes can result in both constructive and destructive interference.

1.2.2 Naive evolution of a quantum walk

Let us attempt to cross directly from a classical random walk to a discrete quantum walk. Let x_i denote the classical positions and $|x_i\rangle$ the corresponding base vectors in a Hilbert space $\mathcal{H}$. Let us start with the quantum walk on a line. In analogy with the classical random walk we would like an evolution operator performing one time step of the walk by acting on the base states as

$$U\left|x_i\right\rangle = \alpha_i \left|x_{i-1}\right\rangle + \beta_i \left|x_i\right\rangle + \gamma_i \left|x_{i+1}\right\rangle$$

for some (possibly position dependent) coefficients α_i, β_i and γ_i. The amplitudes of the walkers state are partially moved to the neighboring sites and partially stay in the original position. (Here we also included the possibility of making no step to show that this does not resolve the problem presented below.) The evolution operator can then be written as

$$U = \sum_i \left(\alpha_i \left|x_{i-1}\right\rangle + \beta_i \left|x_i\right\rangle + \gamma_i \left|x_{i+1}\right\rangle\right) \left\langle x_i\right|.$$

Nonetheless, we require a quantum evolution operator to be unitary [55], i.e. $UU^\dagger = I$, where I is the identity matrix. In our case that is

$$
\begin{aligned}
&UU^\dagger = \\
&= \left(\sum_i \left(\alpha_i \left| x_{i-1} \right\rangle + \beta_i \left| x_i \right\rangle + \gamma_i \left| x_{i+1} \right\rangle \right) \left\langle x_i \right| \right) \left(\sum_j \left| x_j \right\rangle \left(\overline{\alpha_j} \left\langle x_{j-1} \right| + \overline{\beta_j} \left\langle x_j \right| + \overline{\gamma_j} \left\langle x_{j+1} \right| \right) \right) \\
&= \sum_i \left(\alpha_i \left| x_{i-1} \right\rangle + \beta_i \left| x_i \right\rangle + \gamma_i \left| x_{i+1} \right\rangle \right) \left(\overline{\alpha_i} \left\langle x_{i-1} \right| + \overline{\beta_i} \left\langle x_i \right| + \overline{\gamma_i} \left\langle x_{i+1} \right| \right) \\
&= \sum_i \alpha_i \overline{\alpha_i} \left| x_{i-1} \right\rangle \left\langle x_{i-1} \right| + \sum_i \alpha_i \overline{\beta_i} \left| x_{i-1} \right\rangle \left\langle x_i \right| + \sum_i \alpha_i \overline{\gamma_i} \left| x_{i-1} \right\rangle \left\langle x_{i+1} \right| + \\
&+ \sum_i \beta_i \overline{\alpha_i} \left| x_i \right\rangle \left\langle x_{i-1} \right| + \sum_i \beta_i \overline{\beta_i} \left| x_i \right\rangle \left\langle x_i \right| + \sum_i \beta_i \overline{\gamma_i} \left| x_i \right\rangle \left\langle x_{i+1} \right| + \\
&+ \sum_i \gamma_i \overline{\alpha_i} \left| x_{i+1} \right\rangle \left\langle x_{i-1} \right| + \sum_i \gamma_i \overline{\beta_i} \left| x_{i+1} \right\rangle \left\langle x_i \right| + \sum_i \gamma_i \overline{\gamma_i} \left| x_{i+1} \right\rangle \left\langle x_{i+1} \right| ,
\end{aligned}
$$

where the bar represents complex conjugation. The requirement of unitarity results in conditions for the coefficients α, β and γ. The most important is the equality

$$\alpha_i \overline{\gamma_i} = 0$$

(for example $\alpha_2 \overline{\gamma_2} \left| 1 \right\rangle \left\langle 3 \right| = 0 \left| 1 \right\rangle \left\langle 3 \right|$). This requires that one of the coefficients α_i or γ_i for every site x_i is zero. Therefore, the walker can travel from any site only in one direction or in the other. This certainly is not a behavior expected for a quantum counterpart of a random walk.

The above problem is well known and is described more generally e.g. in [52]. It was resolved in the founding work of the field of quantum walks [6] by extending the Hilbert space of the walk by an internal degree of freedom of the walker. Basically the walker is now not only at position x but also facing in some direction of further movement. That is e.g. a walker at position 0 facing to the right.

We stress that non-classical effects in quantum walks result from the interference given by superposition of complex amplitudes and not from the extension of the state space. Random walks with the state space extended in the same way as it is used in discrete quantum walks can be defined. The tossing of the coin then corresponds to a random change of the direction and is followed by a deterministic movement of the walker in the chosen direction. Nevertheless, this does not result in any fundamental advantage – there are still just real-number non-negative probabilities.

1.3 Standard definition of coined quantum walks

1.3.1 Quantum walk on a line

In this chapter we first present the standard definition of a quantum walk on a line. Let us denote vertices of the line graph by an integer index as i and introduce

corresponding base vectors $|i\rangle$. Then we define the so called *position space*

$$\mathcal{H}_p = \text{span}\{|i\rangle \, | i \in \mathbb{Z}\}.$$

As mentioned above, the whole Hilbert space of the quantum walk is obtained by extending the position space by an additional internal system connected to the walker. In this case it is a two-level system having a two-dimensional *coin space*

$$\mathcal{H}_c = \text{span}\{|L\rangle, |R\rangle\}$$

with base vectors associated with directions "left" and "right". We assume the computational basis in the coin space to be $|L\rangle = \begin{bmatrix} 1 \\ 0 \end{bmatrix}$ and $|R\rangle = \begin{bmatrix} 0 \\ 1 \end{bmatrix}$. The whole Hilbert space is a tensor product

$$\mathcal{H} = \mathcal{H}_p \otimes \mathcal{H}_c. \tag{1.3}$$

We will use a shorthand notation for states from the tensor product space: $|i\rangle \otimes |X\rangle \equiv |i, X\rangle$, where $|X\rangle$ represents $|L\rangle$ or $|R\rangle$.

In analogy with the classical random walk, every step of the time evolution is split into two parts: the *coin operation* and the *shift operation*. In quantum walks these are represented by two unitary operators C and S respectively. The time step then evolves the state $|\psi(t)\rangle$ at time t as:

$$|\psi(t+1)\rangle = U \, |\psi(t)\rangle = SC \, |\psi(t)\rangle \, , \tag{1.4}$$

where $U = SC$ is the whole evolution operator of one step.

The coin operator C acts only on the coin space part of the Hilbert space. In the simple case the action of C is independent of the position of the walker and can be described using an operator C_0 defined on the two-dimensional coin space $\mathcal{H}_c$ and the identity I_p on the position space $\mathcal{H}_p$ as

$$C = I_p \otimes C_0.$$

A standard choice of the coin is the two-dimensional Hadamard coin given in the matrix representation as

$$C_0 = H_2 = \frac{1}{\sqrt{2}} \begin{bmatrix} 1 & 1 \\ 1 & -1 \end{bmatrix}. \tag{1.5}$$

The shift operator performs the actual movement of the walker among vertices. Certainly, it moves the walker to the vertex given by the coin part of the current state. The coin state itself is not modified, so

$$\begin{aligned} S \, |i, R\rangle &= |i+1, R\rangle \, , \\ S \, |i, L\rangle &= |i-1, L\rangle \, . \end{aligned}$$

One step of our example walk than modifies the example initial state $|\psi(0)\rangle = |0, R\rangle$ to

$$\begin{aligned}|\psi(1)\rangle = U\,|\psi(0)\rangle = S(I_p \otimes H_2)\,|0, R\rangle = \\ = S\frac{1}{\sqrt{2}}(|0, L\rangle - |0, R\rangle) = \\ = \frac{1}{\sqrt{2}}(|-1, L\rangle - |1, R\rangle).\end{aligned}$$

This definition requires the underlying graph to be a regular lattice which additionally needs to have what we call *global directions* - directions of edges that can be identified in all vertices. This is fulfilled for example for the line graph or the square lattice, but already for a honeycomb lattice and especially for general graphs it is not the case. This is one of the main reasons for introducing our modified definition of quantum walks.

We see that the time evolution of the quantum walk is actually deterministic in the quantum sense. The final quantum state is fully determined by the initial state, the unitary evolution operator, and the time of evolution. The probability enters when we perform a measurement to determine the position of the walker. If we are not interested in the coin state, the probability of finding the walker at position i after t steps is

$$P(x = i, t) = |\,\langle\psi(t)|i, L\rangle\,|^2 + |\,\langle\psi(t)|i, R\rangle\,|^2,$$

which results in a probability distribution over the positions i.

We can choose the form of measurements preformed on our quantum walk and we can also choose their timing at given steps, but these choices will influence the behavior of the walk. In particular, to see a difference between classical and quantum walks, we must let the walk evolve for some time and leave it at least partially undisturbed by measurements. Performing a complete measurement (determining both the position and the coin state) after every step drives the system completely to a classical random walk: the coin operation splits amplitudes into directions, the shift operation moves amplitudes to the neighboring vertices and the measurement collapses the wave function into a new random base state. There is no room for the interference to take place.

One of the first results that raised interest in quantum walks is their ability of fast spreading. An example of the probability distribution of Hadamard quantum walk on a line measured after 100 steps is shown in FIG. 1.2. It can be seen that the deviation of the walkers position from the original point grows linearly with the number of steps, which is a quadratic speedup compared to the classical random walk diffusive spreading.

1.4 Modified definition: the Hilbert space

Let us proceed to our modified definition of quantum walks. With that we aim for two goals: first, we want a definition of quantum walks suitable for any (simple

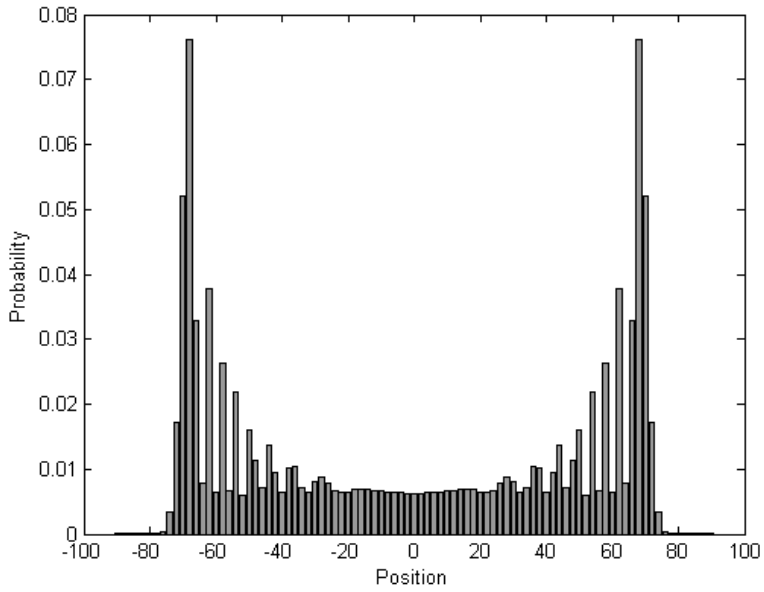

FIG. 1.2. Probability distribution of a Hadamard quantum walk on a line with a balanced initial state $|\psi_0\rangle = |0\rangle \otimes \frac{1}{\sqrt{2}}(|L\rangle + i\,|R\rangle)$ measured after 100 steps. As the number of steps is even, only even positions are shown as only those have non-zero probabilities.

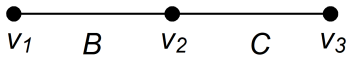

FIG. 1.3. Example of a small simple structure graph with three vertices $V = \{v_1, v_2, v_3\}$ and two undirected edges $E = \{B, C\}$.

connected) undirected graph and second, we want to cover all admissible variants of such walks in a structured way. The first goal was already achieved by so called scattering quantum walks [25]. Our definition actually partially borrows the association of the graph with the Hilbert space of the walk from the scattering walk. While various time evolutions can be chosen for the scattering quantum walk, those are not so conveniently described as in coined quantum walks. Therefore, we introduce the concept of the quantum coin in our definition. Finally, we add the entirely new concept of local permutations, which allows for a simple classification of all possible shifting rules and also allows for a natural incorporation of dynamical percolation in a quantum walk.

A quantum walk is based on an undirected *structure graph* $G(V, E)$, where V is the set of vertices and E the set of undirected edges, both of which are assumed to be finite or at most countably infinite. The structure graph is further assumed to be connected for the simplicity of argument and because a walk on a disconnected graph would only lead to separated walks on its components. On the other hand, simplicity of the structure graph is not required. Therefore, there can be both loops (edges originating and terminating in the same vertex) and parallel edges (multiple edges connecting the same pair of vertices). An example of a structure graph is shown in FIG. 1.3.

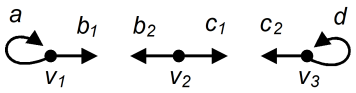

FIG. 1.4. An example of a state graph corresponding to the structure graph in FIG. 1.3. The set of vertices is te same: $V = \{v_1, v_2, v_3\}$. There are six directed edges $E^{(d)} = \{a, b_1, b_2, c_1, c_2, d\}$. Four of these are paired arcs $E_p^{(d)} = \{b_1, b_2, c_1, c_2\}$ and the remaining two are unpaired loops $E_u^{(d)} = \{a, d\}$. (There are no paired loops since the structure graph is simple.) The Hilbert space of the quantum walk is $\mathcal{H} = \mathrm{span}\{|a\rangle, |b_1\rangle, |b_2\rangle, |c_1\rangle, |c_2\rangle, |d\rangle\}$ with vertex subspaces $\mathcal{H}_{v_1} = \mathrm{span}\{|a\rangle, |b_1\rangle\}$, $\mathcal{H}_{v_2} = \mathrm{span}\{|b_2\rangle, |c_1\rangle\}$ and $\mathcal{H}_{v_3} = \mathrm{span}\{|c_2\rangle, |d\rangle\}$.

On top of the structure graph we define a directed *state graph* $G^{(d)}(V, E^{(d)})$. The set of vertices V is the same as for the structure graph. The set of directed edges $E^{(d)}$ is formed by two subsets $E^{(d)} = E_p^{(d)} \cup E_u^{(d)}$. For every undirected edge $e \in E$ from the structure graph we introduce two *paired* directed edges $e_1, e_2 \in E_p^{(d)}$ in the state graph. These edges connect the same vertices as e, each in one direction. The paired edges are mostly arcs connecting two distinct vertices, but an undirected loop l in the structure graph corresponds to two directed paired loops l_1 and l_2 in the state graph, all of them starting and finishing at the same vertex. Appart from paired edges there are so called *unpaired* loops. Those are independent of the undirected edges from E and are typically used to increase degrees of chosen vertices for example on borders of finite cuts of lattices. An example of a state graph is shown in FIG. 1.4.[3]

We use the following *tilde notation*: If directed paired edges $e_1, e_2 \in E_p^{(d)}$ correspond to the same undirected edge $e \in E$, we define $\tilde{e}_1 \equiv e_2$ and $\tilde{e}_2 \equiv e_1$. For an unpaired loop $l \in E_u^{(d)}$ it is trivially $\tilde{l} \equiv l$.

With the state graph defined, we now associate its edges with base states of the walker. The walker is located at the vertex which is the origin of the edge and is facing towards the terminal vertex. This is in analogy with the standard definition of quantum walks for regular lattices, but here the direction of further movement is not understood globally but locally. For every vertex the set of possible directions is given by the neighboring vertices. Nevertheless, it is straightforward to see the equivalence with the standard definition on graphs representing regular lattices.

Written formally, for every directed edge $e^{(d)} \in E^{(d)}$ (an arc or a loop), there is a base state of the walker $|e^{(d)}\rangle$ and the whole Hilbert spaces is the span of all these orthonormal states

$$\mathcal{H} = \mathrm{span}\{|e^{(d)}\rangle \, | e^{(d)} \in E^{(d)}\}.$$

The Hilbert space is no longer of the tensor product form (1.3), but can still be written as a direct sum

$$\mathcal{H} = \bigoplus_{v \in V} \mathcal{H}_v, \tag{1.6}$$

[3]In figures we usually represent directed arcs as arrows beginning in one vertex and pointing towards the end-point instead of as going all the way to the other vertex. This is in correspondence with our understanding of the state of the walker as standing in one vertex and facing towards another.

where $\mathcal{H}_v$ are so called *vertex subspaces*: subspaces spanned by states corresponding to directed edges originating in a given vertex. These concepts are also exemplified in FIG. 1.4.

Due to the form of the Hilbert space (1.6), operators acting on this space can be composed from partial operators acting locally on vertex subspaces as for example the coin operator

$$C = \bigoplus_{v \in V} C_v,$$

where C_v can be for example the Hadamard matrix (1.5). The index v is used to indicate the local version of the operator in the remainder of this work.

Note on terminology simplification: In this work we exploit the bijection between base states of the Hilbert space and directed edges from the state graph and use formulations like "states originating in the vertex v". Also, utilizing the connection between paired directed and undirected edges we can e.g. say "subspace is given by a path in the structure graph", which means the subspace of states on directed edges corresponding to undirected edges included in the path.

Lastly, we introduce one more graph associated with a quantum walk, which will be used in this work. (Its usage is rather specific to investigation of Grover quantum walks with dynamical percolation as introduced in Chapter 3.) It is a *mixed graph* of the walk $G^{(m)}(V, E \cup E_u^{(d)})$. Therefore, it is just the structure graph with added unpaired loops from the state graph. Alternatively, it can be viewed as a graph which we get from the state graph by joining the paired directed edges in pairs into undirected edges.

1.5 Modified definition: the time evolution

The basic concept of a time-discrete unitary evolution is kept the same as in the standard definition

$$|\psi(t+1)\rangle = U\,|\psi(t)\rangle\,. \tag{1.7}$$

The evolution operator U is composed of a shift operator and a coin operator. Differences are introduced mainly in the definition of the shift operator and also in the order in which the operators are applied as is detailed below.

1.5.1 Shift operator

Since our modified definition of the Hilbert space does not assume any global directions that can be identified in all vertices, it is in general not possible to use a shift operator that just keeps some direction as in the standard quantum walk on the line. In general, we have two main requirements for the shift operator to keep the basic notion of a coined quantum walk:

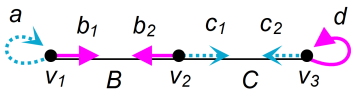

FIG. 1.5. The action of the reflecting shift operator on the example graph from FIG. 1.3. The mapping is depicted using colors and line types, in particular $R\left|b_1\right\rangle = \left|b_2\right\rangle, R\left|b_2\right\rangle = \left|b_1\right\rangle, R\left|c_1\right\rangle = \left|c_2\right\rangle, R\left|c_2\right\rangle = \left|c_1\right\rangle$ and for the unpaired loops $R\left|a\right\rangle = \left|a\right\rangle$ and $R\left|d\right\rangle = \left|d\right\rangle$.

1. The shift operator has to be a permutation on the set of base states corresponding to directed edges in the state graph.[4] This assures unitarity of the evolution.

2. The shift operator has to respect the underlying graph: a state corresponding to an edge (v_1, v_2) must be mapped to a state corresponding to an edge originating in v_2.

There is a canonical shift operator that can be defined on any graph. We call it the *reflecting shift operator* R and is also known as "flip-flop" shift operator [46]. It is easily described using the tilde notation introduced in the above section as

$$R = \sum_{e^{(d)} \in E^{(d)}} \left|\tilde{e}^{(d)}\right\rangle \left\langle e^{(d)}\right|, \tag{1.8}$$

so

$$R\left|e^{(d)}\right\rangle = \left|\tilde{e}^{(d)}\right\rangle$$

for an arbitrary directed edge $e^{(d)} \in E^{(d)}$. In words, amplitudes corresponding to the paired states are swapped in pairs and amplitudes corresponding to unpaired loops are left unchanged. This operator is clearly and unambiguously defined for any graph in question. An example is presented in FIG. 1.5.

Apart from the reflecting shift operator, many other shift operators can be used for any graph. Nevertheless, it is not possible to just map every base state to some arbitrarily chosen base state in the neighboring vertex. We must be careful to avoid mapping two distinct states to one state.

In fact, there is a simple way how to identify all the possible shift operators fulfilling the two requirements above. We first apply the reflecting shift operator R, which is possible on any graph. Then we apply what we call a *local permutation* P - an arbitrary permutation which only permutes edges originating from the same vertices (i.e. does not move the walker from one vertex to another). The final shift operator is then

$$S = PR.$$

It is clear that a shift operator defined in this way fulfills both our requirements and also that any shift operator fulfilling them can be represented in this way. The

[4] Sometimes, phase shifts introduced by the shift operator can be used, but we do not consider those here.

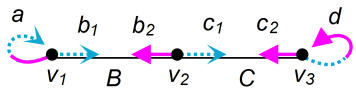

FIG. 1.6. The standard shift operator for the line, which is in our formalism obtained by choosing the swap operator σ_x as the local permutation in all vertices: $S = PR = \left(\bigoplus_{v\in V} \sigma_x\right) R$. The mapping is depicted using colors and line types, in particular $S\left|a\right\rangle = \left|b_1\right\rangle, S\left|b_1\right\rangle = \left|c_1\right\rangle, S\left|c_1\right\rangle = \left|d\right\rangle, S\left|d\right\rangle = \left|c_2\right\rangle, S\left|c_2\right\rangle = \left|b_2\right\rangle, S\left|b_2\right\rangle = \left|a\right\rangle$.

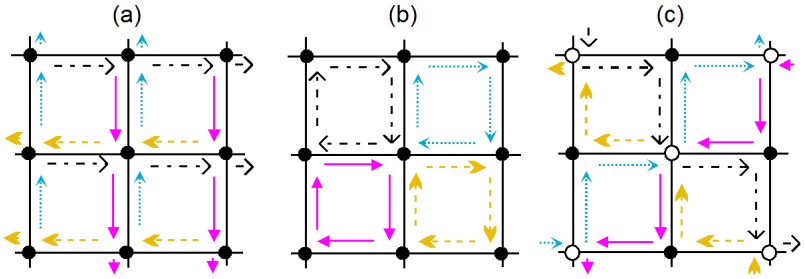

FIG. 1.7. Three examples of shift operators that can be used for a walk on the square lattice: (a) the standard operator keeping walkers direction (local permutation swaps directions left with right and up with down), (b) a *cyclic* shift operator (counter-clock-wise rotation as a local permutation in all vertices) and (c) a *transporting* shift operator (clock-wise rotation in white vertices and counter-clock-wise in black vertices). The mapping is depicted using colors and line types.

reflecting operator moves the walker among vertices in accordance with the graph and the local permutation determines the final direction. Obviously, there is also no room for two states being mapped to a single one as the shift operator is just a subsequent application of two permutations.

There are $\Pi_{v\in V}(\mathrm{d}(v)!)$ possible shift operators for a given graph, where $\mathrm{d}(v)$ is the degree of a vertex $v \in V$. In practice, we typically assume some homogeneity of the medium in which the walker is moving and the local permutation is then the same in all vertices or there are just a few sets of vertices sharing the same local permutations.

For a two-dimensional vertex subspace only two local permutations are possible: the identity I_v and the swap operator σ_x. Using the swap operator in all vertices results in the standard shift operator on the line as illustrated in FIG. 1.6.

With growing degrees of vertices the number of admissible shift operators grows rapidly. FIG. 1.7 presents three chosen variants for a quantum walk on the square lattice. Here we want to point out that the choice of the shift operator is crucial for the dynamics of the resulting quantum walk. Therefore, claims about properties of quantum walks on some graphs using particular coins should always be accompanied by the discussion of the chosen shift operator. The interplay between the shift operator and the coin operator is discussed in detail below.

1.5.2 Coin operator

There is almost no change in meaning of the coin operator C in our modified definition of quantum walks. It is an arbitrary unitary operation which is local at vertices - it only mixes states within the vertex subspaces. In formal terms, it can be stated that all the vertex subspaces are invariant under the action of C, so the coin operator can always be written as

$$C = \bigoplus_{v \in V} C_v,$$

where C_v is a local operator acting in the vertex subspace $\mathcal{H}_v$ of the vertex $v \in V$.

In contrast to regular lattices, in general graphs the degrees may vary among vertices and so dimensions of the vertex subspaces may differ. Therefore, it may not be possible to use the same local coin operation in all vertices. On the other hand, even if the graph is regular, one can obviously choose different local coins in different vertices.

In particular cases studied below we add unpaired loops to the state graph so that it becomes regular and we can use the same coin everywhere.

1.5.3 Labeling states at vertices

The standard representation of operators on finite-dimensional spaces uses matrices. In our case, this mainly applies to the coin operation as in equation (1.5) and also to the local permutations.

The use of matrices, nevertheless, requires choosing and fixing the order of states in the computational basis. For standard quantum walks on regular lattices this is usually not an issue. For example on the line we can choose the order (L, R) in all vertices and so the computational basis is $|L\rangle = \begin{bmatrix} 1 \\ 0 \end{bmatrix}$ and $|R\rangle = \begin{bmatrix} 0 \\ 1 \end{bmatrix}$. This is natural if our one-dimensional walk really progresses along a straight line as in FIG. 1.8 (a). Let us consider a one-dimensional walk which is now placed into some square lattice structure as illustrated in FIG. 1.8 (b). Here the global directions can be identified as vertical (V) and horizontal (H). We can again fix the labeling using these global directions, for example in the order (V, H) in all vertices. While at vertices v_1 and v_3 in FIG. 1.8 this leads to the order (a, b_1) and (c_2, d) in both variants, in the vertex v_2 the (L, R) labeling gives (b_2, c_1) but the (V, H) labeling gives (c_1, b_2). If we choose to apply the Hadamard coin (1.5) in all vertices, then compared to the (L, R) in the (V, H) variant we effectively apply a different coin

$$H' = \sigma_x H \sigma_x^\dagger = \frac{1}{\sqrt{2}} \begin{bmatrix} -1 & 1 \\ 1 & 1 \end{bmatrix} \tag{1.9}$$

in the vertex v_2.

Resolving this issue in a general graph without any global structure of directions would require explicitly defining the ordering of base states in all vertices. In some

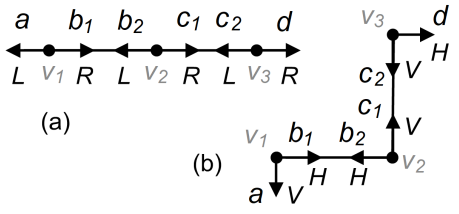

FIG. 1.8. The graph from FIG. 1.3 in two different situations with two corresponding labelings of edges: (a) left/right and (b) vertical/horizontal. Note that the edges b_1 and b_2 have different labels in (a) and have the same label in (b).

cases, the lack of symmetry in the graph can be compensated by symmetry in the represented operators and their matrices themselves. Relabeling of states effectively modifies the matrix in question by multiplying it from both sides by a permutation matrix and its conjugate. (In the example above this was the σ_x swap permutation.) If our matrix is invariant under this transformation, the relabeling actually does not play any role.

In particular, the central coin operator in this work is the Grover coin. If we define the vector $|\phi\rangle = (|1\rangle + |2\rangle + \ldots + |n\rangle)/\sqrt{n}$, the Grover coin has the general form

$$G_n = 2|\phi\rangle\langle\phi| - I \tag{1.10}$$

for arbitrary dimension n. As we mostly work with 3-regular graphs, we are particularly interested in the three-dimensional case

$$G_3 = \frac{1}{3}\begin{bmatrix} -1 & 2 & 2 \\ 2 & -1 & 2 \\ 2 & 2 & -1 \end{bmatrix}. \tag{1.11}$$

From (1.10) we see that the Grover coin commutes with arbitrary permutation matrices. (Both the identity matrix and a matrix with all elements the same commute with all permutation matrices.) Therefore, the Grover matrix is not affected by any change of the ordering of states in a given vertex.

Concerning the local permutations, apart from the identity we mostly work with clock-wise and counter-clock-wise permutations in three-dimensional spaces. The corresponding matrices are not invariant to relabeling, but specific ordering of states in every vertex is not required. For the action of the rotation to be unambiguous, it is sufficient to place the graph into a plane. After such embedding, the meaning of clock-wise or counter-clock-wise rotations is fixed. In fact, the graph does not even need to be planar since eventual crossing of edges has no influence on rotations at vertices.

1.5.4 Order of operators in U

In analogy with the original classical random walk it is natural to always first flip a coin and then make a step according to the result of the coin flip. This approach is also a standard in quantum walks. Nevertheless, we argue that considering the

operators in the opposite order - the shift operator first and the coin operator second - is reasonable and can also bring significant benefits for the study of quantum walks. It sheds light on the relation between different coins and shift operators and in our particular case allows for convenient investigation of quantum walks with dynamical percolation. Further, as consideration of more possible orders of evolution operators is yet another generalization of quantum walks, it can bring some other possibilities not yet discovered.

The standard version of the unitary evolution operator is

$$U^{(1)} = SC = PRC, \tag{1.12}$$

where by the index $^{(1)}$ we indicate the position of the coin operator C in U. The shift operator S is further decomposed into the reflecting shift operator R and the local permutation P.

The variant most heavily used in this work is

$$U^{(3)} = CS = CPR. \tag{1.13}$$

For the original random walk, where the state of the walker is only given by his position in the graph, it does not make sense to first make a step and flip the coin afterwards. Yet, already in the classical random walk with the state space extended by the directions of further movement, this approach can be used without any problems. The walker is initiated in some state, which also includes direction. The walker makes a step and then flips a coin to determine the direction of the following step. The very same holds for quantum walks, where we just apply two unitary operators in one order or the other.

Obviously, since the operators C and S are not commutative, $U^{(1)}$ and $U^{(3)}$ are two different operators. The evolution is in a sense shifted by half of the step. If the initial state of the walker is $|\psi(0)\rangle$, the state at time t with the evolution operator $U^{(1)}$ is

$$|\psi(t)\rangle = \left(U^{(1)}\right)^t |\psi(0)\rangle = (SC)^t |\psi(0)\rangle = C^\dagger (CS)^t C |\psi(0)\rangle = C^\dagger \left(U^{(3)}\right)^t C |\psi(0)\rangle .$$

The final state of the walk, therefore, differs by one application of C on the initial state and one application of $C^\dagger$ on the final sate. In some scenarios, the result can obviously be very different, but we show further that in particular for the asymptotic states of dynamically percolated quantum walks the results for $U^{(3)}$, which are technically much simpler to obtain, can be easily modified for walks with $U^{(1)}$.

1.5.5 Coin-shift interplay

Our definition employing the concept of local permutations in combination with the usage of the version $U^{(3)}$ of the evolution operator reveals a very interesting interplay between the coin operator and the shift operator. Since both C and P in (1.13) are local at vertex subspaces, they can actually be combined and understood as a new coin

$$C' = CP.$$

Every quantum walk can, therefore, be understood as a quantum walk with the reflecting shift operator and some coin, which can also incorporate the local permutation.

Also, one might consider the variant of the evolution operator $U^{(2)} = PCR$. First, it does not make much sense to insert the coin operator between the two parts of the shift operator. Second, the variant $U^{(2)}$ is just $U^{(3)}$ with a different coin $C'' = PCP^\dagger$.

1.6 Percolated quantum walks

1.6.1 The classical question of percolation

A thought experiment inspired by a real-life situation presenting the phenomenon of percolation uses a big block[5] of porous material (stone) submerged in water. The question is, whether the center of the block will be wet or if it will stay dry.

This problem is stated formally in the mathematical theory of graphs. The porous block is represented by an infinite graph (e.g. an infinite square lattice). Then, every edge of the graph is randomly chosen to remain open (with probability p) or is closed (with probability $1-p$) and we ask, what is the probability θ that the origin lies within an infinite component of connectivity (an open cluster) in this modified graph [40].

The interesting result drawing attention to the problem of percolation is that there is some critical probability p_c so that

$$\theta \begin{cases} = 0 & \text{if } p < p_c \\ > 0 & \text{if } p > p_c. \end{cases}$$

Therefore, for $p < p_c$ the probability of "percolation" (existence of an infinite component of connectivity containing the origin) is zero and for $p > p_c$ it is non-zero. This is referred to as a phase transition - a global property of the system exhibits a step change at a given value of a parameter describing local properties. Importantly, this phenomenon of a phase transition is non-trivial ($0 < p_c < 1$) for lattices of dimensionality at least 2 [40].

1.6.2 Percolation in quantum walks

In the field of quantum walks, the term percolation is used to refer to the way of perturbation of a graph by randomly breaking some of its edges rather than to some resulting phenomenon [54].

We could use this process to generate a random graph from a regular lattice and then run a quantum walk on this graph. It that case no modification of the definitions presented above is needed. We would only use percolation to obtain a graph to start

[5] The block is meant to be big compared to the porous micro-structure, so that it can be modeled mathematically as an infinite medium.

with. We do not study this problem in the present work. Instead we focus on a so called *dynamically percolated quantum walks*[6] where a new percolation graph is generated for every step of the walk. In this case, a modification of the quantum walk definition is needed both to deal with closed edges and to incorporate classical randomness in the time evolution.

A dynamically percolated quantum walk also starts with an original undirected structure graph $G(V, E)$ and a directed state graph $G^{(d)}(V, E^{(d)})$, which is based on G and can have some unpaired loops added. We choose a probability p and in every step of the walk a new *percolation graph* $G_K(V, K)$ is generated by randomly choosing some edges in G to be open with probability p or closed with probability $1 - p$. A subset (*configuration*) of open edges is denoted as $K \subset E$.

On the open edges the walker obviously moves just as in the case of non-percolated walk. In contrast, we do not want the walker to pass through closed edges. It is also needed to keep the same Hilbert space of the walk through the time evolution. We therefore keep the state graph $G^{(d)}(V, E^{(d)})$ the same including the paired edges corresponding to closed undirected edges. We keep referring to those as paired, but now *closed paired* edges.

Let us now define the modified time evolution. The coin operator can be kept without any modifications. What needs to be altered is the shift operator. In short, in our formalism we just treat the closed paired edges as unpaired loops and the local permutation is unchanged just as the coin. (This step is simple and natural in our formalism thanks to the fact that the formalism itself was developed with exactly this application in mind.)

We now discuss the modification of the shift operator in more detail. For a given configuration of open edges K we want to define a shift operator S_K which does not move the walker over closed edges. The problem is (would we not employ our new formalism) that if we just keep the walker standing in a state facing towards a closed edge, there may be another state mapped to this one. For example, the walker is standing in the vertex 0 on a line facing to the left. The edge to the left is closed but the one to the right is open and we have the standard shift operator keeping walkers direction. Then we can not map the state $|0, L\rangle$ back to $|0, L\rangle$, because the sate $|1, L\rangle$ is already mapped to $|0, L\rangle$. On the other hand, the state $|0, R\rangle$ is "free", because the walker can not arrive from $|-1, R\rangle$ over a closed edge. In general, we need to map a state of a walker facing towards a closed edge to the state, that would otherwise be the final state of a walker coming over that closed edge. A useful property of the reflecting shift operator R is that the above approach is exactly applied just by treating the closed paired edges as unpaired loops. (Any closed paired edge itself would be the end point for a walker coming from the opposite direction.) This results in a modified reflecting shift operator R_K, which is the same as R for open paired edges and unpaired loops and acts as the identity on closed paired edges. We use this modified reflecting shift operator R_K and then apply the usual local permutation P,

[6] It feels almost like an abuse of the term to say "percolated walks", but we stick to this simplifying terminology anyway.

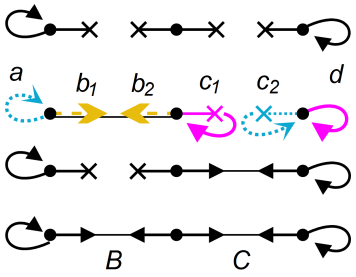

FIG. 1.9. Four possible configurations of percolation graphs $2^E = \{\emptyset, \{B\}, \{C\}, \{B, C\}\} \equiv \{K_\emptyset, K_B, K_C, K_{BC} = K_E\}$ for the example graph in FIG. 1.3. The modified reflecting shift operator R_{K_B} for the configuration K_B is defined as: $R_{K_B}|a\rangle = |a\rangle, R_{K_B}|b_1\rangle = |b_2\rangle, R_{K_B}|b_2\rangle = |b_1\rangle, R_{K_B}|c_1\rangle = |c_1\rangle, R_{K_B}|c_2\rangle = |c_2\rangle, R_{K_B}|d\rangle = |d\rangle$ as indicated by colors and line types of the arrows.

so the step is given as

$$|\psi(t+1)\rangle = U_K^{(3)}|\psi(t)\rangle = CPR_K|\psi(t)\rangle .$$

An example of four possible percolation graphs on our simple example graph with the corresponding action of R_K is shown in FIG. 1.9.

When we study the evolution of a dynamically percolated quantum walk, we can not predict particular configurations K of the percolation graphs in the individual steps. As there is always one unitary operation U_K applied, which is randomly chosen from the set of evolution operators corresponding to all possible configurations $K \in 2^E$, the resulting time evolution is so called *random unitary operation* [45]. It acts on the state of the walker described using a density matrix $\rho(t)$ as

$$\rho(t+1) = \mathcal{S}(\rho(t)) = \sum_{K \subset E} \pi_K U_K \rho(t) U_K^\dagger, \tag{1.14}$$

where π_K is the probability of occurrence of the configuration $K \subset E$.

Note on terminology: In the following we use the abbreviation PCQW for "percolated coined quantum walk" and CQW for just "coined quantum walk". Despite the fact that at some instances we explicitly state "non-percolated CQW", CQW always stands for a quantum walk without percolation.

1.7 Quantum walks with a sink and quantum transport

We aim to study quantum transport using quantum walks. For that purpose we introduce an absorbing *sink*. The walk is initiated in some localized state and when reaching the sink the walker is said to be transported.

1.7.1 Definition of the sink

The implementation of a sink in classical random walks is trivial. In quantum walks, more caution is needed and also there are multiple ways how a sink can be implemented. That is due to the fact that observation of the position of the walker in a quantum walk actually influences the state of the walk. In this work we proceed as follows:

- We choose a *sink subspace* $\mathcal{H}_s$ which is spanned by states corresponding to some chosen directed edges $\mathcal{H}_s = \text{span}\{|s_1\rangle, |s_2\rangle, \ldots\}$. (The sink is not necessarily just one chosen vertex and so the sink subspace does not have to coincide with any of the vertex subspaces.)
- We construct a projector to the sink subspace Π_s and the projector to the complement of the sink subspace $\Pi = I - \Pi_s$.
- After every step a projective measurement is performed to determine if the walker has already reached the sink subspace. This results in a partial collapse of the wave function either to the sink or to its complement.

One step of a quantum walk with a sink is than given as

$$|\psi(t+1)\rangle = \Pi U |\psi(t)\rangle \tag{1.15}$$

for the non-percolated version and as

$$\rho(t+1) = \sum_{K \subset E} \pi_K \Pi U_K \rho(t) U_K^\dagger \Pi \tag{1.16}$$

if the walk is percolated.

The time evolution of the quantum walk with a sink is not trace preserving and the value

$$p(t) = \text{Tr}\left(\rho(t)\right) \tag{1.17}$$

gives the probability that at time t the walker is still present in the graph and has not reached the sink.

1.7.2 Classical and quantum walk transport

If we introduce a sink in the classical random walk on a finite connected graph (and the edges have non-zero probabilities of being chosen for the next step), the walker reaches the sink with probability 1 when the number of steps grows to infinity. In contrast, interference in quantum walks allows the walker to stay trapped in the graph indefinitely. Therefore, it is reasonable to define the *asymptotic trapping probability*

$$p = \lim_{t \to +\infty} p(t) = \text{Tr}\left(\lim_{t \to +\infty} \rho(t)\right)$$

and its complement

$$q \equiv 1 - p = 1 - \mathrm{Tr}\left(\lim_{t\to+\infty} \rho(t)\right) \tag{1.18}$$

the *asymptotic transport probability* (ATP). Most of the remainder of this work is the study of the asymptotic quantum transport represented by the ATP in quantum walks. Let us turn to this question in the following chapter.

Chapter 2

Asymptotic evolution of percolated coined quantum walks

In this chapter we study the asymptotic evolution of dynamically percolated quantum walks in general terms (examples for particular graphs are presented in the next chapter, Chapter 3). Following [42] and [43][1] we apply the general procedure published in [45] to percolated quantum walks while utilizing the modified definition presented in Chapter 1. This was also partially done in [51] (without all the parts employing so called p-attractors) and in a more advanced way in [38]. Similarly as in the previous chapter, we paraphrase all the material here for consistency and extend it with some further comments and details.

From now on we put a further requirement on the structure graph of a quantum walk in investigation - we work only with **finite graphs**. Therefore, it is possible to represent all evolution operators and density operators by finite matrices and pure states by finite vectors.

We start by investigating time evolution of percolated quantum walks without sink and present a modification for walks with a sink afterwards.

2.1 Asymptotic state constructed from attractors

The time evolution of a dynamically percolated quantum walk without a sink is given by the random unitary operation (1.14). If we let the walk evolve for a long time (many time steps), the richness of the unitary dynamics of a non-percolated walk is reduced by the classical randomness introduced by percolation and the system transitions to an asymptotic regime. The asymptotics do not need to be just a single state (density matix) but a limit cycle (several mutually transforming states) can occur [42, 43].

It was shown in [45] that the state of a system evolved by a random unitary operation

[1] Note that in this reference the meaning of the operator denoted as R in the evolution operator is very different from the notation used in this work.

(1.14) (e.g. a percolated quantum walk) in the asymptotic regime can be expressed as

$$\rho_{t\to\infty}(t) = \sum_{\lambda,i} \lambda^t \operatorname{Tr}\left(\rho(0) X_{\lambda,i}^\dagger\right) X_{\lambda,i}, \tag{2.1}$$

where λ are eigenvalues with $|\lambda| = 1$ of the evolution super-operator $\mathcal{S}$ from (1.14) and $X_{\lambda,i}$ are their corresponding eigenvectors called *attractors* indexed by the i orthonormalized with respect to the Hilbert-Schmidt scalar product ($\operatorname{Tr}(X_{\lambda_1,i}^\dagger X_{\lambda_2,j}) = \delta_{\lambda_1\lambda_2}\delta_{ij}$). Attractors are common solutions of all the equations

$$U_K X_\lambda U_K^\dagger = \lambda X_\lambda\,, \quad \text{for all } K \in 2^E \tag{2.2}$$

fulfilling the additional condition $|\lambda| = 1$. (Eigenvaleus with $|\lambda| = 1$ are said to be in the *asymptotic spectrum*. Solutions with $|\lambda| > 1$ are not possible [45] and solutions with $|\lambda| < 1$ are removed from the asymptotic state [45].)

Note that the asymptotic state is independent of the probabilities π_K as long as those are non-zero. Their values clearly influence the non-asymptotic evolution, in particular the rate of convergence towards the asymptotic regime, but those properties are not of our concern in this work.

2.2 Attractors of percolated quantum walks

Using the separation of the evolution operator in the particular case of quantum walks without sink

$$U_K^{(3)} = CPR_K \tag{2.3}$$

it is possible to rewrite the attractor equations (2.2) into the form

$$R_K X R_K^\dagger = \lambda (CP)^\dagger X (CP)\,, \quad \text{for all } K \in 2^E. \tag{2.4}$$

Now we use the fact that the right hand sides of all the equations in (2.4) are the same independently of the configuration K. This allows to solve the problem in two steps.

1. We use one particular configuration $K = \emptyset$ (all the edges are closed), in which case the modified reflecting shift operator is just the identity $R_\emptyset = I$ and we obtain the so called *coin condition*

$$CPX(CP)^\dagger = \lambda X. \tag{2.5}$$

2. Due to the independence of the right hand sides on K, the left hand sides must be mutually equal to each other for all the equations. This gives us the other constrain, the *shift condition*

$$R_K X R_K^\dagger = R_L X R_L^\dagger\,, \quad \text{for all } K, L \in 2^E. \tag{2.6}$$

Both the coin condition and the shift condition are investigated in detail below.

2.2.1 p-attractors

In many cases the search for attractors can be considerably simplified using a procedure published in [43] using so called *common eigenstates*. Those are pure states $|\phi_\alpha\rangle$ which are common eigenstates of all unitary operators U_K

$$U_K |\phi_\alpha\rangle = \alpha |\phi_\alpha\rangle \ , \quad \text{for all } K \in 2^E. \tag{2.7}$$

If $\{|\phi_{\alpha,i}\rangle\}_i$ and $\{|\phi_{\beta,j}\rangle\}_j$ are sets of common eigenstates corresponding to the eigenvalues α and β respectively, then

$$Y_\lambda = \sum_{\alpha\beta^*=\lambda} A^{\alpha,i}_{\beta,j} |\phi_{\alpha,i}\rangle \langle\phi_{\beta,j}| \tag{2.8}$$

is an attractor corresponding to the eigenvalue $\lambda = \alpha\beta^*$ (the asterisk denotes complex conjugation) for arbitrary coefficients $A^{\alpha,i}_{\beta,j}$. We call the attractors obtained in this way from common eigenstates *p-attractors*. The equations for finding common eigenstates can be processed using the decomposition of the evolution operator (2.3) as

$$R_K |\phi_\alpha\rangle = \alpha (CP)^\dagger |\phi_\alpha\rangle \quad \text{for all } K \in 2^E. \tag{2.9}$$

Using the empty configuration $K = \emptyset$ with all edges closed and $R_\emptyset = I$ we have the coin condition

$$CP |\phi_\alpha\rangle = \alpha |\phi_\alpha\rangle \tag{2.10}$$

and from the equality of left hand sides the shift condition

$$R_K |\phi_\alpha\rangle = R_L |\phi_\alpha\rangle \ , \quad \text{for all } K, L \in 2^E. \tag{2.11}$$

We stress that not all attractors are p-attractors. At least the maximally mixed state (proportional to the identity matrix I) is an attractor but it is not a p-attractor.

The difference between p-attractors and general attractors is seen from the fact the p-attractors fulfill not only the condition (2.2) but also a more restrictive one

$$U_{K_1} Y_\lambda U^\dagger_{K_2} = \lambda Y_\lambda \, , \quad \text{for all } K_1, K_2 \in 2^E, \tag{2.12}$$

where there are two possibly distinct configurations K_1 and K_2 instead of just one [43]. As the configuration only influences the reflecting shift operator, this difference translates only to the shift condition which is of the form

$$R_{K_1} Y R^\dagger_{K_2} = R_{L_1} Y R^\dagger_{L_2} \, , \quad \text{for all } K_1, K_2, L_1, L_2 \in 2^E. \tag{2.13}$$

Importantly, it is possible to identify situations in which the maximally mixed state is the only independent[2] non-p-attractor and so the asymptotic evolution can be fully determined from the knowledge of common eigenstates. This is the case for all situations investigated further in this work.

[2] We can obtain new non-p-attractors by combining p-attractors with non-p-attractors, but we clearly only need to find linearly independent attractors.

2.2.2 The coin condition

When working with the coin condition (2.5) for general attractors or (2.10) for common eigenstates we use the fact that both the coin operator and the local permutation are local in vertex subspaces, so CP is a block-diagonal matrix. The coin condition can, therefore, be investigated in separate blocks, which are subsequently merged according to the shift condition to form attractors or common eigenstates.

For a matrix block $X^{v_1}_{v_2}$ corresponding to a pair of vertices $v_1, v_2 \in V$ the coin condition (2.5) requires

$$(C_{v_1}P_{v_1})X^{v_1}_{v_2}(C_{v_2}P_{v_2})^\dagger = \lambda X^{v_1}_{v_2}, \tag{2.14}$$

where C_{v_1}, C_{v_2} and P_{v_1}, P_{v_2} are blocks of matrices C and P respectively.

Here we use a method of rearranging columns of matrix blocks $X^{v_1}_{v_2}$ into long vectors $x^{v_1}_{v_2}$ according to the rule $\langle a, b|x^{v_1}_{v_2}\rangle = \langle a|X^{v_1}_{v_2}|b\rangle$ for all $|a\rangle \in \mathcal{H}_{v_1}, |b\rangle \in \mathcal{H}_{v_2}$. (In practice this just means putting columns of a matrix on top of each other to form a column vector.) In this formalism, the equation (2.14) takes the form of a standard eigenvalue problem

$$(C_{v_1}P_{v_1}) \otimes (C_{v_2}P_{v_2})^* x^{v_1}_{v_2} = \lambda x^{v_1}_{v_2},$$

where the asterisk denotes complex conjugation. This allows us to determine the asymptotic spectrum and a general form of blocks $X^{v_1}_{v_2}$.

In case of common eigenstates the coin condition (2.10) is already in the form of an eigenvalue problem.

2.2.3 The shift condition

Let us write a general pure state as a linear combination of the base states corresponding to directed edges in the state graph

$$|\phi\rangle = \sum_{j \in E^{(d)}} \phi_j \, |j\rangle \, .$$

The reflecting shift operator R can be expressed using the tilde notation as (1.8). When only edges in $K \subset E$ are open, we have a corresponding operator R_K. This operator is also given by a permutation on the set of directed edges, which we denote as k and the R_K is then

$$R_K = \sum_{i \in E^{(d)}} |k(i)\rangle \langle i| \, , \tag{2.15}$$

where $k(\cdot)$ is a permutation mapping i to $\tilde{i}$ if the corresponding undirected edge is open and mapping i back to i otherwise. This is just a formal transition from a permutation map on edges to an operator on the Hilbert space of corresponding states. Using (2.15) and $R_K = R_K^\dagger$, the shift conditions for common eigenstates

(2.11) may be rewritten as

$$R_K^\dagger |\phi\rangle = R_L^\dagger |\phi\rangle \ , \quad \text{for all } K, L \in 2^E,$$
$$\sum_{i \in E^{(d)}} |i\rangle \langle k(i)| \sum_{j \in E^{(d)}} \phi_j |j\rangle = \sum_{i \in E^{(d)}} |i\rangle \langle l(i)| \sum_{j \in E^{(d)}} \phi_j |j\rangle \, ,$$
$$\sum_{i \in E^{(d)}} \phi_{k(i)} |i\rangle = \sum_{i \in E^{(d)}} \phi_{l(i)} |i\rangle \, ,$$

which turns into an equality of vector components

$$\phi_{k(i)} = \phi_{l(i)} \, , \quad \text{for all } i \in E^{(d)}, \ K, L \in 2^E.$$

Suppose a directed edge i corresponds to an undirected edge e and let us choose K and L so that $e \notin K$ and $e \in L$ (the edge is closed in one configuration and open in the other). Then $k(i) = i$ and $l(i) = \tilde{i}$. The shift condition then results in

$$\phi_i = \phi_{\tilde{i}}.$$

Since such pair of configurations can be chosen for any undirected edge and since $i = \tilde{i}$ for any unpaired loop, the shift condition can be expressed as

$$\phi_i = \phi_{\tilde{i}} \, , \quad \text{for all } i \in E^{(d)}. \tag{2.16}$$

This is a very simple and intuitive form of the shift condition. In any common eigenstate the amplitudes for a pair of directed edges corresponding to one undirected edge must always be equal. This shift condition leads to the use of mixed graphs introduced in Appendix A: undirected edges represent pairs of vector elements that must be the same due to the shift condition and further there are the elements corresponding to unpaired loops.

To show the difference between general attractors and p-attractors, we use a straightforward modification of the calculation above to turn the shift condition in the matrix form (2.13) into the form

$$X^{k_1(i)}_{k_2(j)} = X^{l_1(i)}_{l_2(j)} \, , \quad \text{for all } \ i, j \in E^{(d)}, K_1, K_2, L_1, L_2 \in 2^E. \tag{2.17}$$

Let us again suppose that i and j correspond to undirected edges e and f respectively. (In general, it can be $i = j$ or $i = \tilde{j}$, so $e = f$.) It is possible to choose configurations so that for example $e \notin K_1$, $e \in L_1$, $f \notin K_2$ and $f \notin L_2$. Then (2.17) results in

$$X^i_j = X^{\tilde{i}}_{\tilde{j}}. \tag{2.18}$$

Again, this holds even e.g. for $i = j$, in which case the equality is

$$X^i_i = X^{\tilde{i}}_{\tilde{i}}. \tag{2.19}$$

By considering other configurations, we obtain the whole shift condition for p-attractors

$$X^i_j = X^{\tilde{i}}_j = X^i_{\tilde{j}} = X^{\tilde{i}}_{\tilde{j}} \, , \quad \text{for all } \ i, j \in E^{(d)}. \tag{2.20}$$

In case of general attractors, we start with (2.6) and turn it into

$$X^{k(i)}_{k(j)} = X^{l(i)}_{l(j)}, \quad \text{for all} \quad i,j \in E^{(d)}, K, L \in 2^E. \tag{2.21}$$

It is very similar to (2.17) but on each side there is only one permutation map resulting form one configuration of a percolation graph. For cases with $i \neq j$ and $i \neq \tilde{j}$, so $e \neq f$, we can again choose configurations fulfilling $e \notin K$, $e \in L$, $f \notin K$ and $f \notin L$ and get the equality (2.18). In contrast e.g. for $i = j$, we can not make e both open and closed in L simultaneously and so e.g. the equality (2.19) is not required by the shift condition for general attractors. By using other configurations and considering cases with $e = f$, the shift condition for general attractors can be expressed as

$$X^i_j = X^{\tilde{i}}_j = X^i_{\tilde{j}} = X^{\tilde{i}}_{\tilde{j}}, \quad \text{for all} \quad i,j \in E^{(d)}, i \neq j, i \neq \tilde{j}, \tag{2.22}$$

$$X^i_i = X^{\tilde{i}}_{\tilde{i}}, \quad \text{for all} \quad i \in E^{(d)}, \tag{2.23}$$

$$X^i_{\tilde{i}} = X^{\tilde{i}}_i, \quad \text{for all} \quad i \in E^{(d)}. \tag{2.24}$$

Note on restricted percolation: As was already presented in [51] and published in [38], by far not all the possible configurations of the percolation graph are necessary to force the same shift condition as the full percolation model. For example it suffices to use only configurations with just one open edge each. Similarly, the set of configurations with only one edge closed is sufficient. (If we assume at least three undirected edges in the graph in both examples.)

2.2.4 Exclusion of non-p-attractors

In this work, we are particularly interested in percolated quantum walks in which the maximally mixed state is the only non-p-attractor. Therefore, the asymptotic dynamics can be described entirely when the set of p-attractors is known, so we just need to find a basis of the common eigenstates subspace.

The fact that this is the case for percolated quantum walks with the Grover coin and reflecting shift operator or combinations of cyclic shift operators (as described in Chapter 3) is proven in [38]. These proofs are not included in the present work, but the proof for a lazy Grover quantum walk with the standard shift operator is given in section 3.4.2, which serves as a detailed demonstration of the approach. While in this work we are mostly interested in percolated quantum walks with asymptotic dynamics given entirely by p-attractors, this is not always the case. Here we present a simple counter-example.

2.2.5 Example quantum walk with non-trivial non-p-attractors

Let us consider a quantum walk on a graph with just two vertices v_1 and v_2 connected by one edge with directions labeled as L and R as is shown in FIG. 2.1. The basis

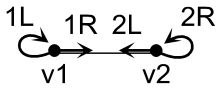

FIG. 2.1. The graph and labeling for the simple example of a percolated quantum walk with non-p-attractors different from the maximally mixed state.

of the Hilbert space consists of four states:

$$|1L\rangle = \begin{bmatrix} 1 \\ 0 \\ 0 \\ 0 \end{bmatrix}, |1R\rangle = \begin{bmatrix} 0 \\ 1 \\ 0 \\ 0 \end{bmatrix}, |2L\rangle = \begin{bmatrix} 0 \\ 0 \\ 1 \\ 0 \end{bmatrix}, |2R\rangle = \begin{bmatrix} 0 \\ 0 \\ 0 \\ 1 \end{bmatrix}.$$

The reflecting shift operator has two possibilities $R_\emptyset$ (the edge is closed) and R_E (the only edge e is open), which have the following matrix forms:

$$R_\emptyset = \begin{bmatrix} 1 & 0 & 0 & 0 \\ 0 & 1 & 0 & 0 \\ 0 & 0 & 1 & 0 \\ 0 & 0 & 0 & 1 \end{bmatrix}, \quad R_e = R_E = \begin{bmatrix} 1 & 0 & 0 & 0 \\ 0 & 0 & 1 & 0 \\ 0 & 1 & 0 & 0 \\ 0 & 0 & 0 & 1 \end{bmatrix}.$$

The local permutation is chosen to be the identity (reflecting walk, $P_{v_1} = P_{v_2} = I$) and the coin in the first vertex v_1 is σ_x and in v_2 it is σ_z, where σ_x and σ_z are Pauli matrices:

$$\sigma_x = \begin{bmatrix} 0 & 1 \\ 1 & 0 \end{bmatrix}, \quad \sigma_z = \begin{bmatrix} 1 & 0 \\ 0 & -1 \end{bmatrix}.$$

Therefore, the whole coin operator is

$$C = \begin{bmatrix} 0 & 1 & 0 & 0 \\ 1 & 0 & 0 & 0 \\ 0 & 0 & 1 & 0 \\ 0 & 0 & 0 & -1 \end{bmatrix}$$

and the two possible evolution operators are

$$U_\emptyset = CR_\emptyset = C,$$
$$U_E = CR_E = \begin{bmatrix} 0 & 0 & 1 & 0 \\ 1 & 0 & 0 & 0 \\ 0 & 1 & 0 & 0 \\ 0 & 0 & 0 & -1 \end{bmatrix}.$$

All Pauli matrices have eigenvalues $+1$ and -1. The eigenvectors for σ_x and σ_z are:

$$|\psi_{x+}\rangle = \begin{bmatrix} 1 \\ 1 \end{bmatrix}, \quad |\psi_{x-}\rangle = \begin{bmatrix} 1 \\ -1 \end{bmatrix},$$
$$|\psi_{z+}\rangle = \begin{bmatrix} 1 \\ 0 \end{bmatrix}, \quad |\psi_{z-}\rangle = \begin{bmatrix} 0 \\ 1 \end{bmatrix}.$$

The shift condition for p-attractors is

$$\phi_{1R} = \phi_{2L}.$$

For the eigenvalue $\alpha_1 = +1$ we can construct a common eigenstate

$$|\phi_+\rangle = \frac{1}{\sqrt{3}} \begin{bmatrix} 1 \\ 1 \\ 1 \\ 0 \end{bmatrix},$$

but for the eigenvalue $\alpha_2 = -1$ the shift condition requires non-zero element for $|2L\rangle$, which is not compatible with the coin condition for the coin σ_z. Therefore, we only have one common eigenstate and it corresponds to the eigenvalue $\alpha_1 = +1$. This results in only one p-attractor and it also corresponds to the eigenvalue $\lambda = 1 \cdot 1 = 1$.

In contrast, it is easily checked that the matrix

$$X_{-1} = \begin{bmatrix} 0 & 0 & 0 & 0 \\ 0 & 0 & 0 & 0 \\ 0 & 0 & 0 & 0 \\ 1 & 1 & 1 & 0 \end{bmatrix} \tag{2.25}$$

fulfills both the equations

$$U_\emptyset X_{-1} U_\emptyset^\dagger = -X_{-1},$$
$$U_E X_{-1} U_E^\dagger = -X_{-1},$$

and so it is an attractor corresponding to the eigenvalue $\lambda = -1$. Clearly, it is not the only obtained p-attractor and it even corresponds to a different eigenvalue.

2.3 Trapped states and asymptotic evolution of walks with a sink

Some of the attractors or common eigenstates of a quantum walk can have zero amplitudes for some directed edges in the state graph. We refer to those as *trapped attractors* and *trapped states* respectively. (Note that attractors are not necessarily valid density operators, so they do not have to be states as for example the attractor in (2.25).) We also say that these attractors/states have limited support on the graph, where by the support we mean the set of directed edges corresponding to non-zero elements in the given trapped attractor/state.

Once we have determined the attractors governing the asymptotic evolution of a percolated quantum walk without a sink, the incorporation of the effect of a sink is relatively simple [56]. We just need to determine the subspace of the attractor space which is orthogonal to the given sink subspace. This is seen from the attractor equation (2.2) when modified for the walk with the sink implemented by the projector

to the complement of the sink subspace Π as

$$\Pi U_K X_\lambda U_K^\dagger \Pi = \lambda X_\lambda\,, \quad \text{for all } K \in 2^E,$$
$$U_K X_\lambda U_K^\dagger = \lambda \Pi X_\lambda \Pi.$$

It is clearly solved by solutions of (2.2) with the additional requirement of zero overlap with the sink subspace. On the other hand, for $|\lambda| = 1$ it is only solved by solutions of (2.2) orthogonal to the sink. The left hand side is an application of a unitary operation and the right hand side is a projection. The only possibility for these to be equal is when $\Pi X_\lambda \Pi = X_\lambda$ and further we are left with the equation (2.2).

Let us now focus on the situation with evolution given only by p-attractors as described in section 2.2.4. The maximally mixed state always overlaps with the sink subspace and is therefore lost in the sink inevitably. If no other non-p-attractors are present, candidates for surviving states that can form the asymptotic state of a walk with sink must be searched for among the trapped common eigenstates. We call trapped states without overlap with the sink *sink resistant* trapped states, in short sr-trapped states.

We presented a method for determining all the common eigenstates in the above sections. Now we need to find a subspace, which is orthogonal to the sink subspace. In general, we can not just discard all the states with some non-zero amplitudes in the sink subspace to obtain a complete set of sr-trapped states. Instead, we must search among all linear combinations of the common eigenstates for a given eigenvalue.

In some situations it is possible to first construct a basis of the trapped states subspace in a clever way so that the part of the subspace overlapping with the sink can be determined easily. If there is a directed sink edge (a base state in the sink subspace) for which only one common eigenstate for a given eigenvalue has non-zero amplitude, then we can just discard this trapped state. As a result, there may be another directed sink edge with the same property. In some cases, this can be repeated for all directed sink edges and we are left with the basis of the sr-trapped states subspace. In all studied cases in this work this approach can be used.

2.3.1 Calculation of the asymptotic transport probability (ATP)

If we are able to obtain an orthonormal basis of the subspace of sr-trapped states for a given PCQW, we can construct a projector to this subspace Π_T. With that the ATP defined in (1.18) can be calculated for an arbitrary initial state ρ_i as

$$q = 1 - \mathrm{Tr}(\Pi_T \rho_i). \tag{2.26}$$

Thanks to the linearity of the trace operation and since the maximally mixed state on the initial subspace $\overline{\rho}_i$ represents the uniform statistical mixture of all possible initial states, we can also directly calculate the average ATP as

$$\overline{q} = 1 - \mathrm{Tr}(\Pi_T \overline{\rho}_i). \tag{2.27}$$

2.4 Results for $U^{(1)}$ from results for $U^{(3)}$

2.4.1 Motivation for using $U^{(3)}$

Our main motivation for using the variant $U^{(3)}$ of the evolution operator in our investigation is the elegant form of the obtained shift condition (2.6). Let us demonstrate the complication with the variant $U^{(1)}$ on the simple case of the search for common eigenstates

$$\begin{aligned} U_K^{(1)} \left|\phi_\alpha\right\rangle &= \alpha \left|\phi_\alpha\right\rangle \ , \quad \text{for all } K \in 2^E, \\ PR_K C \left|\phi_\alpha\right\rangle &= \alpha \left|\phi_\alpha\right\rangle . \end{aligned}$$

In general, the coin operator does not commute with the reflecting shift operator. Therefore, the local permutation has to be kept together with the reflecting shift in the separation

$$C \left|\phi_{\alpha,i}\right\rangle = \alpha R_K (P)^\dagger \left|\phi_{\alpha,i}\right\rangle \quad \text{for all } K \subset 2^E.$$

The empty configuration with $R_\emptyset = I$ results in a very similar shift condition as for $U^{(3)}$ with just C and P commuted, which is no problem for the investigation

$$\begin{aligned} C \left|\phi_{\alpha,i}\right\rangle &= \alpha P^\dagger \left|\phi_{\alpha,i}\right\rangle , \\ PC \left|\phi_{\alpha,i}\right\rangle &= \alpha \left|\phi_{\alpha,i}\right\rangle . \end{aligned}$$

On the other hand, the local permutation P is problematic in the shift condition

$$R_K P^\dagger \left|\phi_{\alpha,i}\right\rangle = R_L P^\dagger \left|\phi_{\alpha,i}\right\rangle \ , \quad \text{for all } K, L \in 2^E.$$

Since the operators R_K and R_L do not commute with the local permutation in general, the local permutation can not be removed from the shift condition. The shift condition can be turned into equalities of vector elements just like (2.16), but those are not equalities of elements corresponding to pairs of directed edges on one undirected edge. They can link arbitrary two elements from the two vertex subspaces. This version is obviously also solvable in some cases, as it was used in [42, 43], but we can not get as far in the systematic analysis as for our version with $U^{(3)}$.

2.4.2 Asymptotics of $U^{(1)}$ without sink

Let us remind that the attractor equation (2.2) with $U^{(3)}$ has the form (2.4)

$$CPR_K X R_K P^\dagger C^\dagger = \lambda X \ , \quad \text{for all } K \in 2^E. \tag{2.28}$$

For comparison, with $U^{(1)}$ this is

$$PR_K C W C^\dagger R_K P^\dagger = \lambda W \ , \quad \text{for all } K \in 2^E, \tag{2.29}$$

where we just for further convenience use W to denote the unknown attractor. Let us now set

$$W = C^\dagger X C.$$

By substituting W into (2.29) and by substituting $X = CWC^\dagger$ into (2.28) we immediately see that X is an attractor for $U^{(3)}$ if and only if W is an attractor for $U^{(1)}$ for the same eigenvalue. Similarly $|\phi\rangle$ is a common eigenstate for $U^{(3)}$ if and only if

$$|\psi\rangle = C^\dagger |\phi\rangle$$

is a common eigenstate for $U^{(1)}$ corresponding to the same eigenvalue. Also, since (2.5) holds for the solution X and (2.10) holds for $|\phi\rangle$, the solutions for $U^{(1)}$ can also be expressed using the local permutation operator P as

$$W = C^\dagger X C = \overline{\lambda} P X P^\dagger, \tag{2.30}$$

$$|\psi\rangle = C^\dagger |\phi\rangle = \overline{\lambda} P |\phi\rangle , \tag{2.31}$$

where the multiplication of an attractor or a common eigenstate by a constant ($\lambda^{-1} = \overline{\lambda}$ or $\alpha^{-1} = \overline{\alpha}$ respectively) is irrelevant. An immediate consequence is that for a reflecting quantum walk ($P = I$) without sink, the attractors and so the asymptotic time evolutions are the same for evolution operators $U^{(3)}$ and $U^{(1)}$.

2.4.3 Asymptotics of $U^{(1)}$ with sink

For walks with a sink, it is clearly possible to just take a modified set of attractors/trapped states as described in the above section and search for their subspace orthogonal to the sink subspace. Nevertheless, in most situations it is possible to directly use the sink resistant attractors or sr-trapped states for the $U^{(3)}$ variant of the evolution operator and transform them into sr-trapped attractors or sr-trapped states for the variant $U^{(1)}$.

Here the attractor equation (2.2) with the added projector to the complement of the sink subspace Π for $U^{(3)}$ is explicitly

$$\Pi C P R_K X R_K P^\dagger C^\dagger \Pi = \lambda X , \quad \text{for all } K \in 2^E \tag{2.32}$$

and for $U^{(1)}$

$$\Pi P R_K C W C^\dagger R_K P^\dagger \Pi = \lambda W , \quad \text{for all } K \in 2^E. \tag{2.33}$$

Due to the fact that Π commutes with C if we assume the sink to always cover whole vertex subspaces, we can use the very same approach as for a walk without sink. We just use solution (2.30) for the walk with $U^{(1)}$. This is in contrast to situations where only some directed edges in vertices act as the sink. If there are vertex subspaces only partially covered by the sink subspace, the operators Π and C do not commute in general and the above approach can not be used. However, the situation can be remedied, as mentioned above. One has to go one step back, construct modified attractors for a walk without sink, and then search for the subspace orthogonal to the sink. Note that the methods for transition from $U^{(3)}$ to $U^{(1)}$ without sink can be used. In particular, as for the reflecting walk the set of attractors is the same for $U^{(3)}$ to $U^{(1)}$, the set of sr-trapped attractors/states is the same even for walks with a sink not covering the whole vertex subspaces.

Chapter 3

Percolated Grover quantum walks on simple 3-regularized graphs

Here we study quantum walks on structure graphs with $\Delta \leq 3$ (every vertex has at most 3 neighbors), where unpaired loops are added so that the state graphs are 3-regular (every vertex has three outgoing and three incoming edges). We call such graphs 3-regularized as detailed in appendix A.

3.1 Motivation for choosing 3-regularity

We consider only connected graphs. In that case a $\Delta = 1$ graph can either be a single vertex or two vertices connected by one edge. Asymptotic properties of percolated quantum walks on graphs with $\Delta = 2$ were studied previously [42] and their possible complexity is also very limited. Such graphs can be chains of vertices either with open ends or joined into a cycle.

Somewhat at the border between $\Delta = 2$ and $\Delta = 3$ graphs is the lazy quantum walk [29] (walk on a line with an additional no-movement state at every vertex). It has a $\Delta = 2$ structure graph, but the state graph is 3-regularized.

An explosion of richness of possible structure graphs comes when considering family of $\Delta = 3$ graphs. It ranges from tree graphs over simple structures like the ladder graph, polyhedra as the cube, the dodecahedron or fullerenes all the way to the honeycomb lattice and graphs representing carbon nanotubes.

For this reason we fix the regularity of the state graph at the value three. In combination with the special choice of the coin to be the Grover matrix this allows us to proceed very far in the analysis of the asymptotic behavior of the corresponding percolated quantum walks.

3.2 The Grover coin

Since the state graph of our quantum walk is 3-regular, all the vertex subspaces are 3-dimensional and we can use the same coin at every vertex. In particular, we choose the well studied Grover coin. The Grover coin is represented by a matrix, which can be defined for arbitrary dimension d by (1.10) and for our particular case of $d = 3$ by (1.11).

The Grover coin has two distinct properties, which we utilize in our investigation:

- It has a degenerate eigenvalue ($\alpha = -1$), which allows for the existence of trapped states (states with limited support on the state graph).
- As a linear combination of the matrix with all elements equal and the identity it commutes with all permutations on the 3-dimensional space.

Due to the fact that the Grover matrix treas all the three inputs the same (it commutes with all permutations on its domain space), there is no need to fix the order of base states in a vertex to apply the coin operation. Therefore, if not required by the local permutation P, there is no need to explicitly specify the order of the base states in the computational basis in vertex subspaces when representing the coin by a matrix.

3.3 Various shift operators

Various shift operators S arise from different local permutations P in our formalism, in particular $S = PR$, where R is the reflecting (or "flip-flop") shift operator.

For a 3-regular state graph, there are 6 possible choices of the local permutation P_v in every vertex $v \in V$. The overall local permutation operation P can in general be given by an arbitrary distribution of these permutations among vertices. Nevertheless, we focus on situations where the same local permutation is chosen for all vertices or at least for a significant fraction of them. In particular, we deal with three scenarios described below.

3.3.1 Reflecting shift operator

If we choose the identity as the local permutation in all the vertices then $S = PR = IR = R$ and we arrive at what we call a *reflecting quantum walk*. An example of the action of this operator is shown in FIG. 3.1.

3.3.2 Cyclic shift operators

Another class of shift operators are those resulting from combinations of clock-wise (CW) and counter-clock-wise (CCW) local rotations P_v^{CW} and P_v^{CCW} respectively.

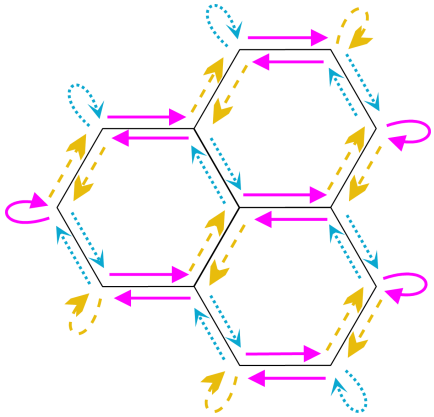

FIG. 3.1. Demonstration of the action of the reflecting shift operator R on a cut of a honeycomb lattice. The state corresponding to a directed edge is mapped to the state corresponding to the edge of the same color and line type beginning in the target vertex.

We can express the cyclic local permutations in the matrix form as

$$P_v^{CW} = \begin{bmatrix} 0 & 0 & 1 \\ 1 & 0 & 0 \\ 0 & 1 & 0 \end{bmatrix}, \quad P_v^{CCW} = \begin{bmatrix} 0 & 1 & 0 \\ 0 & 0 & 1 \\ 1 & 0 & 0 \end{bmatrix}.$$

Here the ordering of base states is relevant, yet it does not have to be specified entirely. To specify a CW or CCW rotation on directed edges, it suffices to place the graph into a plane. (Crossing edges in the planar representation are no problem here, so possible non-planarity of the graph is not relevant.) Then, for the unambiguity of the matrix representation of these rotations we can just say that the base vectors in the computational basis

$$|1\rangle = \begin{bmatrix} 1 \\ 0 \\ 0 \end{bmatrix}, \quad |2\rangle = \begin{bmatrix} 0 \\ 1 \\ 0 \end{bmatrix}, \quad |3\rangle = \begin{bmatrix} 0 \\ 0 \\ 1 \end{bmatrix} \tag{3.1}$$

are always placed in the clock-wise order.

We could again construct the overall local permutation from an arbitrary distribution of cyclic rotations among vertices. Nevertheless, we mostly investigate two special cases in detail. We introduce a *cyclic quantum walk*, where the local permutation is either P_v^{CW} in all vertices or P_v^{CCW} in all vertices. An example of a cyclic walk with P_v^{CW} permutations is shown in FIG. 3.2. We see that in this case without the action of the coin the walker would cycle counter-clock-wise on faces of the lattice.

Next we introduce a *transporting quantum walk*. This walk is only defined on bipartite graphs like the honeycomb lattice or the cube. The bipartity splits the set of vertices into two disjoint groups and we use P_v^{CW} for one group of vertices and P_v^{CCW} for the other group. This typically results (again if not considering the action of the coin) in a zig-zag motion of the walker over the graph as seen in the example in FIG. 3.3.

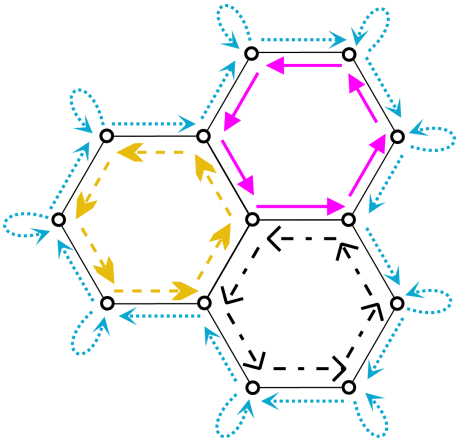

FIG. 3.2. Demonstration of the action of the cyclic shift operator $S = (I_V \otimes P_v^{CW})R$ on a cut of a honeycomb lattice. The state corresponding to a directed edge is mapped to the state corresponding to the edge of the same color and line type beginning in the target vertex. On the border, the walker is moved from a paired edge to a loop and from a loop to the next paired edge.

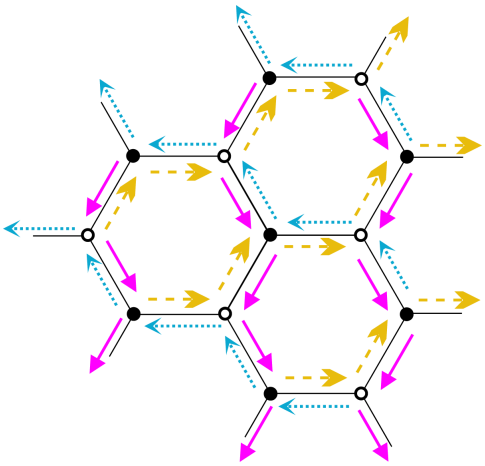

FIG. 3.3. Demonstration of the action of the transporting shift operator with P_v^{CW} in white vertices and P_v^{CCW} in black vertices on a part of a honeycomb lattice. The state corresponding to a directed edge is mapped to the state corresponding to the edge of the same color and line type beginning in the target vertex. In this example only a part of the graph is shown and the graph is assumed to continue in all directions.

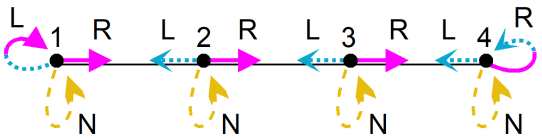

FIG. 3.4. A small graph for the lazy walk with four vertices and three undirected edges. The directed edges (base sates) are labeled as N ("no movement"), L ("left"), R ("right") in every vertex. The action of the standard shift operator is depicted by colors and types of the arrows. The walker is mapped to the state on the edge beginning by the same style as is the end of the original edge.

Apart from cyclic and transporting walks, we also consider some special distributions of cyclic rotations tailored for particular graphs as for example the dodecahedron graph as shown in FIG. 3.10.

3.3.3 Swapping shift operators and the lazy quantum walk

The last three permutations on the three-dimensional spaces leave one state unchanged and swap the other two. In a matrix representation those can be expressed as

$$P_v^{23} = \begin{bmatrix} 1 & 0 & 0 \\ 0 & 0 & 1 \\ 0 & 1 & 0 \end{bmatrix}, \quad P_v^{31} = \begin{bmatrix} 0 & 0 & 1 \\ 0 & 1 & 0 \\ 1 & 0 & 0 \end{bmatrix}, \quad P_v^{12} = \begin{bmatrix} 0 & 1 & 0 \\ 1 & 0 & 0 \\ 0 & 0 & 1 \end{bmatrix}.$$

This kind of a shift operator can be naturally utilized in a so called lazy quantum walk [29].

In a lazy quantum walk, the walker is moving on a line graph as in the most studied case of a quantum walk, but there is the additional possibility for the walker to stay at the given vertex and not to move to any of the neighbors. This is represented in our formalism by a line structure graph (chain of vertices with the nearest neighbors connected) with one unpaired loop added into every vertex in the state graph. Also, as we only use a finite chain of vertices, one more unpaired loop is added at each terminal vertex. Example figures of a structure graph and a state graph of a lazy walk are found in appendix section A.2.1.

For the non-loop edges, the shift operator is required to move the walker into the neighboring vertex but to keep the coin state pointing in the same direction. Therefore, we use the swap local permutation after the reflecting shift to swap the amplitudes corresponding to the non-loop edges. The graph for the lazy walks as well as the action of the shift operator are exemplified in FIG. 3.4.

3.4 Exclusion of non-p-attractors

The search for attractors of a percolated quantum walk is significantly simplified in cases, where there are only p-attractors and the maximally mixed state as the only non-p-attractor. Here we prove that this is the case in examples of our interest.

3.4.1 Reflecting walk and cyclic walks

The fact that the maximally mixed state is the only non-p-attractor for Grover walks on 3-regularized graphs with the reflecting shift operator and for cyclic shift operators (for arbitrary distributions of CW and CCW local rotations among vertices) is shown in the appendix of [38]. We do not present the proof here.

3.4.2 Lazy walk with the standard shift operator

To demonstrate the strategy of the proof and also to be able to tackle this model, we prove here that the same situation as for reflecting and cyclic walks is for the standard lazy quantum walk, i.e. a walk with the swap shift operator. (Walks with all possible distributions of the three swapping operators on arbitrary graphs can be investigated, but for simplicity we restrict ourselves to the lazy walk here.) Obviously, it is also possible to define a lazy quantum walk with the reflecting shift operator. In that case, the general result for reflecting walks applies.

We are to prove that the maximally mixed state is the only independent non-p-attractor. That means that all the other attractors can be expressed as linear combinations of the maximally mixed state and p-attractors. The p-attractors can be constructed from common eigenstates and in contrast to the non-p-attractors they fulfill the condition (2.19) for all edges $i \in E^{(d)}$.

We start with the equation (2.14), which gives a set of eigenvalues and for every eigenvalue λ a general form of the attractor block Ξ_λ given by several parameters $(\alpha, \beta, \ldots)$. In our case, the local permutation is the same in all vertices so it suffices to label the attractor block by the eigenvalue and the vertex labels can be dropped in the general form.

The strategy of the proof is to go through eigenvalues one by one. For eigenvalues $\lambda \neq 1$ we show that the combination of the possible form of attractor blocks Ξ_λ and the less restrictive shift condition (2.22) for general attractors (as compared to the p-attractor shift condition (2.20)) already requires (2.19) for all edges. Note that thanks to (2.22), we immediately obtain

$$X^i_i = X^{\tilde{i}}_i \Rightarrow X^{\tilde{i}}_{\tilde{i}} = X^i_i = X^{\tilde{i}}_i = X^i_{\tilde{i}}. \tag{3.2}$$

Therefore, there are no non-p-attractor for eigenvalues $\lambda \neq 1$. The situation is more complicated for $\lambda = 1$, where there is the one non-p-attractor. Here we show that the combination of the form of attractor blocks and the shift condition for general attractors requires the following:

$$X^i_i = X^{\tilde{i}}_i \Rightarrow \left(X^j_j = X^{\tilde{j}}_j \,, \quad \text{for all} \quad j \in E^{(d)} \right) \tag{3.3}$$

where i is one chosen edge. This also implies

$$X^i_i = X^{\tilde{i}}_i \Rightarrow \left(X^j_j = X^{\tilde{j}}_j = X^j_{\tilde{j}} = X^{\tilde{j}}_{\tilde{j}} \,, \quad \text{for all} \quad j \in E^{(d)} \right). \tag{3.4}$$

This equation requires, that if (2.19) holds for one edge, the whole extended shift condition holds for all the edges and an attractor in question is a p-attractor. We then consider an arbitrary attractor $A \neq I$ corresponding to $\lambda = 1$ and one chosen edge $i \in E_p^{(d)}$. We construct yet another attractor

$$B = zI + wA,$$

where the complex numbers z, w are chosen so that

$$B_i^i = zI_i^i + wA_i^i = zI_{\tilde{i}}^{\tilde{i}} + wA_{\tilde{i}}^{\tilde{i}} = B_{\tilde{i}}^{\tilde{i}}.$$

Since (2.19) holds for one edge i in B, it holds for all edges and B is a p-attractor. Therefore, we can express an arbitrary attractor A as a linear combination of the maximally mixed state I and some p-attractor B as

$$A = \frac{z}{w} I - \frac{1}{w} B.$$

Certainly $w \neq 0$, since $I_i^i \neq zI_{\tilde{i}}^{\tilde{i}}$.

Let us apply this procedure to the case of Grover lazy percolated quantum walk. We label edges as shown in FIG. 3.4 and choose the ordering N, L, R in all vertices, so the local permutation is represented by the matrix P_v^{23} from (3.2). The coin condition (2.14) reads

$$G_3 P_v^{23} \Xi_\lambda (G_3 P_v^{23})^\dagger = \lambda \Xi_\lambda \tag{3.5}$$

and it gives only the eigenvalues -1 and 1. For the eigenvalue $\lambda = -1$, there is a four-dimensional subspace, for which the basis can be chosen in the form

$$\Xi_{-1}^\alpha = \begin{bmatrix} 0 & 1 & 1 \\ -1 & 0 & 0 \\ -1 & 0 & 0 \end{bmatrix}, \quad \Xi_{-1}^\beta = \begin{bmatrix} 0 & 1 & -1 \\ -1 & 0 & 1 \\ 1 & -1 & 0 \end{bmatrix}, \tag{3.6}$$

$$\Xi_{-1}^\gamma = \begin{bmatrix} 0 & 1 & -1 \\ 1 & -1 & 0 \\ -1 & 0 & 1 \end{bmatrix}, \quad \Xi_{-1}^\delta = \begin{bmatrix} -2 & 0 & 0 \\ -1 & 1 & 1 \\ -1 & 1 & 1 \end{bmatrix}. \tag{3.7}$$

The basis is chosen to demonstrate the left-right symmetry of the walk. Since the evolution is the same if we use the order N, R, L and the Grover coin commutes with local permutations, for a given attractor block fulfilling (3.5) the block $P_v^{23} \Xi_\lambda (P_v^{23})^\dagger$ must also be an attractor. This transformation swaps the elements

$$\begin{aligned} \Xi_2^1 &\leftrightarrow \Xi_3^1, \\ \Xi_1^2 &\leftrightarrow \Xi_1^3, \\ \Xi_2^3 &\leftrightarrow \Xi_3^2, \\ \Xi_2^2 &\leftrightarrow \Xi_3^3, \end{aligned}$$

and in our choice of the basis it either leaves the block unchanged or just multiplies it by -1.

An attractor block for the eigenvalues -1 can, therefore, be represented using four free parameters $\alpha, \beta, \gamma, \delta$ as

$$\Xi_{-1} = \begin{bmatrix} -2\delta & \alpha+\beta+\gamma & \alpha-\beta-\gamma \\ -\alpha-\beta+\gamma-\delta & -\gamma+\delta & \beta+\delta \\ -\alpha+\beta-\gamma-\delta & -\beta+\delta & \gamma+\delta \end{bmatrix}. \tag{3.8}$$

We consider two neighboring vertices denoted only as 1 and 2. The corresponding part of the shift condition (2.22) is

$$\begin{aligned} X^{1R}_{1R} &= X^{2L}_{2L}, \\ X^{1R}_{2L} &= X^{2L}_{1R}, \\ X^{1R}_{1L,2R,1N,2N} &= X^{2L}_{1L,2R,1N,2N}, \\ X^{1L,2R,1N,2N}_{1R} &= X^{1L,2R,1N,2N}_{2L}, \end{aligned} \tag{3.9}$$

where multiple indices are just a shorthand for multiple equalities. Next, we combine the coin condition and the shift condition by expressing (3.9) in terms of the elements of the attractor block (3.8), where the equalities are multiplied by different factors for further convenience:

$$\begin{aligned} X^{1R}_{1R} = X^{2L}_{2L} &\to +3\gamma_{11} + 3\delta_{11} = -3\gamma_{22} + 3\delta_{22}, \\ X^{1R}_{2L} = X^{2L}_{1R} &\to -3\beta_{12} + 3\delta_{12} = +3\beta_{21} + 3\delta_{21}, \\ X^{1R}_{1L} = X^{2L}_{1L} &\to -1\beta_{11} + 1\delta_{11} = -1\gamma_{21} + 1\delta_{21}, \\ X^{1R}_{1N} = X^{2L}_{1N} &\to +2\alpha_{11} - 2\beta_{11} + 2\gamma_{11} + 2\delta_{11} = +2\alpha_{21} + 2\beta_{21} - 2\gamma_{21} + 2\delta_{21}, \\ X^{1R}_{2N} = X^{2L}_{2N} &\to -2\alpha_{12} + 2\beta_{12} - 2\gamma_{12} - 2\delta_{12} = -2\alpha_{22} - 2\beta_{22} + 2\gamma_{22} - 2\delta_{22}, \\ X^{1L}_{1R} = X^{1L}_{2L} &\to +1\beta_{11} + 1\delta_{11} = -1\gamma_{12} + 1\delta_{12}, \\ X^{1N}_{1R} = X^{1N}_{2L} &\to -1\alpha_{11} + 1\beta_{11} + 1\gamma_{11} = -1\alpha_{12} - 1\beta_{12} - 1\gamma_{12}, \\ X^{2N}_{1R} = X^{2N}_{2L} &\to +1\alpha_{21} - 1\beta_{21} - 1\gamma_{21} = +1\alpha_{22} + 1\beta_{22} + 1\gamma_{22}, \end{aligned} \tag{3.10}$$

By summing all the equations (3.10) we obtain

$$+8\gamma_{11} + 8\delta_{11} = +8\beta_{21} + 8\delta_{21} \to X^{1R}_{1R} = X^{2L}_{1R}$$

which is exactly (2.19). Therefore, there is no non-p-attractor for the eigenvalue -1.

For the eigenvalue $\lambda = 1$, there is a five-dimensional subspace, for which the basis can be chosen in the form

$$\Xi^{\alpha}_{+1} = \begin{bmatrix} 1 & 0 & 0 \\ 0 & 1 & 0 \\ 0 & 0 & 1 \end{bmatrix}, \quad \Xi^{\beta}_{+1} = \begin{bmatrix} 1 & 0 & 0 \\ 0 & 0 & 1 \\ 0 & 1 & 0 \end{bmatrix}, \quad \Xi^{\gamma}_{+1} = \begin{bmatrix} -1 & 1 & 1 \\ 1 & 0 & 0 \\ 1 & 0 & 0 \end{bmatrix}, \tag{3.11}$$

$$\Xi^{\delta}_{+1} = \begin{bmatrix} 0 & 1 & -1 \\ -1 & 0 & -2 \\ 1 & 2 & 0 \end{bmatrix}, \quad \Xi^{\epsilon}_{+1} = \begin{bmatrix} 0 & 1 & -1 \\ -1 & 2 & 0 \\ 1 & 0 & -2 \end{bmatrix}.$$

An attractor block can be represented using five free parameters $\alpha, \beta, \gamma, \delta, \epsilon$ as

$$\Xi_{+1} = \begin{bmatrix} \alpha+\beta-\gamma & \gamma+\delta+\epsilon & \gamma-\delta-\epsilon \\ \gamma-\delta+\epsilon & \alpha+2\epsilon & \beta-2\delta \\ \gamma+\delta-\epsilon & \beta+2\delta & \alpha-2\epsilon \end{bmatrix}. \tag{3.12}$$

We now consider three vertices denoted only as 1, 2 and 3, where 1 and 2 are adjacent as well as 2 and 3. Here we only present the equalities used in the proof, also already expressed in the coefficients of the blocks

$$\begin{aligned}
X_{1R}^{1R} = X_{2L}^{2L} &\to +1\alpha_{11} - 2\epsilon_{11} = +1\alpha_{11} + 2\epsilon_{11}, \\
X_{2L}^{1R} = X_{1R}^{2L} &\to -1\beta_{12} - 2\delta_{12} = -1\beta_{12} + 2\delta_{12}, \\
X_{3L}^{2R} = X_{2R}^{3L} &\to +1\beta_{23} + 2\delta_{23} = +1\beta_{23} - 2\delta_{23}, \\
X_{1R}^{2N} = X_{2L}^{2N} &\to -2\gamma_{21} + 2\delta_{21} + 2\epsilon_{21} = -2\gamma_{21} - 2\delta_{21} - 2\epsilon_{21}, \\
X_{1R}^{3N} = X_{2L}^{3N} &\to +2\gamma_{31} - 2\delta_{31} - 2\epsilon_{31} = +2\gamma_{31} + 2\delta_{31} + 2\epsilon_{31}, \\
X_{1R}^{3R} = X_{2L}^{3R} &\to -1\alpha_{31} + 2\epsilon_{31} = -1\beta_{31} - 2\delta_{31}, \\
X_{1N}^{2R} = X_{1N}^{3L} &\to +2\gamma_{21} + 2\delta_{21} - 2\epsilon_{21} = +2\gamma_{21} - 2\delta_{21} + 2\epsilon_{21}, \\
X_{2N}^{2R} = X_{2N}^{3L} &\to -2\gamma_{22} - 2\delta_{22} + 2\epsilon_{22} = -2\gamma_{22} + 2\delta_{22} - 2\epsilon_{22}, \\
X_{1L}^{2R} = X_{1L}^{3L} &\to -1\beta_{21} - 2\delta_{21} = -1\alpha_{21} - 2\epsilon_{21}.
\end{aligned} \tag{3.13}$$

By summing all the equations in (3.13) we obtain

$$\alpha_{11} + \alpha_{22} - 2\epsilon_{11} - 2\epsilon_{22} = \beta_{21} + \beta_{32} - 2\delta_{21} - 2\delta_{32}. \tag{3.14}$$

The equality (3.14) implies that if (2.19) holds for the first pair of vertices, so in particular

$$X_{1R}^{1R} = X_{1R}^{2L} \to \alpha_{11} - 2\epsilon_{11} = \beta_{21} - 2\delta_{21},$$

it also holds for the other pair, so

$$\alpha_{22} - 2\epsilon_{22} = \beta_{32} - 2\delta_{32} \to X_{2R}^{2R} = X_{2R}^{3L}.$$

Due to the left-right symmetry and the transitional invariance the equality (2.19) holds for all directed edges. Therefore, as described above, the maximally mixed state is the only independent non-p-attractor for the eigenvalue $\lambda = 1$ and also for the whole lazy Grover quantum walk with the standard shift operator.

3.5 Reflecting Grover walk

3.5.1 Search for common eigenstates

Since the maximally mixed state is the only non-p-attractor, the knowledge of all the common eigenstates allows us to determine the asymptotic behavior of a percolated

reflecting Grover walk. We start with the coin condition (2.10), which in this case with $P_v = I$ is

$$G_3 \left|\phi_v\right\rangle = \alpha \left|\phi_v\right\rangle . \tag{3.15}$$

There are two eigenvalues 1 and -1.

We start with the eigenvalue 1, which has only one corresponding eigenvector of the form

$$\left|\phi_v^{+1}\right\rangle = \begin{bmatrix} 1 \\ 1 \\ 1 \end{bmatrix} . \tag{3.16}$$

This is trivially extended to a whole common eigenstate – it just has all the elements equal. Obviously, this state is not sr-trapped independently of the position of the sink.

The eigenvalue -1 has degeneracy 2 so the whole subspace orthogonal to (3.16) contains corresponding eigenvectors. The basis can be chosen for example as any pair from the following triplet of vectors

$$\left|\phi_v^{-1,1}\right\rangle = \begin{bmatrix} 1 \\ -1 \\ 0 \end{bmatrix} , \quad \left|\phi_v^{-1,2}\right\rangle = \begin{bmatrix} 0 \\ 1 \\ -1 \end{bmatrix} , \quad \left|\phi_v^{-1,3}\right\rangle = \begin{bmatrix} 1 \\ 0 \\ -1 \end{bmatrix} . \tag{3.17}$$

The degeneracy of the eigenvalue -1 allows for a very rich set of common eigenstates. As described in [38], we provide a very specific recipe how to construct a basis of the subspace of common eigenstates $\mathcal{H}_{(-1)}$ for any **planar** (this is a new requirement) simple 3-regularized graph and usually it is also easy to determine the subspace of sr-trapped states.

We use the following strategy: First, we determine the dimension of the subspace of common eigenstates. Second, we construct a set of linearly independent common eigenstates with the required number of elements, which is, therefore, a basis.

The whole Hilbert space $\mathcal{H}$ of the walk has dimension $\dim(\mathcal{H}) = 3\#V$. The subspace $\mathcal{H}_{(-1)}$ is extracted from $\mathcal{H}$ by $\#V$ coin conditions (the sum of vector elements in every vertex must be equal to zero to assure local orthogonality to the vector (3.16)) and $\#E$ shift conditions (vector elements on the same undirected edge must be the same (2.16)). Therefore, if all the conditions are independent, we have $\dim(\mathcal{H}_{(-1)}) = 2\#V - \#E$. It is proven in detail in an appendix of [38] that this set of conditions is dependent if and only if the underlying graph of the walk is actually 3-regular (there are no added unpaired loops) and it is bipartite. In that case, after removing one of the conditions the remaining set is independent. In short, the idea of the proof is the following: First we use all the shift conditions requiring equality of elements on the same undirected edge. Then we try to construct the coin condition in one vertex from the others. We start with the conditions for neighboring vertices and the shift condition forces us to include more and more terms with alternating signs to cancel out the unwanted elements in the linear combination. The elements corresponding to loops can not be canceled out and the whole process can be completed successfully

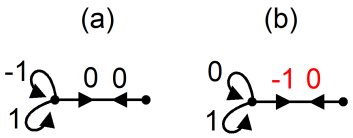

FIG. 3.5. Two possible situations after adding the fist block (3.17) in construction of a common eigenstate for the reflecting Grover percolated quantum walk: (a) the special case where we immediately obtain a common eigenstate and (b) the situation where the shift condition requires addition of another block since the red elements are not equal.

only for a bipartite graph – the coin condition of one partition of vertices is multiplied by $+1$ and the other by -1. Clearly, any missing condition also breaks the process even on a 3-regular bipartite graph.

As a result, we search for

$$N_1 = 2\#V - \#E + 1 \tag{3.18}$$

independent common eigenstates for walks on 3-regular bipartite graphs and

$$N_2 = 2\#V - \#E \tag{3.19}$$

in all other cases.

Importantly, we show below that the common eigenstates for the percolated reflecting Grover quantum walk are in most cases trapped states as described in section 2.3. Therefore, their presence allows the walker to avoid a sink introduced in the walk indefinitely and therefore reduce the asymptotic transport probability. We devote the whole next chapter, Chapter 4, to the investigation of the asymptotic transport by reflecting Grover walks on various examples of graphs. Here we construct the set of common eigenstates using a procedure, which allows all the common eigenstates to be on a small support.

The construction of common eigenstates uses the one-vertex blocks (3.17). Let us start with the zero vector and add one of these blocks in one vertex. It can be a special case that both the non-zero elements correspond to loops and we have a complete common eigenstate. This is illustrated in FIG. 3.5 (a) and an example of this situation are the border states in the lazy quantum walk as described in section 4.2. Nevertheless, in most cases the shift condition requires the addition of more blocks to neighboring vertices (with plus or minus signs) as shown in FIG. 3.5 (b).

After addition of each new block one of the three following situations can occur:

1. There is some vector element corresponding to a paired edge which is not equal to the other element in the pair. (Again as in FIG. 3.5 (b).) Another block must be added.

2. All vector elements corresponding to unpaired loops are zeros and all the shift conditions are satisfied. In this case we have actually constructed an even closed graph walk corresponding to a common eigenstate. The states illustrated in

FIG. 3.6 (a) and (b) are of this type. The correspondence between the common eigenstate and the graph walk can be summarized as follows: We start with all vector elements zeros. We go through the graph walk and alternate between adding $+1$ and -1 to the pairs of vector coefficients on the undirected edges in the walk.

3. All the shift conditions are satisfied and there are two unpaired loops with non-zero coefficients. An example of the resulting common eigenstate is in FIG. 3.6 (c). Alternatively, there can be just one unpaired loop with the coefficient $+2$ or -2 as in FIG. 3.6 (d). We have formed a capped graph walk (as introduced in appendix section A.1.5) on the mixed graph of the quantum walk. (Note that the even closed graph walks from the above case can also be thought of as being defined on the mixed graph.) Construction of the common eigenstate corresponding to a capped graph walk is analogous to the one for an even closed graph walk above. We only add the needed values $+1$ or -1 to the elements on the capping unpaired loops.

The above procedure can be applied on any 3-regularized graph, but now we restrict ourselves to planar graphs. First, we need the planarity to prove independence and second, we need the Euler's formula to prove completeness.

To build the basis, we use four types of common eigenstates illustrated in FIG. 3.6. The states in FIG. 3.6 (a) and (b) correspond to even closed graph walks and those in (c) and (d) to capped graph walks. We refer to those as A-type, B-type, C-type and D-type states respectively. An A-type state uses an even closed walk around one even-edged face of the graph. A B-type state also uses an even closed walk, but now it circumscribes two odd edged faces connected by a path, which is traversed twice. A C-type state is given by a simple capped graph walk connecting two distinct unpaired loops. Finally, a D-type state is also given by a capped graph walk, but beginning and ending by the same unpaired loop with usage of one odd-edged face. In general, we could also construct states where instead of going back through the same path, we could use different edges, but we do not need such states for the construction of the basis. Also, it is easily seen that for example a D-type like state with an even-edged face is just an A-type state, since the other elements cancel out during the second passage.

Now we construct a basis of the common eigenstates. The procedure differs for four possible situations depending on the graph of the quantum walk.

- **3-regular structure graph (no unpaired loops in the state graph):** We combine the Euler's formula (A.1)

$$\#V + \#F - \#E = 2$$

with an equality valid for all 3-regular structure graphs (every vertex has three edges and if we sum them over vertices, every edge is counted twice)

$$3\#V = 2\#E$$

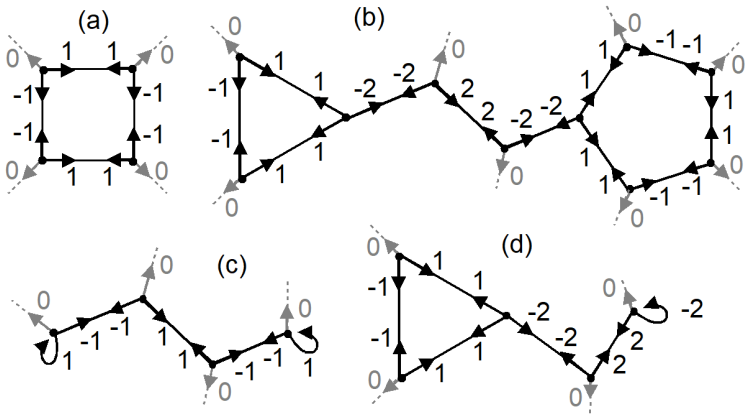

FIG. 3.6. Four types of common eigenstates for the eigenvalue -1 in the percolated reflecting Grover walk on simple planar 3-regularized graphs. These are further denoted as (a) A-type, (b) B-type, (c) C-type and (d) D-type states. The types differ by the corresponding type of graph walk: an even closed graph walk in (a) and (b) and a capped graph walk in (c) and (d) and by the number and the type of faces used (odd-edged or even-edged).

into the equality

$$2\#V - \#E = \#F - 2. \tag{3.20}$$

- **Graphs with only even-edged faces:** A planar graph with all faces even-edged is bipartite, and so we need $N_1 = 2\#V - \#E + 1 = \#F - 1$ common eigenstates as stated in (3.18). In this case we just use one A-type state for each face except one. Typically, we exclude the outer face. The number of states is correct. Their mutual independence is proven by the following contradiction: Let us try to obtain one of the A-type states corresponding to some face from the others. Coefficients of the linear combination for the neighboring faces are given immediately and this spreads on through the graph. Eventually, we reach the excluded face and the linear combination requires a non-zero coefficient for the corresponding state, which is not included in our set. (We have not ruled out the possibility that we encounter some inconsistency earlier, but this would only support the contradiction.)
- **Graphs with $\#F_e$ even-edged and $\#F_o > 0$ odd-edged faces:** For this case we first prove a known fact that the number $\#F_o$ is even. In fact we only need this, to be certain that there are more odd-edged faces than just one. For every number $i \geq 3$ we denote the number of faces with i edges as $\#F_i$. Then the following equality holds $\sum_{i=3}^{\infty} i\#F_i = 2\#E$, because every edge is shared by two faces so it is counted twice in the sum. For an even-edged face with $i = 2k$ the number $2k\#F_{2k}$ is always even. Therefore, the number of odd-edged faces $\#F_o = \sum_{k=1}^{\infty} \#F_{2k+1}$ must be even to make the left hand side even.

  Now we can just construct $\#F_e - 1$ A-type states (with the omitted face chosen arbitrarily) and $\#F_o - 1$ B-type states by connecting one fixed

odd-edged face to all the others with arbitrary connecting paths. This gives us exactly $\#F_e - 1 + \#F_o - 1 = \#F - 2 = 2\#V - \#E = N_2$ common eigenstates as required by (3.19). The independence is proven absolutely analogously as for the previous case.

- **3-regularized graphs with $\#L$ unpaired loops:** For this case there is a similar condition as in the graphs without loops. It comes from the fact that every vertex is connected to three edges in the mixed graph and by summing all these connections the undirected edges are counted twice and the unpaired loops once, so

$$3\#V = 2\#E + \#L.$$

In combination with Euler's formula, which still holds for the structure graph of the walk, the above equality results in

$$2\#V - \#E = \#F + \#L - 2.$$

  - **Graphs with only even-edged faces:** Due to the presence of unpaired loops, we still only search for $N_2 = 2\#V - \#E = \#F - 1 + \#L - 1$ common eigenstates. We again use $\#F - 1$ A-type states and add $\#L - 1$ C-type states by connecting one chosen and fixed loop to all the others with arbitrary connecting paths. The independence of the A-type states was proven above and the C-type states are independent because each of them has non-zero element on an unpaired loop, where all the other states have a zero element.
  - **Graphs with $\#F_e$ even-edged and $\#F_o > 0$ odd-edged faces:** We again need $N_2 = 2\#V - \#E = \#F + \#L - 2 = \#F_e - 1 + \#F_o - 1 + \#L$ common eigenstates. We use $\#F_e - 1$ A-type states and $\#F_o - 1$ B-type states as for graphs without unpaired loops. Then we add $\#L$ D-type states where every loop is connected to some odd-edged face by an arbitrary connecting path. The independence for A-type and B-type states follows from the very same argument as in graphs without unpaired loops and the independence for D-type states from the same observation as for C-type states above.

Let us note that analogous states as depicted in FIG. 3.6 resulting from even closed graph walks or capped graph walks are common eigenstates also for walks on non-planar graphs. The problem there is that there are no faces defined and we cannot use the Euler's formula. Therefore, we can not in general provide a construction of a complete and independent set – a basis.

3.5.2 Eigenstates of non-percolated quantum walks

As the common eigenstates are common for all the evolution operators corresponding to different configurations of a percolation graph, these are also eigenstates of

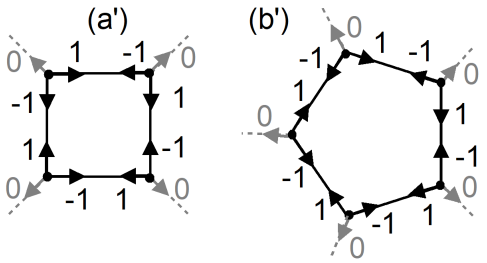

FIG. 3.7. Two types of of additional eigenstates for the eigenvalue -1 in the non-percolated reflecting Grover walk on simple planar graphs. These are further denoted as (a') A'-type and (b') B'-type states. These states are derived from A-type and B-type states in FIG. 3.6 and can be defined on faces with arbitrary number of edges.

the non-percolated walk governed by the evolution operator for all edges open. Nevertheless, the asymptotic dynamics of non-percolated walks can be much richer with a variety of other eigenstates. Without percolation, the entire unitary evolution is only restricted by the presence of the sink.

From the knowledge of common eigenstates of the percolated reflecting Grover walk we are able to determine some of the additional trapped eigenstates of the non-percolated version. In particular, we introduce A'-type and B'-type states usable on general graphs demonstrated in FIG. 3.7. They are similar to A-type and B-type states but the elements for a pair of directed edges on every undirected edge have opposite signs and the B'-type states only use one face each. The A'-type and B'-type states are excluded in percolated walks by the shift condition. Note, that due to the loops, similar states obtained by modification of C-type and D-type states are not eigenstates of the non-percolated walk.

In some cases (for example for the ladder graph as described in section 4.3) the A'-type and B'-type states are the only additional sr-trapped eigenstates in the non-percolated walk. (In such case all the other eigenstates overlap with the sink subspace.) On the other hand, in many situations there are other sr-trapped states, for which we do not have any general recipe.

3.6 Cyclic Grover walks

Similarly to the reflecting Grover walks, it was proven in [38] that the Grover walk with combinations of cyclic local permutations have no non-p-attractors other than the maximally mixed state. Therefore, we just need to identify the common eigenstates to determine the asymptotic behavior.

3.6.1 Search for common eigenstates

We again start with the coin condition (2.10), which for the cyclic walks has two possible forms depending on the direction of the rotation $P_v = P^{CW}$ or $P_v = P^{CCW}$

in the given vertex

$$G_3 P_v^{CW} |\phi_v\rangle = \alpha |\phi_v\rangle , \tag{3.21}$$
$$G_3 P_v^{CCW} |\phi_v\rangle = \alpha |\phi_v\rangle .$$

The matrices for P^{CW} and P^{CCW} are just a (conjugate) transpose of each other and so $G_3 P^{CW}$ and $G_3 P^{CCW}$ have the same spectrum and the same eigenvectors just corresponding to the conjugate eigenvalues. There are three distinct eigenvalues $\alpha_1 = 1, \alpha_2 = \mathrm{e}^{i\pi/3}$ and $\alpha_3 = \mathrm{e}^{-i\pi/3}$.

For the eigenvalue $\alpha_1 = 1$ there is again just the state (3.16), which is extended by the shift condition to the common eigenstate with all elements equal.

The eigenvectors for the two remaining eigenvalues $\alpha_2 = \mathrm{e}^{i\pi/3}$ and $\alpha_3 = \mathrm{e}^{-i\pi/3}$ can be described using three elements, which we denote by letters $r = 1$, $g = \mathrm{e}^{i\frac{2\pi}{3}}$, $b = \mathrm{e}^{-i\frac{2\pi}{3}}$. The letters stand for red, green and blue, the colors which are used to represent these values in figures below.

For $\alpha_2 = \mathrm{e}^{i\pi/3}$ in an eigenvector for P^{CW} the values are organized as

$$|\phi_v^{\alpha_2,CW}\rangle = \begin{bmatrix} r \\ g \\ b \end{bmatrix} = g \begin{bmatrix} b \\ r \\ g \end{bmatrix} = b \begin{bmatrix} g \\ b \\ r \end{bmatrix} \tag{3.22}$$

and for P^{CCW} as

$$|\phi_v^{\alpha_2,CCW}\rangle = \begin{bmatrix} r \\ b \\ g \end{bmatrix} = b \begin{bmatrix} g \\ r \\ b \end{bmatrix} = g \begin{bmatrix} b \\ g \\ r \end{bmatrix} , \tag{3.23}$$

when the base states (3.1) are ordered in the clock-wise order. For $\alpha_3 = \mathrm{e}^{-i\pi/3}$ the eigenvectors just swap their roles so

$$|\phi_v^{\alpha_3,CW}\rangle = |\phi_v^{\alpha_2,CCW}\rangle , \tag{3.24}$$
$$|\phi_v^{\alpha_3,CCW}\rangle = |\phi_v^{\alpha_2,CW}\rangle . \tag{3.25}$$

Therefore, by complex conjugation we can switch between eigenvectors for P^{CW} and for P^{CCW} or between eigenvectors corresponding to α_2 and corresponding to α_3.

When illustrated on the graphs, we can describe the eigenstates so that for the eigenvalue α_2 the values r, g, b must be in clock-wise order at vertices with P^{CW} local permutation and in counter-clock-wise order at vertices with P^{CCW}. Analogously, for α_3 the values r, g, b must be in counter-clock-wise order at vertices with P^{CW} local permutation and in clock-wise order at vertices with P^{CCW}. This specification is sufficient for the construction of common eigenstates.

Note that there can not be any zero elements in the common eigenstates so none of the common eigenstates can be trapped. Therefore, we do not study transport by quantum walks with cyclic local permutations as it is always 100 %. Instead, we are interested in the presence of non-trivial asymptotic behavior.

The common eigenstate for the eigenvalues $\alpha_1 = 1$ is present for walks on all graphs and for all distributions of cyclic local permutations. A walk having only one p-attractor resulting from this common eigenstate and the maximally mixed state attractor has trivial asymptotic dynamics described by the equation (2.1) – there is no change of the state in the asymptotic regime. In contrast, there is nontrivial evolution in the form of asymptotic cycles over three time steps if the other p-attractors resulting from common eigenstates corresponding to α_2 and α_3 are present. These are not present for all distributions of rotations among vertices. If they are, we say that the quantum walk is *asymptotically non-trivial*. Note also that by complex conjugation (i.e. by swapping colors green and blue) of a common eigenstate for α_2 we obtain a common eigenstate for α_3 and vice versa. This is seen from the form of one-vertex blocks (3.22) and (3.23) and from the fact, that by swapping colors the shift condition can not be violated. Therefore, we always either have both non-trivial common eigenstates or none.

If the structure graph and the distribution of cyclic permutations is given, it is simple to check for the existence of non-trivial common eigenstates and actually to construct them in the process. We just start at some arbitrary vertex and color edges of the mixed graph in accordance with the combination of the direction of rotation in this vertex and the chosen eigenvalue α_2 or α_3, for which we want to construct the common eigenstate. This fixes coloring in the neighboring vertices. We simply go through vertices and we either color the whole mixed graph of the walk and obtain the common eigenstate or we encounter a conflict (two edges of the same color in one vertex or wrong ordering of colors in a vertex enforced by the neighboring vertices) and the common eigenstate does not exist.

Let us have a look at some simple examples. It is demonstrated in FIG. 3.8 that both the cyclic and the transporting shift operators presented above in FIG.3.2 and FIG. 3.3 give a valid edge-3-coloring and so the corresponding quantum walks have non-trivial asymptotic evolution. For comparison similar operators on the cube graph are shown in FIG. 3.9. While the shift operator distributing P^{CW} and P^{CCW} according to the bipartition of the cube graph (the transporting shift operator) leads to non-trivial dynamics, the cyclic operator with P^{CW} in all vertices results in asymptotically trivial evolution.

The above ideas are agregated in the interesting result presented in [38]: A percolated Grover quantum walk with cyclic local permutations is asymptotically non-trivial if and only if its structure graph is edge-3-colorable. The association between the common eigenstates and an edge-coloring of the structure graph is the following: If we have a common eigenstate corresponding to α_2 or α_3 for some distribution of cyclic permutations, we can simply color the edges of the structure graph by colors given by the vector elements on the edges. (The elements for the two directed edges associated with one undirected edge are the same due to the shift condition.) Reversely, if we have an edge-3-coloring of the structure graph, we embed the graph into a plane, place a P^{CW} rotation into vertices where the colors red, green and blue are in clock-wise order and P^{CCW} into others. The state with elements given by colors of the edge-3-coloring is a common eigenstate for a walk with this distribution of local permutations corresponding to the eigenvalue α_2. (If there is an unpaired

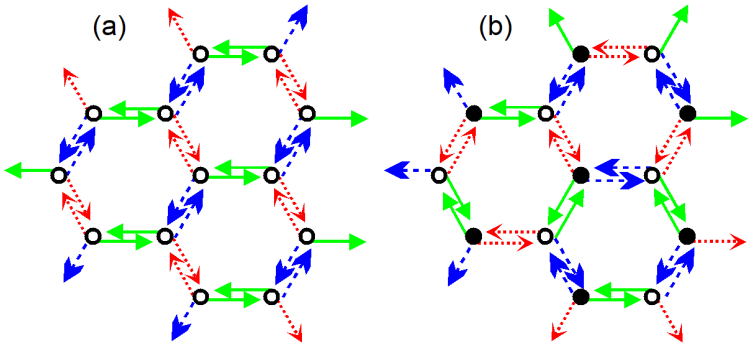

FIG. 3.8. Coloring of parts of the honeycomb lattice for (a): cyclic shift operator with P^{CW} in all vertices from FIG. 3.2 and (b) the transporting shift operator from FIG. 3.3. (For the coloring, it is not relevant whether on the border there are loops or edges leading to other vertices.) Colors of edges are also indicated by line types: red dotted, blue dashed, green solid. For illustration, the directed edges of the state graph are colored in this figure, from which the coloring of the mixed graph is obvious. White vertices represent P^{CW} and black vertices P^{CCW} local rotation. Both of these shift operators imply a valid edge-3-coloring of the structure graph and so lead to non-trivial asymptotic dynamics.

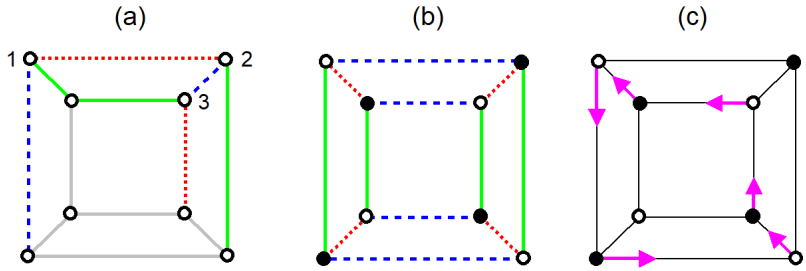

FIG. 3.9. Coloring of graphs for (a): cyclic shift operator with P^{CW} in all vertices and (b) a shift operator with P^{CW} in the white vertices and P^{CCW} in the black vertices. Colors of edges are also indicated by line types: red dotted, blue dashed, green solid. In (a) there is a conflict showing that this configuration of cyclic permutations does not lead to non-trivial asymptotic evolution. Three vertices are labeled by a number representing the order in which they are used for coloring. In contrast, the distribution in (b) gives a valid edge-3-coloring of the graph and so non-trivial common eigenstates. Further, in (c) the action of the shift operator from (b) is indicated. There are three more similar cycles in the whole shift operator.

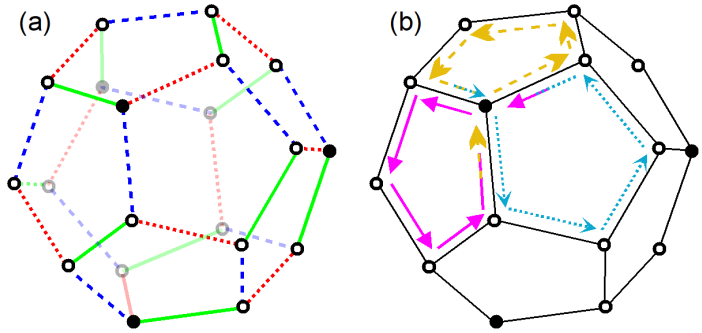

FIG. 3.10. Non-triviality of a walk on the dodecahedron: (a) an edge-3-coloring of a dodecahedron graph and (b) the action of the shift operator corresponding to the distribution of P^{CW} and P^{CCW} local permutations given by the coloring. Colors of edges are also indicated by line types: red dotted, blue dashed, green solid. White vertices represent P^{CW} and black vertices P^{CCW} local rotation, where the direction is given by embedding the graph on a sphere. There are three more cycles similar to the one shown in (b) in the whole shift operator.

loop in a vertex, we just give it the remaining value and if there are two unpaired loops, we can assign the two elements arbitrarily.) The same state is a common eigenstate for a walk with all the P^{CW} and P^{CCW} rotations interchanged, just for the eigenvalue α_3 or a common eigenstate for α_3 is obtained simply by a complex conjugation of the one for α_2.

Another example of an edge-3-colorable graph is the one of a dodecahedron. The edge-3-coloring is shown in FIG. 3.10 (a). This coloring induces a distribution of local rotations at vertices, which in turn results in non-trivial asymptotic evolution of the walk. This walk has a rather special shift operator, the action of which is illustrated in FIG. 3.10 (b). Here the formalism of local permutations is very helpful as this complex shift operator is simply described by a distribution of P^{CW} and P^{CCW}.

Finally, let us have a look at graphs of carbon nanotubes introduced in appendix section A.2.5. These graphs can be obtained by folding sheets of the honeycomb lattice and so their properties with respect to the non-triviality of the asymptotic evolution are derived from those presented in FIG. 3.8 with some additional effects at junctions.

We investigate $(n, 0)$ zig-zag and (n, n) armchair nanotubes. For both of these cases the cyclic shift operator (with the same orientation of rotations in all vertices) results in an asymptotically non-trivial walk regardless of the choice of the chirality. This is seen from the fact that with the coloring shown in FIG. 3.8 (a) in all cases we join (identify) edges of the same color when folding the lattice into a tube.

The situation is more complicated in the case of the transporting shift operator with coloring shown in FIG. 3.8 (b). In (n, n) armchair tubes there are also no conflicts in the coloring. This is exemplified in FIG. 3.11 (a). In contrast, for $(n, 0)$ zig-zag tubes it depends on the value of n. Only if the n is a multiple of three we are joining edges of the same color when forming the tube. In other cases there is a conflict in the

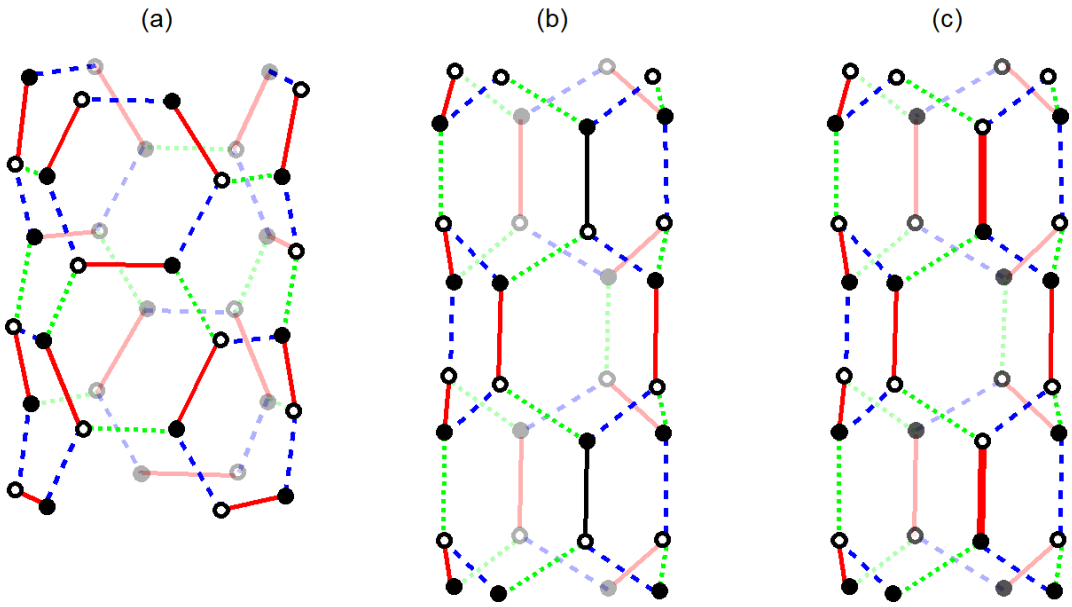

FIG. 3.11. Non-triviality of walks on the nanotubes: (a) an edge-3-coloring of a $(3,3)$ nanotube graph, (b) the problem with coloring of the $(4,0)$ tube where the blue and red edges at the junction do not correspond with the chosen direction of rotation at vertices and (c) correction of the problem by changing directions of rotation at vertices at the junction. Colors of edges are also indicated by line types: red dotted, blue dashed, green solid. White vertices represent P^{CW} and black vertices P^{CCW} local rotation, where the direction is given by embedding the graph on a torus.

coloring as shown in FIG. 3.11 (b) and the resulting walk is asymptotically trivial. Nevertheless, a small modification of the shift operator can correct the coloring as illustrated in FIG. 3.11 (c).

3.7 Lazy Grover walk (swapping local permutation)

Here we study Grover quantum walks with the swapping shift operator used in the lazy walk graph presented in appendix section A.2.1. For this case we have checked that the only non-p-attractor is the maximally mixed state, see section 3.4.2.

We start the search for the common eigenstates (and so the p-attractors) with the coin condition (2.10). We remind the reader of the choice of the ordering of states in every vertex as N, L, R, so the coin condition incorporates the local permutation P_v^{23} in the form (3.2) and requires

$$G_3 P_v^{23} |\psi_v\rangle = \alpha |\psi_v\rangle . \tag{3.26}$$

The spectrum contains only the values $+1$ and -1 as in the reflecting walk, but here the degenerate eigenvalue is $+1$. For the eigenvalue -1 there is only one eigenvector

$$|\psi_v^{-1}\rangle = \begin{bmatrix} -2 \\ 1 \\ 1 \end{bmatrix} . \tag{3.27}$$

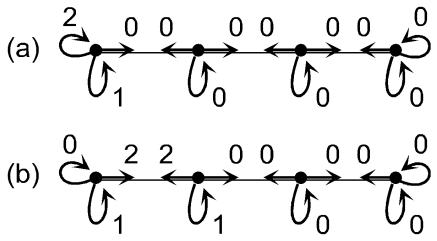

FIG. 3.12. Examples of common eigenstates corresponding to the eigenvalue +1 for the percolated Grover lazy quantum walk with the standard shift operator: (a) a border state with just two non-zero elements and (b) an inner state with four non-zero elements. The states are not normalized nor mutually orthogonal. The state in (a) is further denoted as $|t_0\rangle$. The state in (b) is denoted as $|t_1\rangle$ and the other inner states as $|t_i\rangle$ with the index i increasing from the left to the right.

The shift condition requires the resulting common eigenstate to have the same element for all the $|L\rangle$ and $|R\rangle$ states and the element doubled in magnitude with the opposite sign in all the $|N\rangle$ states. Therefore, this common eigenstate is not trapped. On the other hand, this state induces non-trivial asymptotic dynamics in a walk without a sink.

For the eigenvalue +1 the basis of the eigen-subspace can be chosen as

$$|\psi_v^{+1,I}\rangle = \begin{bmatrix} 1 \\ 0 \\ 2 \end{bmatrix}, \quad |\psi_v^{+1,II}\rangle = \begin{bmatrix} 1 \\ 2 \\ 0 \end{bmatrix}. \tag{3.28}$$

In other form, the coin condition requires

$$2\psi_{v,N} = \psi_{v,L} + \psi_{v,R}$$

for all vertices $v \in V$. The set of coin conditions and shift conditions is clearly independent - every element of a paired edge only appears in one shift condition and every element on an unpaired loop only appears in one coin condition. Therefore, we can not compose any of the conditions from the others. As a result, we search for

$$M = 2\#V - \#E = \#V + 1 \tag{3.29}$$

independent common eigenstates, where we have used the fact that $\#E = \#V - 1$ for the lazy walk graph. It is easy to construct this basis. There are two border states shown in FIG. 3.12 (a) and $\#E = \#V - 1$ inner states shown in FIG. 3.12 (b). (Only the inner states are presented in [56], since the PCQW on a closed ring is investigated therein.) These states are trapped and if the sink is placed in one end-vertex, most of them are also sr-trapped. A complication is that to calculate the asymptotic transport probability these states need to be orthonormalized. We address the orthogonalization later.

The asymptotic transport probability for the percolated quantum walk can be calculated from the overlap of the orthonormalized sr-trapped common eigenstates with

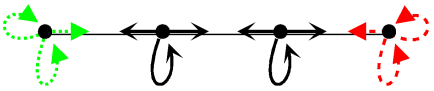

FIG. 3.13. Depiction of the initial subspace with green dotted arrows and the sink subspace with red dashed arrows for lazy quantum walks.

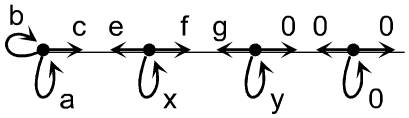

FIG. 3.14. The notation for the description of orthogonalized sr-trapped states $|t'_i\rangle$ for the lazy PCQW. For the state $|t'_i\rangle$ we denote the coefficient for the $|N\rangle$ state in the right-most vertex as y_i and the coefficient for the $|N\rangle$ state in the vertex to the left as x_i. For $|t'_0\rangle$ we define $x_0 = 0$.

the initial state of the walk. Due to linearity, we can also obtain the average transport probability if we take the maximally mixed sate on the initial subspace as the initial state.

For the study of transport we have to choose the initial position of the walker and the position of the sink. We naturally initiate the walker in one of the end vertices (e.g. in the left one) and place the sink to the other end vertex. Therefore, the initial and sink subspaces correspond to the two vertex subspaces as indicated in FIG. 3.13.

To calculate the ATP for the percolated quantum walk, we first need to identify the set of sr-trapped states. It is simple since the right border state is the only one overlapping with the R state in the sink vertex. We remove this trapped state and then the right-most inner trapped state is the only one overlapping with the $|N\rangle$ state in the sink vertex. We also remove this one and now none of the remaining trapped states overlaps with the sink subspace and so all these are sr-trapped.

To obtain the ATP it is possible to use a brute-force numerical orthonormalization of the sr-trapped states and then calculate their overlap with the initial state. Nevertheless, in this case we can use the translational invariance of the walk to obtain the average ATP directly from a recursive relation.

We start with the left border trapped state in FIG. 3.12 (a) and denote it as $|t_0\rangle \equiv |t'_0\rangle$. (We use lower-case letters for non-normalized states with integer coefficients and upper-case letters for normalized versions. Also, with a prime we denote the states from the orthogonalized set.) The other states are constructed in a systematic manner. For this we use the following notation for two particular elements of the states $|t'_i\rangle$ as x_i and y_i as described in FIG. 3.14 and also we denote the sum of squares of all the elements of $|t'_i\rangle$ as N_i^2, so N_i is the normalization constant of the state: $|T'_i\rangle = 1/N_i\,|t'_i\rangle$.

Next we construct $|t'_{i+1}\rangle$:

1. We start with $|t'_i\rangle$ and just add a particular multiple of the state $|t_{i+1}\rangle$ shown in FIG. 3.12 (b). With the notation introduced in FIG. 3.14 that is in particular $|t'_{i+1}\rangle = |t'_i\rangle + y_{i+1}\,|t_{i+1}\rangle$, where the value of y_{i+1} needs to be determined.

2. The state $|t'_{i+1}\rangle$ is automatically orthogonal to all the states $|t'_j\rangle$ for $j < i$ as it does not differ from $|t'_i\rangle$ on supports of the states $|t'_j\rangle$. We just need to ensure $\langle t'_i|t'_{i+1}\rangle = 0$ and that is

$$0 = \langle t'_i|t'_{i+1}\rangle = N_i^2 - y_i^2 + y_i x_{i+1}.$$

Here we used the fact that all the elements of the state $|t'_i\rangle$ are the same in $|t'_{i+1}\rangle$ except the element y_i.

3. The requirement of orthogonality is satisfied if we set

$$x_{i+1} = \frac{N_i^2 - y_i^2}{-y_i}.$$

4. Then from our linear combination and from the form of the state $|t_{i+1}\rangle$ we just have $x_{i+1} = y_i + y_{i+1}$, so

$$y_{i+1} = x_{i+1} - y_i.$$

5. The coefficients for arcs connecting vertices with loops corresponding to x_{i+1} and y_{i+1} (denoted as f and g in FIG. 3.14) have values $2y_{i+1}$.

6. Finally, using the form of the state $|t_i\rangle$ we calculate the new normalization constant as

$$N_{i+1}^2 = N_i^2 - y_i^2 + x_{i+1}^2 + (2 \cdot 2^2 + 1)y_{i+1}^2.$$

7. Examples of the constructed orthogonalized states are in FIG. 3.15.

8. Using these recursive relations initialized by the state $|t'_0\rangle$ as $x_0 = 0$, $y_0 = 1$ and $N_0^2 = 5$ we can calculate x_i, y_i and N_i^2 for arbitrary i and also the average (for maximally mixed initial state) trapping contribution from the given orthonormalized state for $i > 0$ as

$$p_i = \mathrm{Tr}(\rho_{mm} |T'_i\rangle \langle T'_i|) = \frac{1}{3}\frac{1}{N_i^2}\mathrm{Tr}(P_{v_0} |t'_i\rangle \langle t'_i|) = \frac{1}{3}\frac{1}{N_i^2}(4 + 16 + 100) = \frac{40}{N_i^2},$$

where ρ_{mm} is the maximally mixed initial state and P_{v_0} is the projector to the initial subspace in the vertex v_0. For $i = 0$ the contribution to trapping from the state $|T'_0\rangle$ is $p_0 = 1/3$. (This is trivially the overlap of any pure state localized in the 3-dimensional initial subspace with the maximally mixed state on this subspace.)

The results for the lazy walk chain of length up to 30 are shown in FIG. 3.16. For comparison the ATP for the non-percolated walk is also included. (It can be obtained by calculation of a sufficient power of the evolution operator (1.15), here $t = 2^{30}$, and applying it to the initial state.)

In FIG. 3.16 we see that the ATP is the same for PCQW and CQW. This means that there are no additional sr-trapped states in the non-percolated walk. (We checked

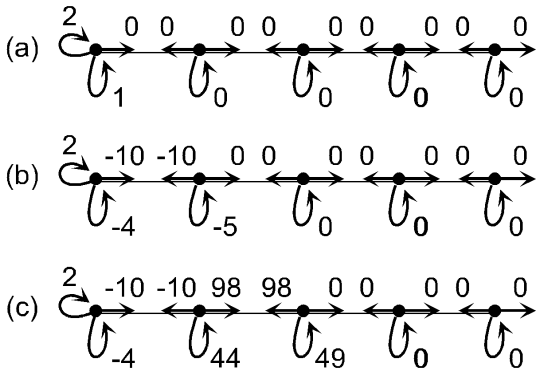

FIG. 3.15. The first three orthogonalized sr-trapped states for the lazy PCQW: (a) the state $|t_0\rangle = |t'_0\rangle$, (b) the state $|t'_1\rangle$ and (c) the state $|t'_2\rangle$.

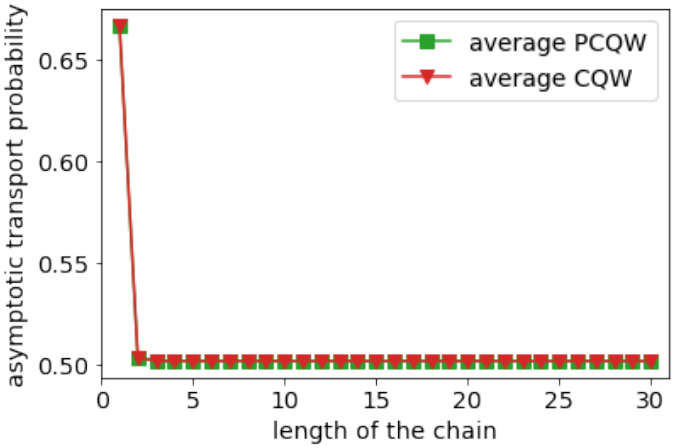

FIG. 3.16. The average ATP for the lazy walk chain of length up to 30 for percolated (PCQW) and non-percolated (CQW) Grover quantum walks. (The values for PCQW and CQW coincide for all lengths.) The result for CQW is obtained numerically with 2^{30} steps.

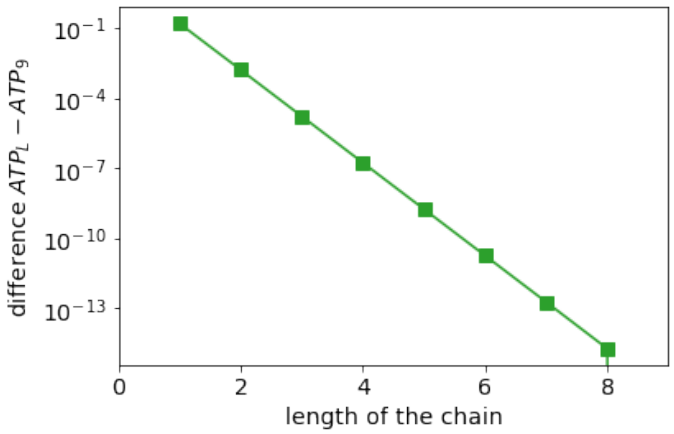

FIG. 3.17. The average ATP of the percolated lazy Grover quantum walk on a chain of length up to 8 plotted as the difference from q_9 on a semi-log scale.

this numerically up to the length 30.) Further, FIG. 3.17 demonstrates that the contribution from trapped states for longer chains drops exponentially with length. Therefore, the difference becomes negligible very fast. In fact, for $L > 10$ the difference in ATP in different lengths is below the precision of our calculation, which is about 10^{-15}.

When considering the asymptotic transport for particular pure initial states, the whole range of possible ATP can be achieved for the lazy walks: the initial state with (3.27) in the initial vertex is orthogonal to all the trapped states and therefore results in 100% ATP. In contrast, the trapped state $|t_0'\rangle$ as shown in FIG. 3.12 (a) is localized in the initial vertex and the walk initiated in this state has zero ATP.

Chapter 4

Reflecting Grover QW asymptotic transport on examples of 3-regularized graphs

In this chapter we use the results obtained in section 3.5 to study quantum transport by reflecting Grover quantum walks on various graphs presented in appendix section A.2. The majority of these results were published in restricted versions in [48] and [49].

For all graphs we take the same approach:

- Using the recipe from section 3.5 we determine the set of all trapped states (common eigenstates) for the percolated version of the walk in dependence on the structure parameters of a particular graph.
- We choose the initial position and the position of the sink, or precisely we choose the initial subspace and the sink subspace from the Hilbert space. (None of the two is required to always cover whole vertex subspaces.) We place the initial site and the sink to natural positions of the graph (e.g. investigating transport from one end of a nanotube to the other) but also take into account the known set of trapped states, which allows us to determine the interesting cases. Therefore, in some cases we study multiple initial/sink position variants.
- We identify the set of sr-trapped states for the particular placements of the sink subspace.
- We calculate the asymptotic transport probability in dependence of a particular initial state localized in the initial subspace. In all cases we look at the average transport (2.27) (ATP averaged over all admissible initial states). Further, we also investigate transport for pure initial states with some distinct properties, i.e. maximizing/minimizing the ATP or e.g. maximizing the difference in the ATP over the range of a structure parameter of the graph.
- We use the results and insights obtained for percolated walks to investigate the non-percolated versions. Apart from the common eigenstates of the percolated

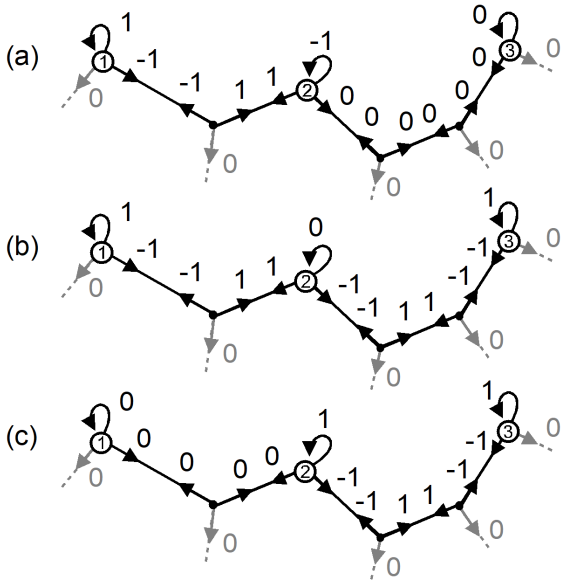

FIG. 4.1. Illustration of the different choices of the C-type states: (a) the state $|t_{12}\rangle$, (b) the state $|t_{13}\rangle$ and (c) their combination $|t_{23}\rangle = |t_{13}\rangle - |t_{12}\rangle$.

walk we are able to construct some other trapped eigenstates and actually for example in the case of the ladder these turn out to be all the trapped states present in the non-percolated walk. Further, we calculate the ATP in non-percolated walks numerically for the initial states identified in the percolated version. (Exploration of the transport for a set of initial states representatively covering the initial subspace is the main challenge for the numerical approach.)

4.1 Different bases of C-type states

If the state graph under investigation contains loops and all the faces are even-edged the recipe in section 3.5 instructs to construct C-type trapped states (see FIG. 3.6) by connecting one fixed loop to all the other loops. The advantage of this approach is that it is general and independent of the graph in question (as long as the assumptions of planarity and connectedness hold). In many situations, nevertheless, different choices of the basis for the subspace of C-type states are advantageous. In particular, it is usually easier to work with C-type states connecting near loops in the graph.

Suppose we have three loops l_1, l_2, l_3 and two C-type states: $|t_{12}\rangle$ corresponding to a path between l_1 and l_2 and $|t_{13}\rangle$ corresponding to a path between l_1 and l_3, where $|t_{13}\rangle$ goes along the same path as $|t_{12}\rangle$ all the way to the vertex with l_2. If we choose both states to have the same sign of the element corresponding to l_1, the state $|t_{23}\rangle = |t_{13}\rangle - |t_{12}\rangle$ is just a C-type state connecting the loops l_2 and l_3. This is illustrated in FIG. 4.1. The idea is to use $|t_{12}\rangle$ and $|t_{23}\rangle$ instead of $|t_{12}\rangle$ and $|t_{13}\rangle$. The new states are clearly independent and since their number is the same we obtain a new basis.

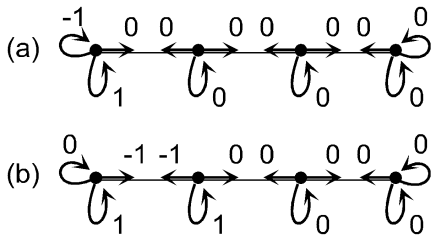

FIG. 4.2. Examples of C-type common eigenstates for the percolated reflecting Grover lazy quantum walk corresponding to the eigenvalue -1: (a) a border state with just two non-zero elements and (b) an inner state with four non-zero elements. The states are not normalized nor mutually orthogonal.

4.2 Lazy walk

We already investigated transport in the lazy Grover quantum walk with the standard shift operator (keeping the direction of the walker's movement) in section 3.7. Here we look at the quantum walk on the lazy walk graph (line with additional loops) described in section A.2.1 with the reflecting shift operator.

Since the lazy walk graph has many loops and has no faces, the trapped states for the reflecting lazy walk are very similar to those for the standard one and also their number is the same. Due to the absence of faces, we only use C-type states from FIG. 3.6. We apply the approach from section 4.1 where we connect the closest loops and the states only overlap on loops as seen in FIG. 4.2.

The structure graph is not 3-regular, so the dimension of the subspace of trapped states is given by (3.19) and it is

$$N_2 = 2\#V - \#E = \#V + 1 \tag{4.1}$$

as for the standard shift lazy walk. There are again two border states localized at the border vertices with an example shown in FIG. 4.2 (a) and $\#E = \#V - 1$ inner states exemplified in FIG. 4.2 (b).

Naturally, we place the initial state to one border vertex and the sink to the other as indicated in FIG. 3.13. Then one of the border states and one of the inner states overlap with the sink and we are left with $\#V - 1$ sr-trapped states.

To be useful for calculations, the basis of sr-trapped states has to be orthonormalized. We can do this numerically, but actually it is possible to reuse the procedure from section 3.7 for the lazy walk with the standard shift operator with just a slight modification. At the point 5 of the process, the elements on the arcs between the new vertex with non-zero elements and its left neighbor have values $-y_{i+1}$ instead of $2y_{i+1}$ and the normalization constant is modified accordingly as

$$N_{i+1}^2 = N_i^2 - y_i^2 + x_{i+1}^2 + 3y_{i+1}^2.$$

Examples of the constructed orthogonalized states are in FIG. 4.3.

Again, using the recursive relations, now initialized by the state $|t_0'\rangle$ as $x_0 = 0$, $y_0 = 1$ and $N_0^2 = 2$ we can calculate x_i, y_i and N_i^2 for arbitrary i and the contribution from

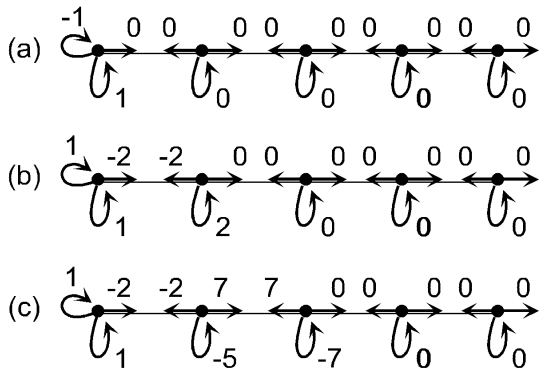

FIG. 4.3. The first three orthogonalized sr-trapped states for the reflecting Grover lazy PCQW: (a) the state $|t_0\rangle = |t'_0\rangle$, (b) the state $|t'_1\rangle$ and (c) the state $|t'_2\rangle$.

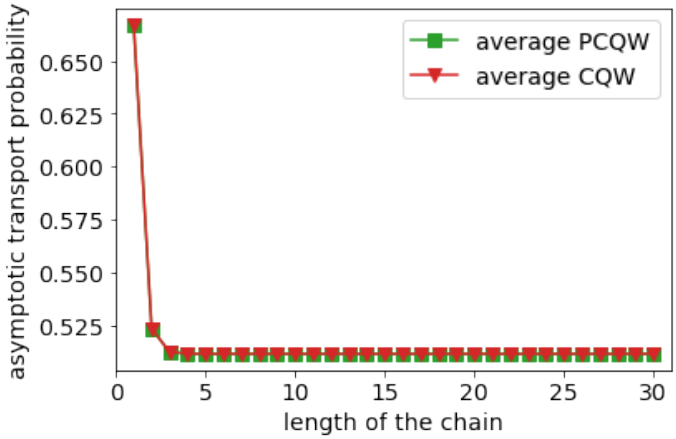

FIG. 4.4. The average ATP for the lazy walk chain of length up to 30 for Grover lazy percolated (PCQW, green squares) and non-percolated (CQW, red triangles) quantum walks. (The values for PCQW and CQW coincide for all lengths.) The result for CQW is obtained numerically with 2^{30} steps.

the given orthonormalized state for $i > 0$ to the average trapping is

$$p_i = \mathrm{Tr}(\rho_{mm} |T'_i\rangle \langle T'_i|) = \frac{1}{3}\frac{1}{N_i^2}\mathrm{Tr}(P_{v_0} |t'_i\rangle \langle t'_i|) = \frac{1}{3}\frac{1}{N_i^2}(1+1+4) = \frac{2}{N_i^2},$$

where ρ_{mm} is the maximally mixed initial state and P_{v_0} is the projector to the initial subspace in the vertex v_0. For $i = 0$ the contribution to trapping from the state $|T'_0\rangle$ is again trivially $p_0 = 1/3$.

The result for the lazy walk chain of length up to 30 is shown in FIG. 4.4. For comparison, the ATP for the non-percolated walk is also included. Again, there is no contribution from any additional trapped states in the non-percolated walk. Also, the contribution from new trapped states for longer chains in PCQW drops exponentially. In fact the FIG. 4.4 looks almost the same as FIG. 3.16 and so we present a comparison of the ATP for the two lazy walks with different shift operators in FIG. 4.5.

Finally, also with the reflecting shift operator, pure initial states can be found re-

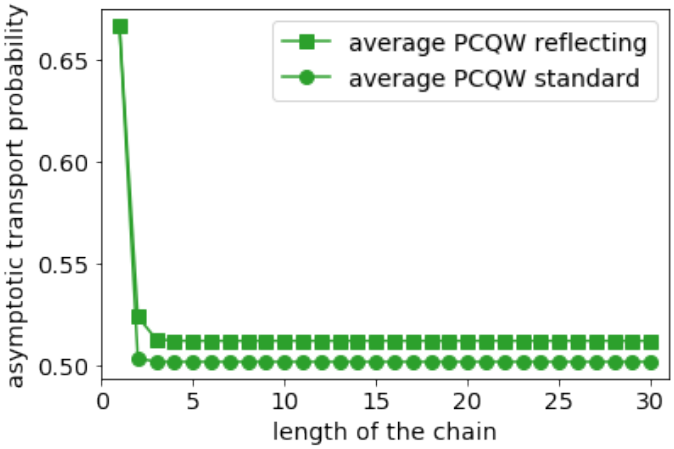

FIG. 4.5. Comparison of the average ATP for the lazy walk chain of length up to 30 for the reflecting Grover lazy PCQW for the two variants of the shift operator: reflecting (green squares) and standard (green circles).

sulting in the whole range of the ATP from 0 % (initial state $|t_0\rangle$) to 100 % (initial state with all three elements the same).

4.3 Walk on a ladder graph

The ladder graph presented in appendix section A.2.2 is in a certain sense an extension of the line graph. It is also a simple structure linearly growing in one direction only determined by its length L. For the ease of the notation let us always place the ladder vertically and denote base states on directed edges as $|h\rangle$ for "horizontal", $|u\rangle$ for "up" and $|d\rangle$ for "down", and when displayed in the vector form let us put the coefficients in this order.

From the point of view of the transport and trapped states in reflecting Grover quantum walks the main difference compared to the lazy walk is the presence of faces in the ladder graph. For a ladder of length L we therefore use L A-type states shown in FIG. 4.6 (a). (We do not use the outer face, which would correspond to a state going over all the $2L + 2$ non-inner edges of the ladder.) Further, due to the presence of four loops in the border vertices we add three C-type states. For those we again use the modified set. We use two C1-type short path states on the ends of the ladder shown in FIG. 4.6 (b) and one C2-type connecting path state shown in FIG. 4.6 (c). The presence of the connecting path state will result in very counter-intuitive effects, which can not be observed in the lazy walk, where all the trapped states are localized on a fixed number vertices (two or three) independently of the size of the whole graph.

For the non-percolated walk we can further identify L A'-type states shown in FIG. 4.6 (d). Notably, these are orthogonal to all the trapped states for the percolated walk (but obviously not among themselves). It turns out from our numerical simulations that for the ladder graph these are the only additional states contributing to the

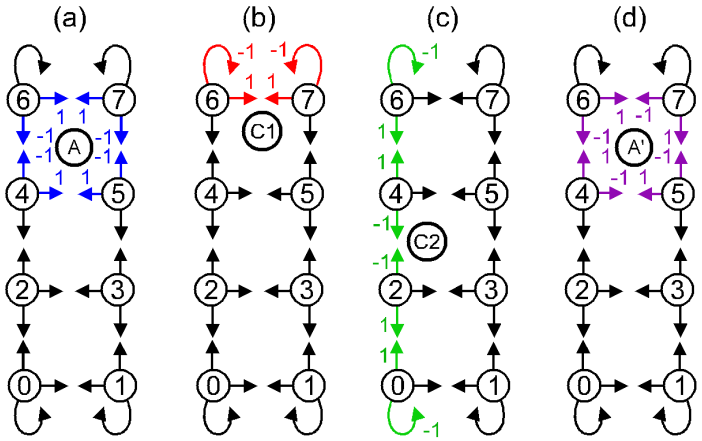

FIG. 4.6. Types of trapped states in the reflecting Grover PCQW on the ladder graph: (a) A-type face cycle state, (b) C1-type short path state and (c) C2-type connecting path state and (d) an additional A'-type trapped state for the non-percolated CQW.

trapping in reflecting Grover CQWs (for the investigated choices of the sink and the initial subspace).

The form of the subspace of sr-trapped states depends on the position of the sink. For the ladder we investigate two variants: the one-vertex sink and the loops sink shown in FIG 4.7. With the one-vertex sink we first remove the top short path C1-type trapped state as the only one overlapping with the up-state in the sink subspace and then the top A-type face cycle state. (As advised in the recipe for the construction we choose the connecting C2-type state so that it has no overlap with the sink.) In the case of the loops sink, we remove the short path state and very importantly also the C2-type connecting path state.

Similarly to the sink we have the same two variants for the initial subspace. This results in four possible scenarios for investigation of the transport: vertex-to-vertex transport, vertex-to-loops transport, loops-to-vertex transport and loops-to-loops transport as shown in FIG. 4.7 (a), (b), (c) and (d) respectively.

One more natural variant could be an initial subspace or the sink subspace spread on both vertices on one end of the ladder. Nevertheless, the knowledge of the trapped states shows that this does not bring much new interesting phenomena. In the case of the sink, the set of sr-trapped states is the same as for the loops sink only with the top A-type state removed, which has the smallest overlap with the initial state after orthonormalization and therefore only small quantitative impact. On the initial state end this mostly just combines properties of the one-vertex and loops initial state. The only notable difference is that as the initial subspace covering both vertices contains the whole short path C1-type sr-trapped state, there can be complete trapping.

Let us start with the results for the loops-to-loops transport presented in FIG. 4.8. In this variant the behavior of the ATP with respect to the length is qualitatively completely analogous to the one for the lazy walk shown in FIG. 4.4. This is not surprising. The C2-type connecting state, which has no analogy in the lazy walk,

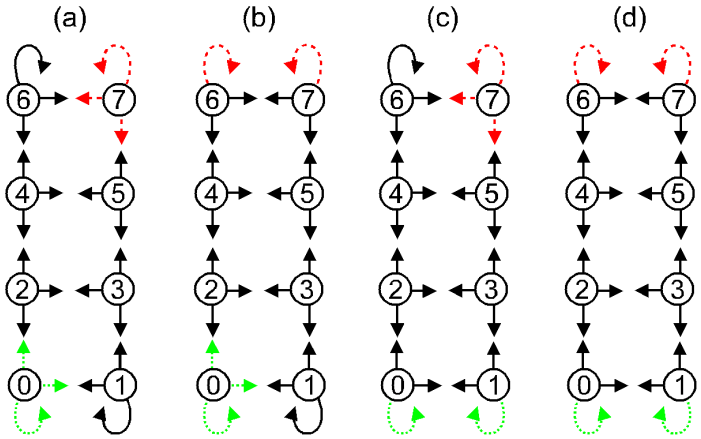

FIG. 4.7. Illustrations of the analyzed configurations of the initial subspace with green dotted arrows and the sink subspace with red dashed arrows for the ladder graph: (a) and (b) one-vertex initial state, (c) and (d) loops initial state, (a) and (c) one-vertex sink and (b) and (d) loops sink. According to these choices we use the terms vertex-to-vertex transport for (a), vertex-to-loos transport for (b), loops-to-vertex transport for (c) and loops-to-loops transport for (d). For the vertex-to-vertex variant we choose to maximize the distance between the initial vertex and the sink.

is excluded by the sink. Further, the A'-type additional trapped states in the non-percolated CQW are orthogonal to both the initial subspace and to all the other trapped sates and can not contribute to trapping. Therefore, by lengthening the ladder we just add more A-type states with smaller and smaller overlap with the initial subspace after orthonormalization.

Next we take a look at the vertex-to-loops transport on the ladder shown in FIG. 4.9. The difference from the loops-to-loops transport is that the one-vertex initial subspace is not orthogonal to the additional A'-type states in the non-percolated CQW. As a result, with every increment of the length, not only one A-type state but also one A'-type state contributes to trapping and the non-percolated CQW exhibits lower overall ATP.

The most interesting and counter-intuitive transport effect is present in the one-vertex sink variants. For simplicity we start with the loops-to-vertex transport. As seen in FIG. 4.10 the ATP actually increases with the length of the ladder. That means that the walker is more likely to traverse a longer ladder than a shorter one. This behavior has to our knowledge no analogy in the domain of classical random walks. Our access to the analytic form of the trapped states in PCWQs allows to explain this effect easily. The reason is the presence of the C2-type connecting state, which is sr-trapped for this sink type. As the ladder grows, this state is simply spread over more edges and it has more non-zero elements. Therefore, after normalization the coefficients in the initial subspace have lower magnitudes and the state has a smaller overlap with the maximally mixed initial state (or with other initial states). This effect is clearly competing with the addition of new A-type states, but as was seen earlier, their influence diminishes fast. In particular, already from the length $L = 2$ onward the ATP increases with the length. Note that as we have loops type initial state there is no influence of the A'-type states and the transport is the same

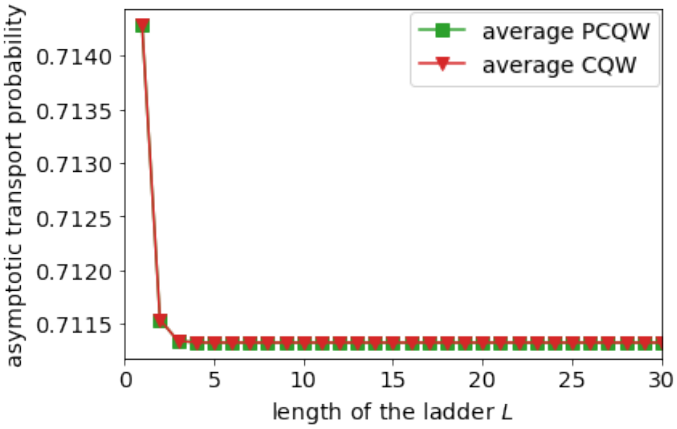

FIG. 4.8. The average loops-to-loops ATP for the ladder graph of length up to 30 for the reflecting Grover PCQW (green squares) and CQW (red triangles). The values of ATP for PCQW and CQW coincide for all lengths. The result for CQW is obtained numerically with 2^{30} steps. The C2-type connecting path state overlaps with the sink and the initial subspace is orthogonal to the A'-type states in the CQW. Therefore, the ATP is only influenced by the A-type states and the C1-type state on the bottom end of the ladder.

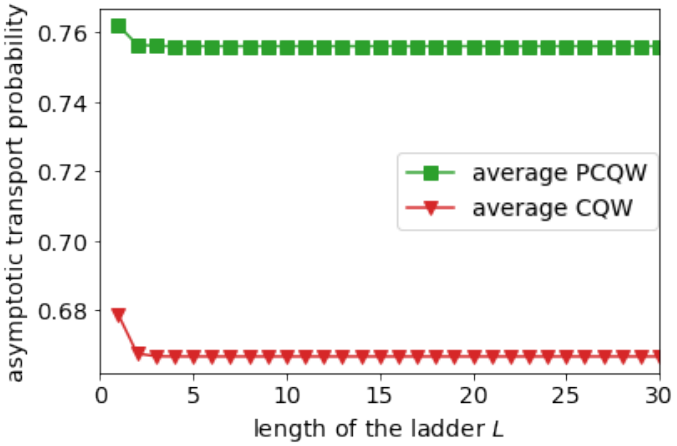

FIG. 4.9. The average vertex-to-loops ATP for the ladder graph of length up to 30 for the reflecting Grover PCQW (green squares) and CQW (red triangles). The result for CQW is obtained numerically with 2^{30} steps. The connecting path state overlaps with the sink, but here the A'-type states overlap with the initial state, which results in decreased ATP in the CQW.

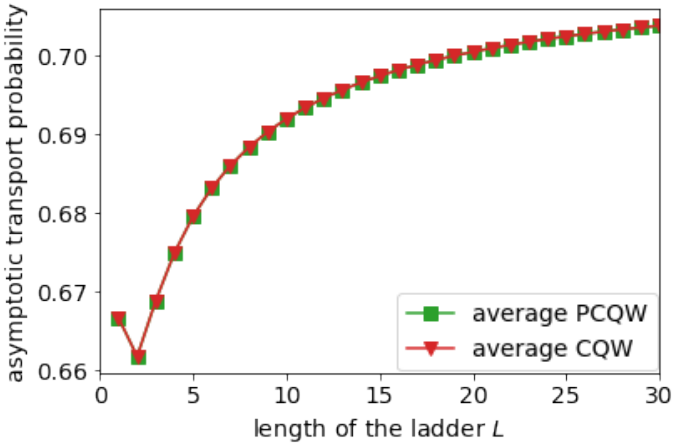

FIG. 4.10. The average loops-to-vertex ATP for the ladder graph of length up to 30 for the reflecting Grover PCQW (green squares) and CQW (red triangles). The result for CQW is obtained numerically with 2^{30} steps. We observe the counter intuitive behavior of increasing ATP with the length of the ladder. Only when extending from $l = 1$ to $l = 2$ the influence of the added A-type state outweighs the influence of stretching of the connecting path state. The A'-type states are orthogonal to the initial subspace, so the ATP for PCQW and CQW coincide.

for PCQW and CQW.

Finally, we have the vertex-to-vertex transport shown in FIG. 4.11, where the phenomena form vertex-to-loops and loops-to-vertex variants meet. The C2-type connecting state is present and we observe an increase of the ATP with length of the ladder. Simultaneously, the initial state overlaps with the A'-type states and so the ATP for the non-percolated walk is decreased, but still showing the improving ATP with increasing distance. (For $L = 1$ the ATP for PCQW and CQW is the same since both the only A-type and the only A'-type states overlap with the sink.)

In both the loops-to-vertex and vertex-to-vertex transport the increment of the average ATP with growing length has magnitude of about 0.05. This is non-negligible itself, but in FIG. 4.12 we further present the ATP for a pure initial state with particularly significant growth of the ATP with length. The increase is monotonous for both PCQW and CQW and for the PCQW it is over 0.2 in magnitude.

We can examine some more extreme behavior for particular initial states. As mentioned above, unless we allow the initial state on both end vertices, none of the trapped states lies entirely in the initial subspace and complete trapping is not possible. On the other hand, complete transport is trivially possible in all one-vertex initial state variants for the initial state $\frac{1}{\sqrt{3}}(|0,h\rangle + |0,u\rangle + |0,d\rangle)$. Also the loops-to-loops transport reaches 100 % for the initial state $\frac{1}{\sqrt{2}}(|0,d\rangle - |1,d\rangle)$. The same initial state also maximizes loops-to-vertex transport, but again due to the C2-type connecting path state the ATP is never equal to one as seen in FIG. 4.13, so there is no full-transport initial state in this variant.

Finally, in FIG. 4.14 we demonstrate that the effect of the sink type diminishes for longer ladders. This is due to the fact that the influence from both the connecting

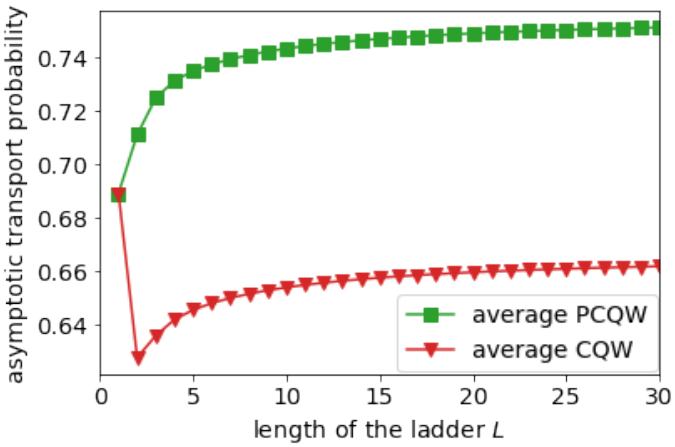

FIG. 4.11. The average vertex-to-vertex ATP for the ladder graph of length up to 30 for the reflecting Grover PCQW (green squares) and CQW (red triangles). The result for CQW is obtained numerically with 2^{30} steps. In constrast to the loops-to-vertex transport in FIG. 4.10 the one-vertex initial subspace overlaps with the A'-type states reducing the ATP in the CQW.

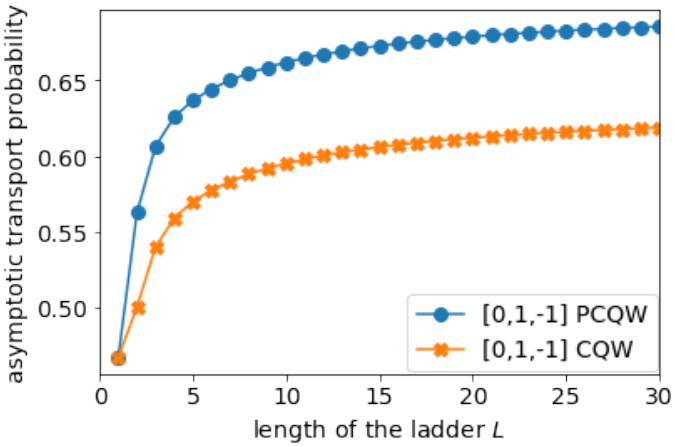

FIG. 4.12. The vertex-to-vertex ATP for the ladder graph of length up to 30 for the reflecting Grover PCQW (blue circles) and CQW (orange crosses) for the initial state $\frac{1}{\sqrt{2}}(|0,u\rangle - |0,d\rangle)$. The result for CQW is obtained numerically with 2^{30} steps. This particular initial state exhibits the maximal increase of the ATP with length of the ladder.

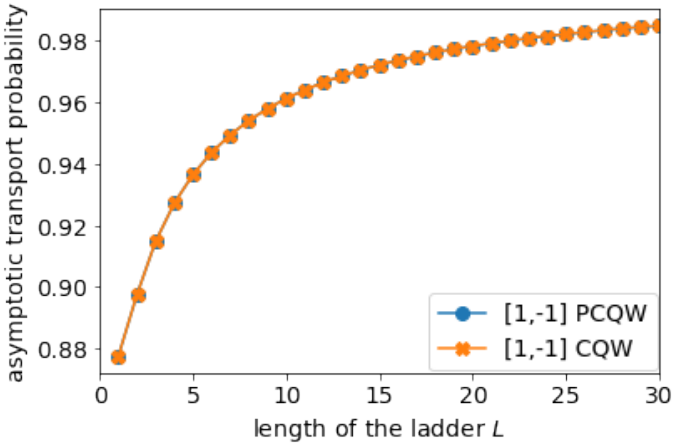

FIG. 4.13. The loops-to-vertex ATP for the ladder graph of length up to 30 for the reflecting Grover PCQW (blue circles) and CQW (orange crosses) for the initial state $\frac{1}{\sqrt{2}}(|0,d\rangle - |1,d\rangle)$. The result for CQW is obtained numerically with 2^{30} steps. This initial state has the highest ATP among all possible initial states for the loops-to-vertex transport on the ladder graph. There is no fully transported initial state.

path state and the newly added A-type states decreases.

4.4 Carbon nanotube structures

Structures of carbon nanotubes presented in appendix section A.2.5 represent yet another step of increasing complexity of graphs which naturally grow in one dimension. In fact, regarding the lengthening of the tube we will see, that the qualitative transport properties for reflecting Grover quantum walks on nanotube structures are very similar to those on the ladder, especially for the percolated walks. In particular, all the transport effects presented for the ladder can be found in the transport on nanotubes. In contrast to both the lazy walk on a chain and to the ladder the nanotubes have the so called chirality controlling their diameter and the way in which hexagonal faces are organized. This is a new – additional free parameter and it is worth to study its influence on the transport efficiency. In this case length is not the only control parameter for ATP.

For simplicity of arguments we always place the tube vertically with the walker initiated somewhere at the bottom end and with the sink at the top end.

The set of trapped states is very analogous to the ladder graph as shown in FIG. 4.15. Graphs of carbon nanotubes are also planar graphs only having even-edged faces as already discussed in appendix section A.2.5. We construct A-type states for all the hexagonal faces. From the example of a planar embedding of a nanotube structure in FIG. A.16 we see that apart from the outer face there is one more even-edged face on the bottom end of the tube. (It is convenient to use the top end with sink as the outer face for the subsequent identification of the subspace of sr-trapped states.) Then we add the C-type states. The (n,n) tubes have $4n$ loops

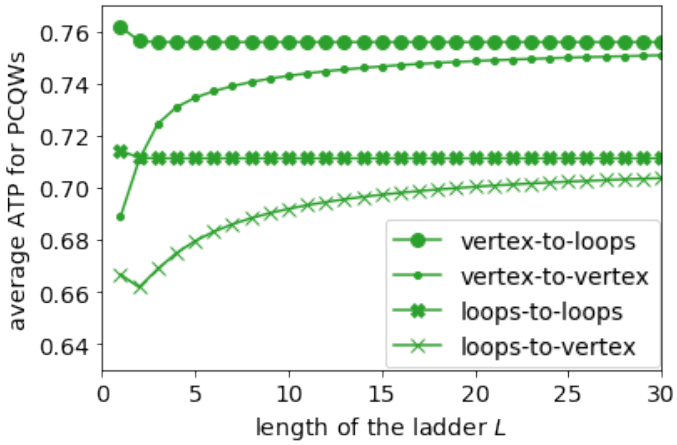

FIG. 4.14. All four variants of average ATP for the ladder graph of length up to 30 for the reflecting Grover PCQW demonstrating that the influence of the sink type diminishes with growing length of the ladder. It is seen that the ATP for vertex-to-loops transport (big circles) converges to the one for vertex-to-vertex transport (small points) and the ATP for loop-to-loops transport (solid crosses) converges to the one for loops-to-vertex transport (thin crosses).

and the $(n, 0)$ tubes have $2n$ loops. That means to construct $4n - 1$ and $2n - 1$ C-type states respectively. We use $2n - 1$ C1-type short path states on every end of an (n, n) tube and $n - 1$ C1-type states on every end of an $(n, 0)$ tube. Finally, we add the important C2-type connecting path state.

For nanotube structures we again investigate one-vertex type and loops type initial subspaces and sinks as shown in FIG. 4.16. According to their choices we again use the terms vertex-to-vertex transport, vertex-to-loos transport, loops-to-vertex transport and loops-to-loops transport. For the vertex-to-vertex variant we choose to maximize the distance between the initial vertex and the sink, which is at the expense of symmetry for $(2n, 0)$ tubes.

The loops sink removes all the C1-type states on the top end of the tube and the C2-type connecting path state. The one-vertex sink removes one C1-type short path state and one A-type state. (When constructing the trapped states we already choose the connecting path state to avoid the sink and leave out one short path state, which would otherwise overlap with the sink.) The remaining states are sr-trapped and we orthonormalize them numerically.

In analogy with the investigation of the walk on the ladder graph we again start with the simplest variant of loops-to-loops transport shown in FIG. 4.17. For percolated walks the result is qualitatively completely the same as for the ladder - with increasing length the transport decreases due to new A-type states and the ATP levels to a given value exponentially fast as is seen in FIG. 4.18. As the A'-type states are orthogonal to the loops type initial state, the ATP for CQW and PCQW is the same for all (n, n) tubes and for $(2n + 1, 0)$ tubes. Nevertheless, the ATP is lower for CQW on $(2n, 0)$ tubes. This is because there are more trapped states then the A'-type states in CQWs. In particular, here we can identify trapped states

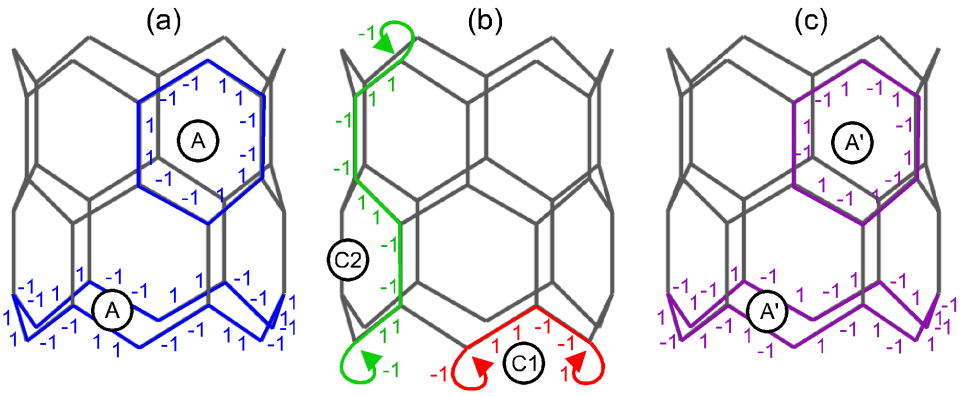

FIG. 4.15. Types of trapped states in the reflecting Grover PCQW on nanotube graphs: (a) A-type face cycle states, (b) C1-type short path state and C2-type connecting path state and (c) additional A'-type trapped states for the non-percolated CQW.

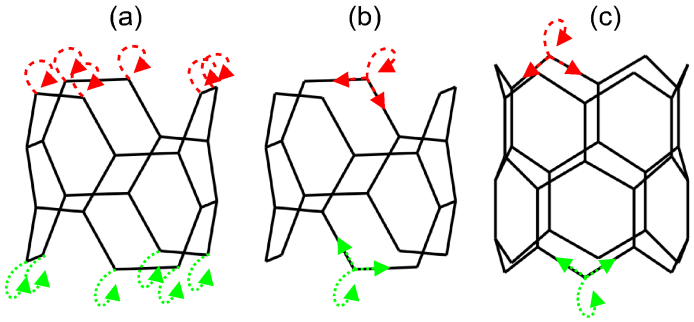

FIG. 4.16. Depiction of variants of the initial subspace with green dotted arrows and the sink subspace with red dashed arrows for example nanotubes: (a) loops initial state and loops sink on a $(3, 3)$ tube, (b) one-vertex sink and one-vertex initial subspace on a $(3, 3)$ tube and (c) one-vertex sink and one-vertex initial subspace on a $(6, 0)$ tube.

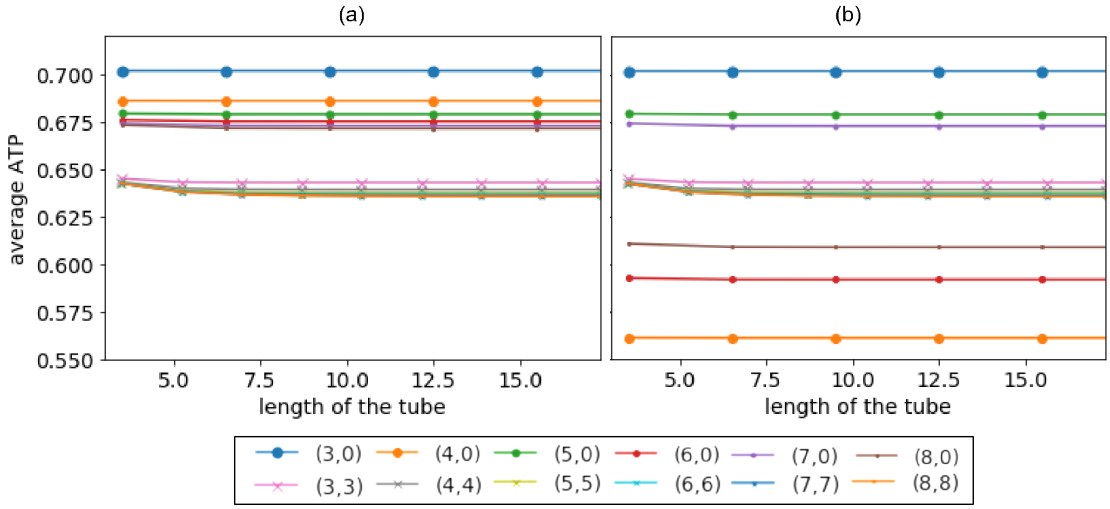

FIG. 4.17. The loops-to-loops average ATP for the reflecting Grover (a) percolated (PCQW) and (b) non-percolated (CQW) quantum walks in dependence on the length of a nanotube for different chiralities. The result for CQW is obtained numerically with 2^{30} steps. There is a monotonous decrease of the ATP with length of the tube resulting form A-type states, which is clearly illustrated in FIG. 4.18. As the A'-type states are orthogonal to the loops type initial subspace the ATP is lower in the CQW in (b) only for $(2n, 0)$ tubes, where additional trapped states are present (exemplified in FIG. 4.19).

localized on the bottom ring of vertices as depicted in FIG. 4.19.

For the additional trapped state in FIG. 4.19 we observe an effect analogous to the one with the connecting path state for the ladder graph - as the width of the tube increases the state has more elements and after normalization its overlap with the initial state decreases. Therefore, the transport is higher on tubes with higher n.

When we switch to the one-vertex initial state the results in FIG. 4.20 are again influenced by the presence of the trapped state shown in FIG. 4.19. Further, the A'-type states are no longer orthogonal to the initial subspace and so they induce lower ATP in the non-percolated CQW for all chiralities and all values of n.

With the one-vertex sink we see an analogy with the walk on the ladder for PCQWs as shown in FIG. 4.21 (a). Due to the presence of the C2-type connecting state we again observe the increase of the ATP with the length of the tube, which is counter-intuitive but already known from the ladder. Nevertheless, it is interesting that this phenomenon also appears in the physically realistic and more complex structures of carbon nanotubes. When we turn to CQWs, the results in FIG. 4.21 (b) may look rather messy at first. The ATP in $(2n, 0)$ tubes is decreased by the trapped state in FIG. 4.19. The A'-type states are out for this type of the initial state, but there are more trapped states in CQWs, which only appear for specific combinations of chiralities and tube lengths. As an example that can be conveniently presented we show the trapped state causing the initial drop of ATP for $(3, 0)$ tube in FIG. 4.22. For lengths where similar trapped states are not present we just have the same ATP as for the PCQW as is also best visible for the $(3, 0)$ tube.

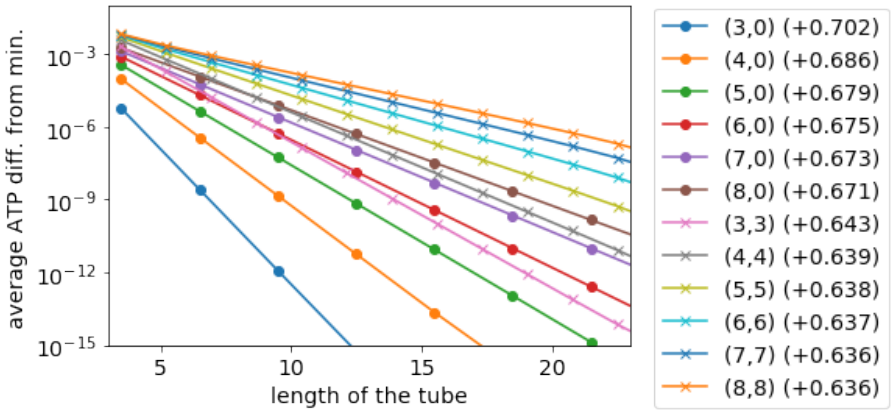

FIG. 4.18. The loops-to-loops average ATP for the reflecting Grover PCQW in dependence on the length of a nanotube for different chiralities plotted on a semi-log scale as a difference from the minimal value indicated on the right. The differences clearly drop exponentially in all cases.

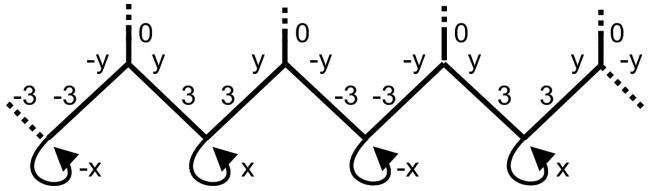

FIG. 4.19. Additional trapped state present in non-percolated CQWs on $(2n, 0)$ tubes. The values are $x = -2 + i\sqrt{8}$ and $y = 1 + i\sqrt{8}$ and it is an eigenstate corresponding to the eigenvalue $\lambda = (1 - i\sqrt{8})/3$. The complex conjugate of this state is clearly also an eigenstate of the CQW.

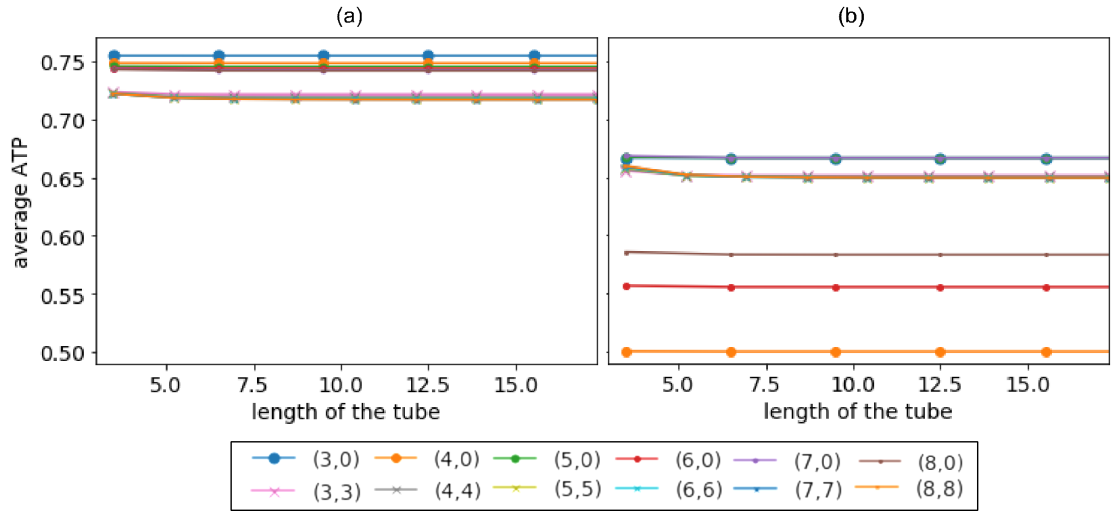

FIG. 4.20. The vertex-to-loops average ATP for the reflecting Grover (a) percolated (PCQW) and (b) non-percolated (CQW) quantum walks in dependence on the length of a nanotube for different chiralities. The result for CQW is obtained numerically with 2^{30} steps. Note, that the figures (a) and (b) are plotted with a common vertical axis for easy comparison. The situation is similar to the loops-to-loops transport in FIG. 4.17, only now the ATP in the CQW in (b) is further decreased by the the overlap of A'-type states with the initial subspace.

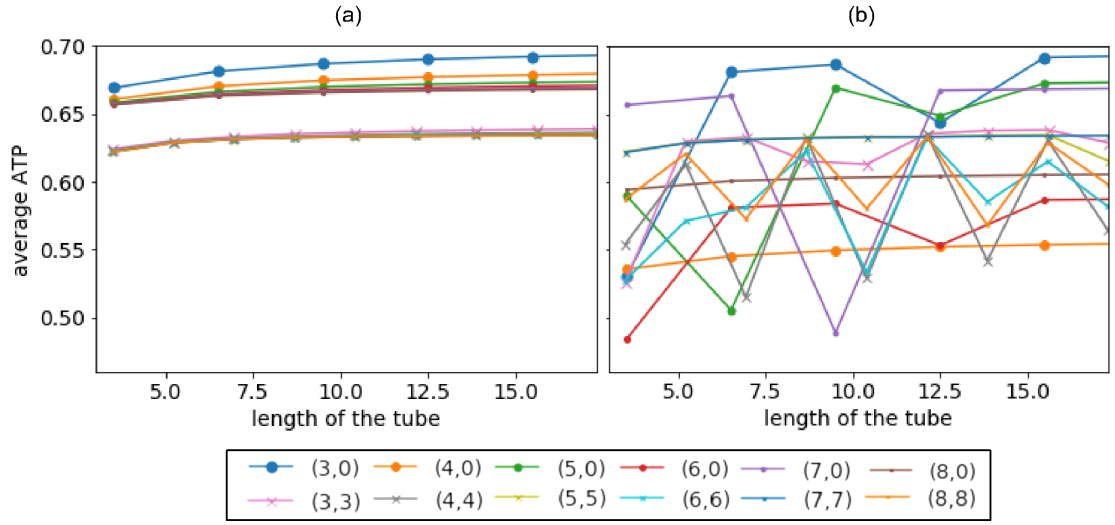

FIG. 4.21. The loops-to-vertex average ATP for the reflecting Grover (a) percolated (PCQW) and (b) non-percolated (CQW) quantum walks in dependence on the length of a nanotube for different chiralities. The result for CQW is obtained numerically with 2^{30} steps. For the PCQW in (a) we see an increase of the ATP with length of the tube given by the presence of the C2-type connecting path trapped state as for the ladder graph. The ATP in the CQW in (b) is now reduced not only in $(2n, 0)$ tubes by the trapped states exemplified in FIG. 4.19, but also by other trapped states only appearing for some combinations of chirality and length as e.g. the state in FIG. 4.22. This results in a non-monotonous dependence of the ATP on the length of the tube.

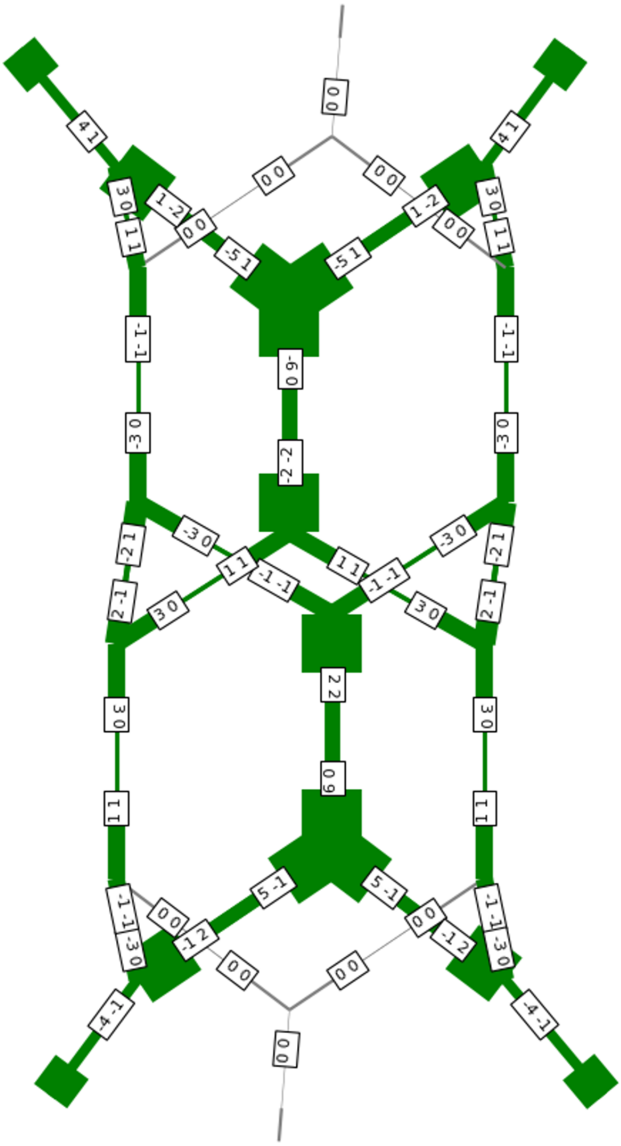

FIG. 4.22. An additional trapped state present in non-percolated CQWs on the $(3, 0)$ tube of the minimal investigated length (two basal length segments). It is an eigenstate corresponding to the eigenvalue $\lambda = (-1 + i\sqrt{8})/3$ and for every edge there is a pair of coefficients a, b (always closer to the beginning of the edge) and the corresponding vector element has value $a + b\sqrt{8}i$. Width of the edges represents magnitudes of the elements.

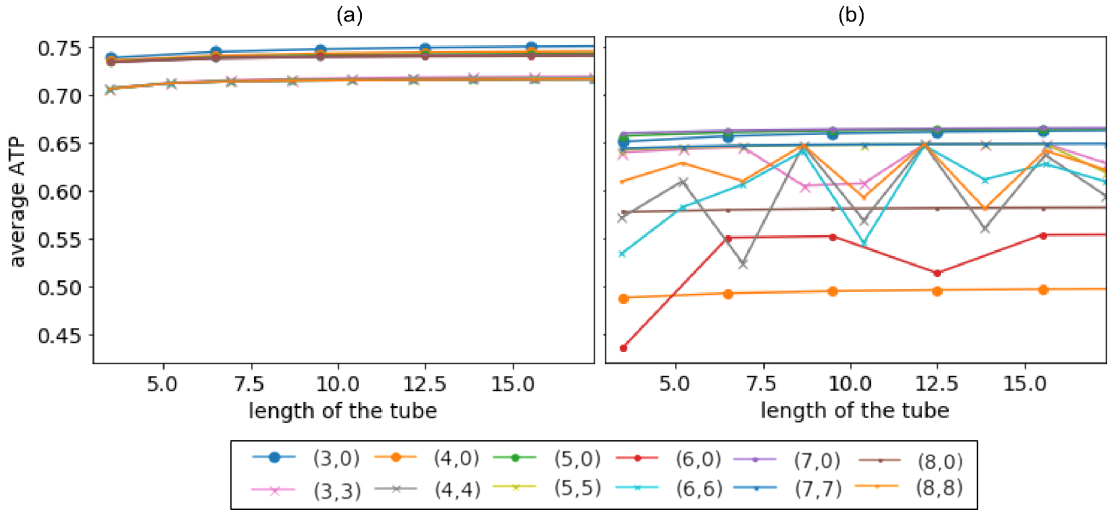

FIG. 4.23. The vertex-to-vertex average ATP for the reflecting Grover (a) percolated (PCQW) and (b) non-percolated (CQW) quantum walks in dependence on the length of a nanotube for different chiralities. The result for CQW is obtained numerically with 2^{30} steps. In comparison to the loops-to-vertex transport in FIG. 4.21 here is the additional effect of A'-type states in the CQW in (b). Further, there can be other influences given by the change of the initial subspace as e.g. the fact that the state presented in FIG. 4.22 does not contribute here.

The results for vertex-to-vertex transport in FIG. 4.23 are very similar to the loops-to-vertex case. Primarily, there is the additional influence of the A'-type states. Further, we can for example notice a change for the $(3,0)$ tube. Because the trapped state in FIG. 4.22. has all elements zeros in the initial subspace, it does not reduce ATP for the initial length in the case of one-vertex type sink.

The results for all sink / initial subspace variants show a quantitative separation of the transport on (n,n) tubes and $(n,0)$ tubes by percolated walks. This is mainly given by the different shape of the bottom end of the tube forming the short path states. While for $(2n,0)$ tubes there are $2n$ C1-type states spanning over two undirected edges and therefore having 6 non-zero elements, for (n,n) tubes there are n C1-type states on one undirected edge with 4 non-zero elements and n states on three undirected edges with 8 non-zero elements.[1] Clearly, the states first need to be orthonormalized before calculation of the ATP, but the difference in the average ATP between $(2n,0)$ and (n,n) tubes can actually be well estimated directly. For example the loops type maximally mixed initial state has diagonal elements $\frac{1}{2n}$, the trapped states are normalized by $\frac{1}{\sqrt{6}}$ in $(2n,0)$ tubes and by $\frac{1}{\sqrt{4}}$ or $\frac{1}{\sqrt{8}}$ in (n,n) tubes, and every trapped state overlaps with the initial state on two loops. Therefore, the difference in average ATP can be estimated as

$$\overline{q}_{(2n,0)} - \overline{q}_{(n,n)} \simeq \left(1 - \frac{1}{2n}\left(2n \cdot 2 \cdot \frac{1}{6}\right)\right) - \left(1 - \frac{1}{2n}\left(n \cdot 2 \cdot \frac{1}{4} + n \cdot 2 \cdot \frac{1}{8}\right)\right) = \frac{1}{24},$$

[1] Above, we constructed the basis of trapped states in such a way that we omitted one C1-type state on every end of the tube as being linearly dependent. Nevertheless, dependent A-type states can be removed instead, which is more convenient for our current reasoning.

which agrees reasonably well with the observed difference. Clearly, there are further factors influencing the actual ATP. Obviously, there is the orthonormalization and the presence of A-type states. Interestingly, the interplay of these effects results in yet another surprising observation - the ATP is higher for thinner tubes. This again contradicts our intuition from the classical world since addition of another parallel paths connecting the initial position and the final destination would be expected to improve transport.

4.5 Cayley trees

As the last example of graphs for investigation of quantum transport by reflecting Grover quantum walks we choose the Cayley trees introduced in appendix section A.2.6. This allows us to explore different dependencies of the quantum transport on the structure parameters of the graph not possible with linear structures of the line, ladder or tubes. First, the number of vertices and so the dimension of the Hilbert space grows exponentially with the order of a Cayley tree k and second by permanently breaking one link we can cut out a whole branch of the tree for the entire time span of the walk and observe the effect of this modification on the ATP.

We study quantum walks on 3-regular graphs so we choose Cayley trees with inner vertices of degree 3. Then the particular graph is determined by the choice of the order k, which we always choose as $k \geq 1$. A Cyley tree of the order k has $\#V = 1 + 3(2^k - 1)$ vertices, $\#E = 3(2^k - 1)$ undirected edges, $\#L = 3 \cdot 2^k$ unpaired loops after 3-regularization and no faces (or technically it has the outer face covering the whole embedding plane). In comparison to the linear structures studied above, the dimension of the Hilbert space $\dim(\mathcal{H}) = 3(1 + 3(2^k - 1))$ grows exponentially with the structure parameter k.

To study transport in reflecting Grover PCQWs we construct $N_2 = 2\#V - \#E = (3 \cdot 2^k) - 1$ C-type trapped states. We construct the basis by placing the graph into a plane and by using C-type states for all paths connecting neighboring loops as indicated in FIG. 4.24 (c). This gives $3 \cdot 2^k$ states and we remove one of the states corresponding to the longest path. The same approach can be used for Cayley trees with one or two branches removed or actually for any connected tree graph. For every tree graph $\#E = \#V - 1$ holds and every 3-regularized tree graph will have exactly $3\#V - 2\#E = 2\#V + \#E + 1 - 2\#E = 2\#V - \#E + 1$ loops resulting in $N_2 = 2\#V - \#E$ independent C-type states.

We initiate the walker in the central vertex of the graph and place the sink in one of the leafs as shown in FIG. 4.25. The figure also shows how the base states in the initial subspace $|b_1\rangle$ ("branch 1"), $|b_2\rangle$ and $|b_s\rangle$ ("branch with sink") relate to the position of the sink and the removal of branches. We choose the position of the sink and the embedding into plane in such combination that the one trapped state left out overlaps with the sink. By the presence of the sink, two more trapped states are removed and we are left with $3 \cdot 2^k - 3$ sr-trapped states.

For the calculation of transport, the sr-trapped states need to be orthonormalized.

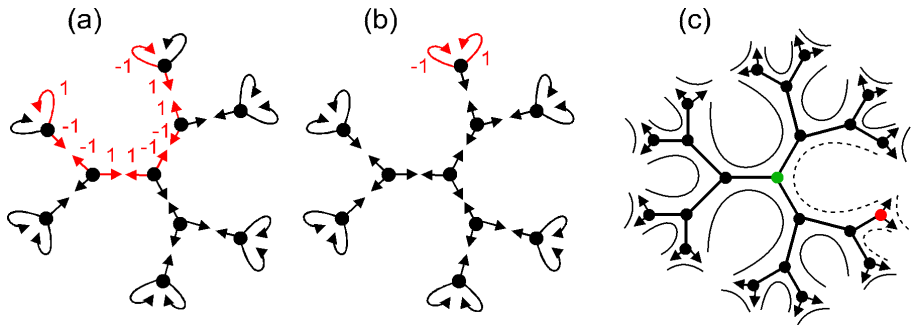

FIG. 4.24. Examples of trapped states for the reflecting Grover PCQW on Cayley trees of the order $k = 2$: (a) a trapped state on multiple vertices and (b) a trapped state localized in one vertex. Further, in (c) all the trapped states for a Cayley tree with $k = 3$ are represented by curved lines. The dashed lines represent trapped states overlapping with the sink, which are further removed. In (c) loops are represented just as directed edges pointing out of the graph.

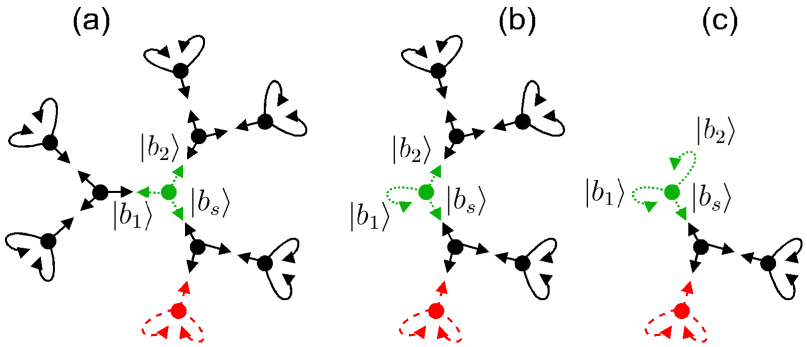

FIG. 4.25. Illustration of the initial subspace (green dotted arrows) and the sink subspace (red dashed arrows) on (a) a standard Cayley tree and Cayley trees with (b) one and (c) two branches removed; all of the order $k = 2$. Notation for the base states in the initial subspace $|b_1\rangle$, $|b_2\rangle$ and $|b_s\rangle$ in relation to the position of the sink and the removed branches is indicated.

We perform the orthonormalization numerically in most cases. Nevertheless, an approach of a partial analytical orthonormalization was published in an appendix of [48]. It allows to give a closed form formula of the ATP for the initial state resulting in maximal trapping.[2] We present the procedure here in detail since it is also very useful for an intuitive understanding of the other transport phenomena on Cayley trees.

We use the symmetry of Cayley tree graphs to construct a new orthogonal basis of sr-trapped states. Let us first note that the sr-trapped states constructed above and shown in FIG 4.24 are mostly in a one-to-one correspondence with vertices which are in the middle of the corresponding path. The only exception is the root vertex, which is central for two sr-trapped states. From these two we now choose the one on the two non-sink branches (with non-zero amplitudes for $|b_1\rangle$ and $|b_2\rangle$). For each of these trapped states we construct one new trapped state according to the following recipe:

- Let us take some vertex in the tree. It has one edge going towards the root vertex. (If we choose the root vertex itself, the role of this edge is played by the edge on the sink branch.) The remaining two edges lead to two symmetrical branches of the tree. (One of those can contain the sink.)
- We connect every non-sink loop in one branch with one non-sink loop in the second branch by a capped graph walk (in this case just a path with loops on the ends). If none of the branches contains the sink, every loop is an end-point of one capped graph walk. If one of the branches contains the sink, the sink loops are not used and the two loops in the vertex closest to the sink vertex are used twice.
- For each of the capped graph walks we construct a C-type state and we sum the C-type states so that all the coefficients on loops on one branch have the same sign.

Examples of the newly formed states are in FIG. 4.26. We denote the states exemplified in FIG. 4.26 (d) as *sink affected* and the others as *sink non-affected*.

Finally we construct one additional state from the second sr-trapped state going through the root vertex in a similar way. We just consider the two main branches of the Cayley tree without sink as one branch of the state and the last main branch with the sink as the other branch of the state. Every loop on the branch with sink basically plays a role of two loops. An example of this state for $k = 3$ is shown in FIG. 4.27 (b). We denote this state as $|\tilde{t}_2\rangle$ [3] and the second state containing the root vertex constructed earlier, which is shown in FIG. 4.27 (a), as $|t_1\rangle$.

All the sink non-affected states are orthogonal both mutually and to all the sink affected states. This is because the states either have disjoint supports or one support

[2]Some of the elements of the orthogonal basis remain only partially determined and so we can calculate the ATP only for the particular initial state orthogonal to these not fully known trapped states.

[3]The tilde indicates that this is not the final state used. The lower-case letter indicates that this is a non-normalized version of the vector with integer coefficients.

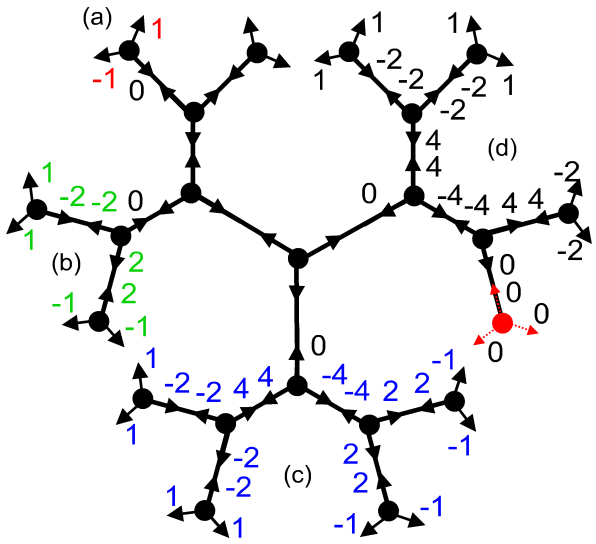

FIG. 4.26. Examples of the newly constructed sr-trapped states: (a), (b) and (c) are states not affected by the sink and (d) is a state affected by the sink. These are four different states depicted in one figure. For each state all the other coefficients following the zero in the central vertex of this state are zeros. Coefficients are color-coded for visual aid.

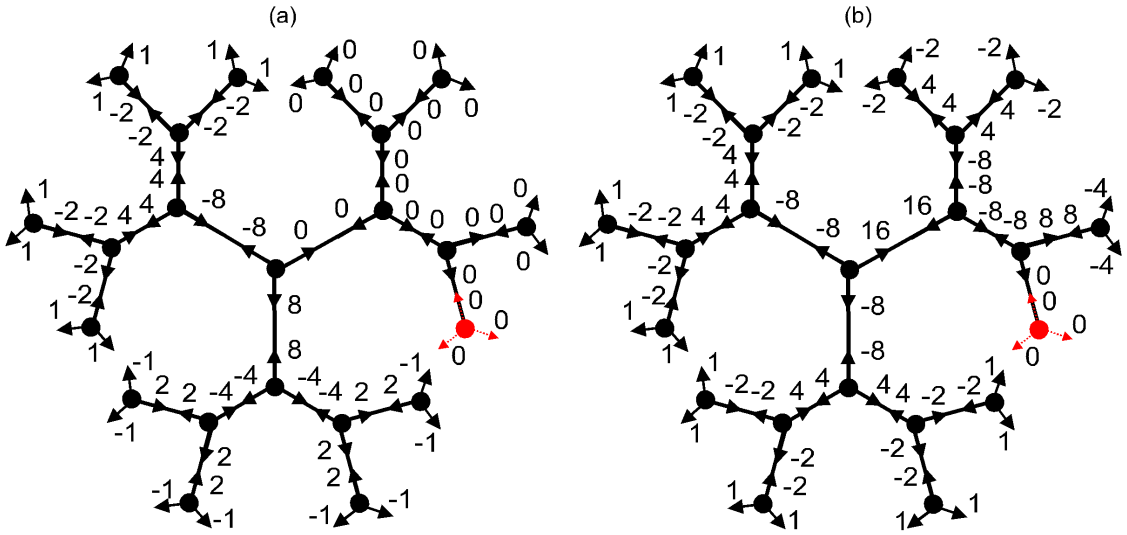

FIG. 4.27. Examples of the states (a) $|t_1\rangle$ and (b) $|\tilde{t}_2\rangle$ for $k = 3$.

is a subset of the other. In the later case the state with smaller support has two anti-symmetric branches aligned with two similar symmetric branches of the other state as illustrated in FIG. 4.26. In contrast, the sink-affected states are not mutually orthogonal as is seen for example by comparing FIG. 4.26 (d) and FIG. 4.27 (b).

Importantly, if we have an orthonormal basis, only states overlapping with the initial subspace can contribute to trapping. In our new basis those are only states $|t_1\rangle$ and $|\tilde{t}_2\rangle$. Yet, the basis is not orthogonal. In fact, we are not able to orthogonalize the sink-affected states analytically. Nevertheless, only some partial knowledge will be sufficient for our purposes:

- A Gram-Schmidt orthogonalization performed on the set of sink-affected states replaces the state $|\tilde{t}_2\rangle$ with a state $|t_2\rangle$, which only differs from $|\tilde{t}_2\rangle$ on the main branch of the graph with sink by addition of multiples of the other sink-affected states. The coefficients on the two main branches without sink do not undergo any changes.

- We denote the normalized version of $|t_2\rangle$ as $|T_2\rangle$ and the normalization constant as N_2, so $||T_2|| = 1$ ($||T_2||$ is a short-hand notation for $||\,|T_2\rangle\,||$) and $|T_2\rangle = \frac{1}{N_2}|t_2\rangle$. Similarly, we introduce a normalized vector $|T_1\rangle = \frac{1}{N_1}|t_1\rangle$. The value of N_1 is calculated below. The value of N_2 is unknown, but we know that $(N_2)^2 > 3(N_1)^2$. To show this we consider a state $|\tilde{\tilde{t}}_2\rangle$, which is constructed similarly as $|\tilde{t}_2\rangle$ with the only difference that we ignore the sink completely in the construction of the capped graph walks and use the sink loops normally. An example of this state is shown in FIG. 4.28. It is easily seen that $||\tilde{\tilde{t}}_2||^2 = 3||t_1||^2$. Further, by the construction of trapped states in reflecting Grover walks, the sum of elements at vertices must be zero also for the state $|t_2\rangle$ and since the equal splitting in $|\tilde{\tilde{t}}_2\rangle$ minimizes the norm, we have $||t_2||^2 > ||\tilde{\tilde{t}}_2||^2 = 3||t_1||^2$, and so $(N_2)^2 > 3(N_1)^2$.

- We denote the restrictions of the states $|T_1\rangle$ and $|T_2\rangle$ to the initial subspace as $|\tau_1\rangle = \frac{2^k[1,-1,0,\ldots]}{N_1}$ and $|\tau_2\rangle = \frac{2^k[1,1,-2,\ldots]}{N_2}$ respectively. (We understand these as non-normalized vectors on the whole Hilbert space with all elements outside the initial subspace zeros.) We note that $|\tau_1\rangle$ and $|\tau_2\rangle$ are orthogonal and thanks to the relation for N_1 and N_2 the inequality $||\tau_2|| < ||\tau_1||$ holds.

Using the results above we can write the trapping probability for an arbitrary normalized initial state $|x\rangle$ as

$$\begin{aligned} p(|x\rangle) &= |\,\langle T_1|x\rangle\,|^2 + |\,\langle T_2|x\rangle\,|^2 \\ &= |\,\langle \tau_1|x\rangle\,|^2 + |\,\langle \tau_2|x\rangle\,|^2 \\ &= ||\tau_1||^2 \left|\langle \frac{\tau_1}{||\tau_1||}|x\rangle\right|^2 + ||\tau_2||^2 \left|\langle \frac{\tau_2}{||\tau_2||}|x\rangle\right|^2 \end{aligned} \tag{4.2}$$

which can be bounded thanks to $||\tau_2|| < ||\tau_1||$ as

$$p(|x\rangle) \leq ||\tau_1||^2 \left(\left|\langle \frac{\tau_1}{||\tau_1||}|x\rangle\right|^2 + \left|\langle \frac{\tau_2}{||\tau_2||}|x\rangle\right|^2\right) \tag{4.3}$$

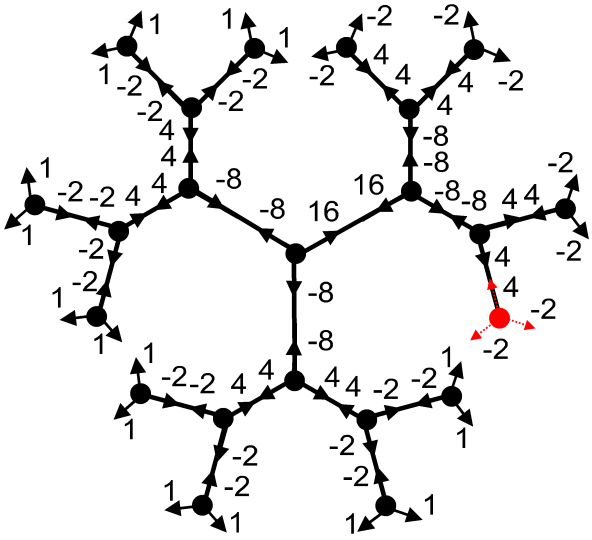

FIG. 4.28. The state $|\tilde{\tilde{t}}_2\rangle$ for $k = 3$.

and from Bessel's inequality we obtain

$$q(|x\rangle) \leq ||\tau_1||^2. \tag{4.4}$$

Note that the form of all the states and therefore also the value of $q(|x\rangle)$ are dependent on the order of the tree k.

Since for the initial state $|\psi_1\rangle = \frac{|\tau_1\rangle}{||\tau_1||} = \frac{1}{\sqrt{2}}(|b_1\rangle - |b_2\rangle)$ we obtain

$$p(|\psi_1\rangle) = ||\tau_1||^2, \tag{4.5}$$

there is no initial state resulting in more trapping. Thanks to the symmetry, it is actually possible to calculate N_1 directly for any order k as

$$(N_1(k))^2 = 2^{k+1} + \sum_{i=0}^{k-1} 2^{2+i}(2^{k-i})^2 = 2^{k+1}(2^{k+2} - 3)$$

and so the ATP for the initial state $|\psi_1\rangle$ is

$$q(k, |\psi_1\rangle) = 1 - |\langle\psi_1|T_1\rangle|^2 = 1 - \frac{(2 \cdot 2^k)^2}{2 \cdot (N_1(k))^2} = 1 - \frac{2^k}{2^{k+2} - 3}.$$

The ATP for walks on Cayley trees with different k is plotted in FIG. 4.29 for the initial state $|\psi_1\rangle$, for an orthogonal state $|\psi_2\rangle = \frac{|\tau_2\rangle}{||\tau_2||} = \frac{1}{\sqrt{6}}(|b_1\rangle + |b_2\rangle - 2|b_s\rangle)$ and the average ATP. The average ATP also contains contribution from the state $|\psi_3\rangle = \frac{1}{\sqrt{3}}(|b_1\rangle + |b_2\rangle + |b_s\rangle)$, which is fully transported for any k.

We see that even for Cayley trees, after an initial decent, the average ATP increases with the order k and so with increasing distance separating the initial vertex and the sink. For the maximally trapping state $|\psi_1\rangle$ we even have this result analytically for arbitrary k.

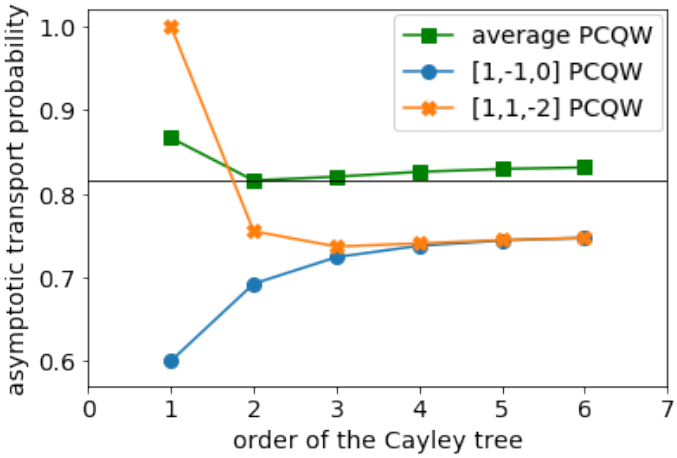

FIG. 4.29. The average ATP (green squares) and the ATP for the initial states $|\psi_1\rangle = \frac{1}{\sqrt{2}}(|b_1\rangle - |b_2\rangle)$ (blue circles) and $|\psi_2\rangle = \frac{1}{\sqrt{6}}(|b_1\rangle + |b_2\rangle - 2\,|b_s\rangle)$ (orange crosses) in the reflecting Grover PCQW on Cayley trees in dependence on the order of the tree k. The ATP for both the minimal transport initial state $|\psi_1\rangle$ and the orthogonal state $|\psi_2\rangle$ increase (at least from some point) with growing order of the tree. This translates also to the average transport, which also contains a contribution from the fully transported state $\frac{1}{\sqrt{3}}(|b_1\rangle + |b_2\rangle + |b_s\rangle)$.

We can use our analytical insights to explain the observed phenomena. There are again two competing effects: 1) there is an exponentially growing number of new trapped states with any increase of the order k and 2) the states $|T_1\rangle$ and $|T_2\rangle$ are more spread with more non-zero coefficients outside of the initial subspace $\mathcal{H}_i$. The normalization then reduces coefficients of these states inside $\mathcal{H}_i$, which reduces trapping. Since the state $|\psi_1\rangle$ only overlaps with $|T_1\rangle$ and $|\psi_2\rangle$ only overlaps with $|T_2\rangle$, the result in FIG. 4.29 is very representative. While for $|\psi_1\rangle$ the effect of spreading of the trapped state $|T_1\rangle$ is dominant from the beginning, for $|\psi_2\rangle$ the influence of the new trapped states appearing with the growing order k is only suppressed for higher orders. For any other initial state we obtain some combination of these two behaviors with the addition of transport due to possible overlap with the fully transported state $|\psi_3\rangle$.

4.5.1 Non-percolated CQWs on Cayley trees

The comparison of transport between percolated and non-percolated reflecting Grover CQWs on Cayley trees is plotted in FIG. 4.30. We see that for the initial state $|\psi_2\rangle = \frac{1}{\sqrt{6}}(|b_1\rangle + |b_2\rangle - 2\,|b_s\rangle)$, the ATP for PCQW and CQW is the same except from the orders $k = 5$ and $k = 9$ with drops in the ATP caused by additional trapped states. We investigate these interesting additional trapped states in detail below. These drops are also visible in the average ATP. The average ATP for CQW is further reduced compared to the percolated case since the initial state $|\psi_1\rangle = \frac{1}{\sqrt{2}}(|b_1\rangle - |b_2\rangle)$ is completely trapped in the non-percolated walk. An example state contributing to the complete trapping of this state is shown in FIG 4.31. It is

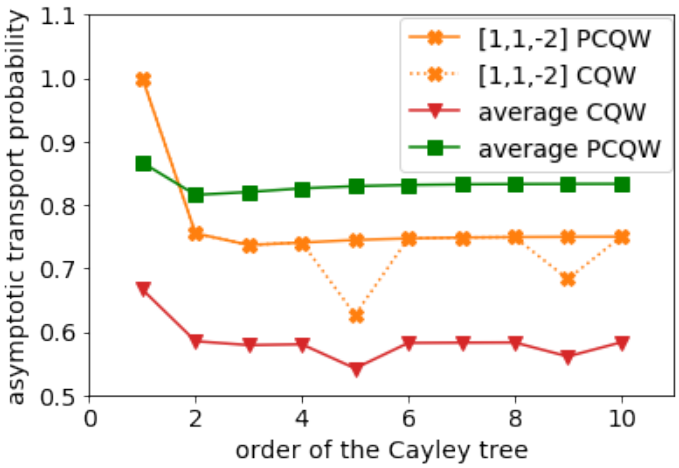

FIG. 4.30. The average ATP for reflecting Grover PCQW (green squares) and CQW (red triangles) and the ATP for the initial state $|\psi_2\rangle = \frac{1}{\sqrt{6}}(|b_1\rangle + |b_2\rangle - 2\,|b_s\rangle)$ (orange crosses) for PCQW (solid line) and CQW (dotted line) in dependence on the order of the tree k. There are drops of the ATP for the values (orders) $k = 5$ and $k = 9$ for the initial state $|\psi_2\rangle$ given by additional trapped states. The state $|K5\rangle$ for the order $k = 5$ is depicted in FIG. 4.33. The average ATP for the CQW is reduced for the given orders by these drops and also for all orders by the fact that the state $|\psi_1\rangle$ is completely trapped due to the presence of trapped states like e.g. the one in FIG. 4.31.

actually directly visible that the initial state $|\psi_1\rangle$ can never reach the sink. It enters the two main branches with the same magnitudes and opposite signs of elements. Due to symmetry it always returns to the root vertex in this way and so the coin never maps any non-zero amplitude to the state $|b_s\rangle$.

Additional trapped states $|K5\rangle$, $|K9\rangle$, and others

Let us take a closer look at the additional trapped states causing the drops of the ATP for $k = 5$ and $k = 9$ in FIG. 4.30, which we denote as $|K5\rangle$ and $|K9\rangle$. Particularly we want to understand why such states appear only for certain orders of the tree. We also show that, as expected, similar states appear after each enlargement

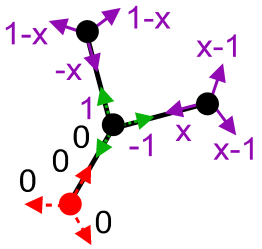

FIG. 4.31. An additional trapped state in non-percolated reflecting Grover CQW on a Cayley tree with order $k = 1$. The value of x is $x = (2 + i\sqrt{5})/3$ and it is also the corresponding eigenvalue for this state.

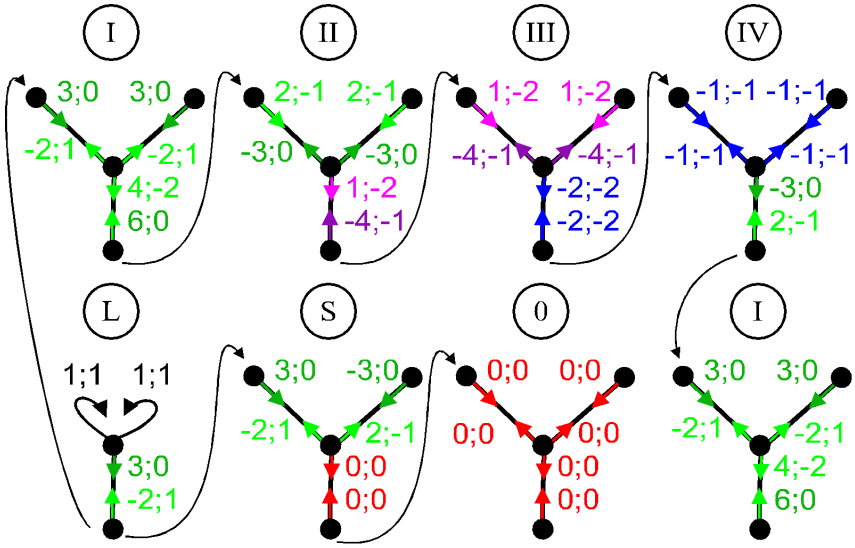

FIG. 4.32. Basic blocks forming the states $|K5\rangle$ and $|K9\rangle$. Every directed edge corresponding to a vector element is labeled by two coefficients $a;b$ indicating the value of the coefficient $\frac{a+bi\sqrt{5}}{3}$. It can be checked that by application of the reflecting shift operator and the Grover coin, the values in the central vertex of every block are transformed to x-times the original values, where $x = \frac{2+i\sqrt{5}}{3}$ is the eigenvalue of the eigenstates $|K5\rangle$ and others. There are four standard blocks I to IV, an L block with two loops used in leafs of the tree, the 0 block of all zeros and the S block allowing to connect the zero block in the sink vertex with the rest of the state. Arrows and colors indicate, how the clocks can be connected together. Important role is played by the I blocks, which can be connected to L blocks, II blocks and IV blocks.

of the tree by four orders.

Let us start with the state $|K5\rangle$. In fact, there are two complex conjugate states corresponding to the eigenvalues $x = \frac{2+i\sqrt{5}}{3}$ and $\overline{x} = \frac{2-i\sqrt{5}}{3}$. For simplicity, we just talk about the state $|K5\rangle$ as corresponding to x. The state can be understood as formed by blocks described in FIG. 4.32. The particular composition of the state $|K5\rangle$ from the blocks is shown in FIG. 4.33.

For the formation of the state $|K5\rangle$ it is important that there is the block I in the central vertex, since only this block allows connecting the same type of block (the block IV) in all directions. This is the reason why similar states are not present for orders $k < 5$. (For the order $k = 1$ the sink covers the whole sink branch of the tree and additional sr-trapped states can not be formed.)

Instead of the L blocks we can put the IV blocks in the leafs of the graph. Then we connect the whole sequence of blocks III, II and again I. From this we see how the state $|K9\rangle$ is formed and also similar states $|K13\rangle$ and others with the step of four orders.

The existence of these additional trapped states is a nice demonstration of the fact that the global structure of the underlying graph can be relevant for transport by quantum walks.

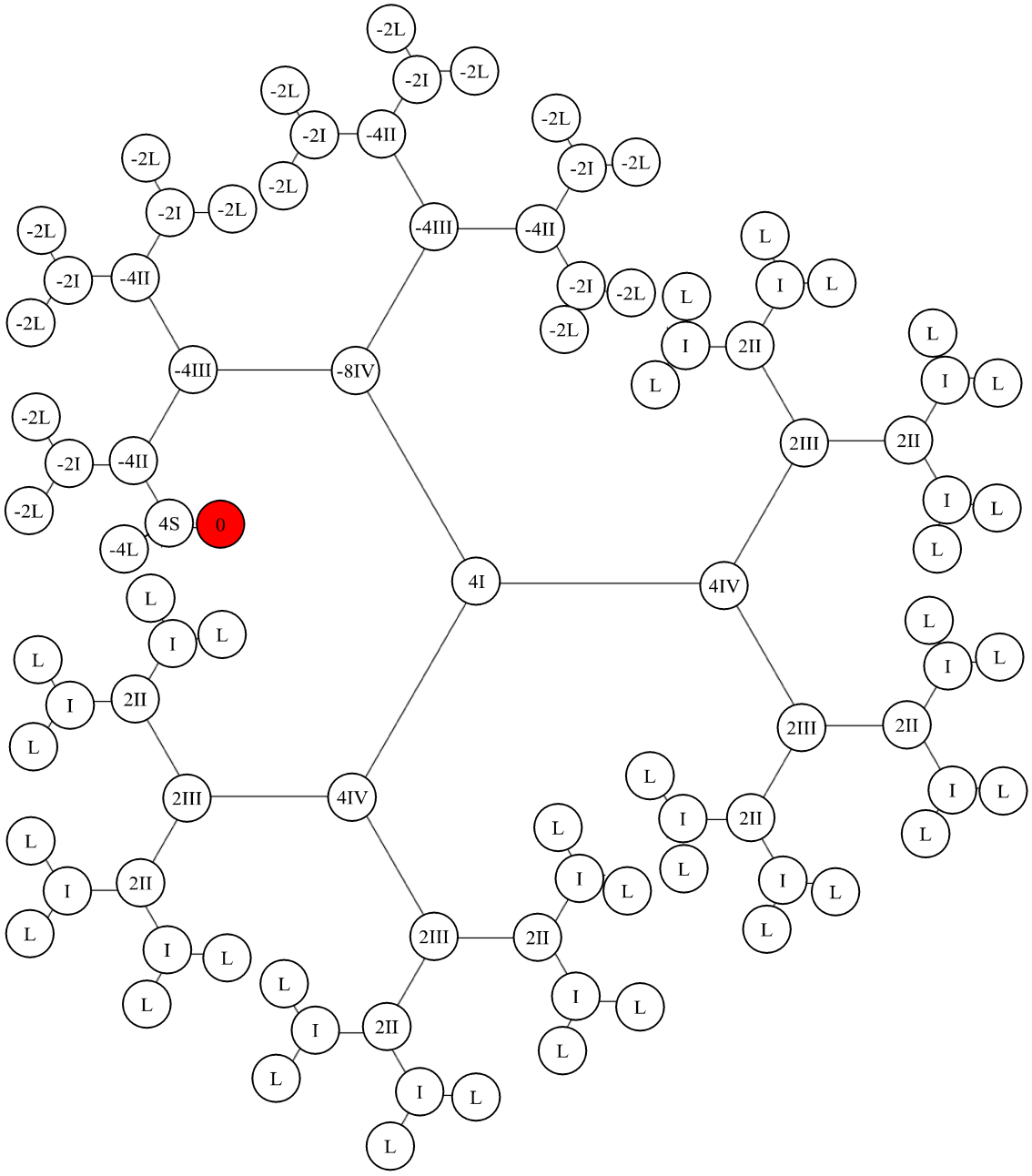

FIG. 4.33. The $|K5\rangle$ state composed from the blocks described in FIG. 4.32. Numbers before designations of the block types denote particular multiples of the blocks used in the construction of the state (before normalization). The sink vertex, where the symmetry of the sate is broken, is indicated by red color.

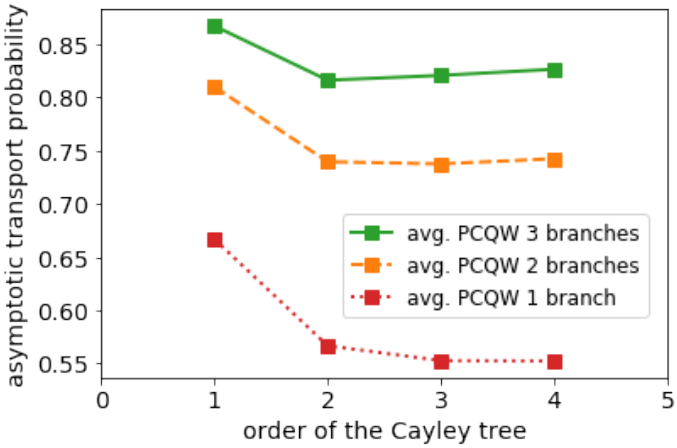

FIG. 4.34. The average ATP for reflecting Grover PCQW on a Cayley tree with all three branches (green solid line), with one non-sink branch removed (orange dashed line) and with both non-sink branches removed (red dotted line) in dependence on the order of the tree k. We see that by removing dead-end branches without the sink the ATP actually decreases, so the walker is more likely to be trapped outside of the sink.

4.5.2 Removing branches in Cayley trees

The Cayley tree graphs allow us to investigate the effect of removal of branches as indicated in FIG. 4.25. The FIG. 4.34 shows another surprising effect - the removal of dead-end branches (without sink) actually decreases the probability of the walker being transported from the root vertex to the sink. This is in a direct contrast to the standard expectation. One would think that removing the possibility of the walker wandering in a dead-end branch would increase transport efficiency. The explanation is similar as for the increase of the ATP with the order of the tree. Here, by removing a branch the trapped states overlapping with the initial subspace $\mathcal{H}_i$ loose a lot of coefficients out of $\mathcal{H}_i$ and the whole weight lies on the loop in the root vertex, which increases trapping.

While in PCQWs the removal of branches decreases the ATP, for CQWs this is not always the case. As seen in FIG 4.35 for the state $|\psi_1\rangle$ the removal of one branch breaks the symmetry of the walk and the ATP increases to non-zero values in CQW. By removing the other non-sink branch the symmetry is restored and the ATP drops back to zero. (For the walk with both non-sink branches removed the initial state $|\psi_1\rangle$ is actually directly a trapped state on a pair of loops.)

We see again an overall increase of the ATP with growing order in the variant with one branch removed. Nevertheless, the CQW has a richer set of trapped states and the development of the ATP is actually not monotonous.

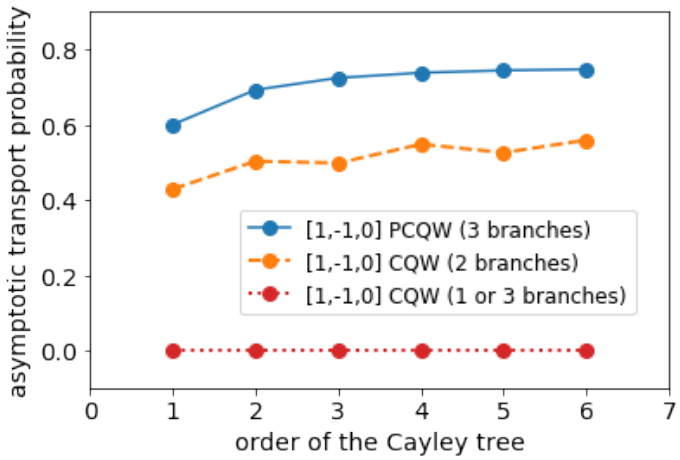

FIG. 4.35. The ATP for reflecting Grover quantum walk on a Cayley tree with the initial state $|\psi_1\rangle = \frac{1}{\sqrt{2}}(|b_1\rangle - |b_2\rangle)$ for a PCQW (blue solid line) and CQW on a tree with one non-sink branch removed (orange dashed line) and CQW on a tree with all three branches or with both non-sink branches removed (red dotted line, the values are the same) in dependence on the order of the tree k. For CQW the removal of a branch can both increase and decrease the ATP. Also the variant with one removed branch proves that the ATP can grow with the order in the CQW.

Conclusions

Quantum walks represent a simple yet very versatile model allowing the study of various non-classical properties of quantum systems. In this work we investigated discrete quantum walks disrupted by so called dynamical percolation.

There are several ingredients constituting a specific quantum walk. First, there is a distinction in the time resolution. In analogy with the classical random walks there are time-continuous quantum walks and time-discrete quantum walks. In the present work we dealt only with discrete quantum walks. In these walks the evolution is described by a successive application of discrete evolution operators on the state of the quantum walker.

Second, there is the medium in which the quantum walker is moving. It is described by the abstract object of a graph - a set of sites called vertices with some pairs of them connected by edges. (Concepts from the mathematical theory of graphs used in this work are presented in Appendix A.) There are multiple ways how the state of the walker can be related to the components of the graph underlying a quantum walk. The requirement of unitarity of the evolution does not permit to just identify base states in the walker's Hilbert space with the vertices of the graph. The standard approach is to introduce a Hilbert space associated with vertices as so called position space and add a coin space. The coin space represents an additional quantum degree of freedom joined with the walker and its base states are associated with directions of the walker's movement. The main drawback of this approach is that it can only be used on regular lattices, like the line or a square lattice, where the global directions associated with the coin states can be used in all vertices. For example the honeycomb lattice is not of this kind as it is not possible to continue in a direction of a given edge in the neighboring vertex. The so called scattering quantum walk utilizes another approach allowing to overcome this obstacle. It uses a directed graph where vertices are connected (usually in both directions) by directed arcs and these correspond to the base states of the walker. An important part of this work is a modified definition of a discrete quantum walk presented in Chapter 1, which combines concepts of coined and scattering quantum walks. We identify states of the walker with edges in a directed graph, but still use a coin operator in the time evolution. This allows both to define such quantum walk on a large class of general graphs and to investigate various types of evolutions given by different coins.

Another aspect defining a quantum walk is the way in which the shift operator moves the walker among vertices of the graph. Usually, one of the following two options is chosen without much discussion: On regular lattices allowing for continuation in

a given direction the shift operator usually moves the walker to a the neighboring vertex and leaves the coin state unchanged. On more general graphs usually a reflecting (flip-flop) shift operator is used – it moves the walker to the neighboring vertex and changes the coin state to the one pointing back towards the original position. In our modified definition presented in Chapter 1 we introduced the concept of local permutations – the shift operator is composed of the subsequent actions of the reflecting shift operator and a permutation operator shuffling states corresponding to edges in vertices locally. This approach allows for a convenient classification of all admissible shift operators on different graphs. We used our definition to study discrete quantum walks disrupted by dynamical percolation. In such processes in every step during the walk only a subset of edges in the graph is chosen to be open for this step and the remaining edges are closed not allowing the walker to traverse between vertices. The concept of local permutations allows for a direct introduction of dynamical percolation in quantum walks with arbitrary shift operators. Without local permutations it can be rather non-trivial to adequately modify the shift operator in case of broken edges in the graph. In our approach the modified shift operator results directly from the formalism.

Our approach differs from the standard one in the ordering of the coin and shift operations in the evolution step. In contrast to classical random walks (but without any trouble for quantum walks) we mostly first apply the shift operator and then the coin operator. Obviously, the evolution does not differ too much as the coin operation is then followed by the shift in the next step and so on. The difference may be more dramatic when e.g. a projective measurement is introduced in each time step (in our case representing transport to a sink). Changing the order of the coin and the shift operation turns out to be very convenient for our investigation of time-asymptotic evolution of percolated quantum walks. Further, it reveals a tight relationship between the choice of the coin and the choice of the shift operator. In particular, a walk with arbitrary shift operator can be thought of as a walk with the reflecting shift operator and a coin modified accordingly. Importantly, we presented how our results can often be used to answer the same questions in quantum walks with the standard order of operations, where the coin is applied first.

In Chapter 2 we presented an approach for the investigation of the time-asymptotic evolution of dynamically percolated quantum walks. The central part is the search for so called attractors, which define the asymptotic evolution of systems governed by random unitary operations. Percolated quantum walks represent an example of such system since for every step of the walk a configuration of the percolation graph and the corresponding evolution operator is chosen randomly. In the case of quantum walks it is possible to use the separation of the evolution operator into the coin operator and the shift operator and break up the search for attractors into two steps: There is a local coin condition specified by the choice of the coin and the local permutation determining the form of basal matrix blocks. Those are then joined together according to the shift condition, which is given by the graph structure. A further and in fact fundamental simplification of the search is possible using so called p-attractors. Those are attractors formed from states which are common eigenstates of all the evolution operators for all possible configurations of the percolation graph simultaneously. We used this procedure heavily in the subsequent

chapters. In fact, in all our studied cases of percolated quantum walks the asymptotic dynamics is given purely by p-attractors and the maximally mixed state as the only remaining independent non-p-attractor. For some of the investigated walks our proofs of this property are not included in this dissertation as they are lengthy and were published in [38]. We gave a new proof for one version of lazy percolated quantum walk explicitly in Chapter 3 to demonstrate the general approach.

We modeled the transport by quantum walks. For that we introduced an absorbing sink at some position in the graph and extended every step of the walk by a projective measurement to determine if the walker has already reached the sink. The formal definition of the sink and its incorporation into the time evolution was given in Chapter 1 and its influence on the asymptotic behavior was discussed in Chapter 3. The interference in quantum walks allows for the existence of the non-classical phenomenon of asymptotic trapping. In some cases the walker can stay trapped in the graph avoiding the sink indefinitely. Therefore, it is reasonable to study the asymptotic transport probability (ATP) that the walker is transported to the sink. Mathematically, the trapping is caused by eigenstates of the dynamics with limited support on the graph. We call those trapped states and their subset additionally having zero overlap with the sink sr-trapped states (sink resistant).

In Chapter 3 we focused our attention to discrete quantum walks with the Grover coin on 3-regularized graphs. The Grover coin is heavily used in research for its symmetry and applicability for arbitrary dimension of the coin space. The choice of 3-regular graphs is natural as in contrast to 2-regular graphs the family of 3-regular graphs is very rich and contains a multitude of very non-trivial structures with examples described in Appendix A. We investigated three choices of the shift operator in combination with the Grover coin: the simple reflecting shift operator, a class of shift operators resulting from arbitrary distributions of local rotations and the swapping shift operator used in the lazy quantum walk. For the reflecting Grover percolated quantum walks we presented in detail a general procedure for construction of the subspace of common eigenstates (used for the construction of p-attractors and the whole asymptotic dynamics) for arbitrary planar 3-regularized graphs. This allows the identification of all the trapped states and the calculation of the ATP (after orthonormalization of the trapped states, which can be performed at least numerically). For cyclic Grover percolated quantum walks we presented a relation between an edge-3-coloring of the underlying graph and non-stationarity of the asymptotic evolution of the walk. In particular, we showed how an edge-3-coloring of the graph induces a distribution of local rotations with which the percolated quantum walk exhibits 3-step cycles in the asymptotic dynamics. In the remainder of Chapter 3 we investigated the lazy Grover percolated quantum walk with the standard shift operator (keeping the walker's direction to the left/right after a displacement). We identified all the common eigenstates (and so all the trapped states) and even provided recursive relations allowing for a direct calculation of the average ATP (without the need for a numerical orthonormalization of the common eigenstates) for transport from one side of the chain graph to the other. In this simple model we just observe a decrease of the average ATP with the length of the chain given by the presence of additional trapped states.

The main application of our theoretical results is presented in Chapter 4. We applied our methods to several types of example graphs ranging from the lazy walk on a line through the ladder graph towards carbon nanotube structures and the Calyley trees. In all cases we investigated transport in reflecting Grover quantum walks, for which the recipe for construction of trapped states was given in Chapter 3. We primarily investigated percolated versions of the walks, but also obtained results for walks without percolation numerically. For this the insights from percolated walks are very advantageous since all the trapped states in percolated walks are also trapped states in non-percolated walks. Therefore, the understanding of the percolated version allowed us to identify interesting scenarios for numerical studies. Primarily, we were able to choose interesting placements of the sink and the initial position of the walker and also the particular initial states.

With growing complexity of the graphs more and more transport phenomena arising from changes of their structure parameters occur. For the lazy walk the transport is the same for percolated and non-percolated walks and we just observed a monotonous decrease of the ATP which levels to a certain value exponentially fast with growing length of the chain. This is in a tight analogy with the results for the lazy quantum walk with the standard shift operator from Chapter 3 and the difference is purely quantitative. For the ladder graph the same behavior can be seen if we choose both the initial state and the sink to be on the pairs of loops on ends of the ladder. Nevertheless, when we use a one-vertex sink, a trapped state spreading over the whole length of the ladder is sr-trapped. This leads to probably the most interesting and counter-intuitive result of this work – the ATP for the ladder with one-vertex sink actually grows with the length of the ladder. This is very unexpected as the walker is more likely to traverse a longer ladder than a shorter one. We also explained the source of this effect using the knowledge of trapped states. Analogous effect was actually also found in walks on carbon nanotube structures and Caley trees. For Cayley trees there is another similar phenomenon that the ATP can be decreased by removing dead-end (without sink) branches of the graph. For nanotubes we further presented some quantitative observations as is the dependence of the ATP on the chirality of the tube. For all cases we also investigated the non-percolated version of the walks. As the percolation can only remove trapped states from the asymptotic regime, the ATP in non-percolated walks can be the same or lower compared to percolated walks. There are no additional trapped states in non-percolated lazy walks and in walks on the ladder there is just one additional type of states, which can be identified completely. For both nanotubes and Cayley trees there are multiple additional trapped states bringing high complexity into the dependence of the ATP on structure parameters of the graphs. We identified and presented some examples of such states. In walks on nanotubes some of the trapped states only appear for some combinations of the chirality and length resulting in sudden drops of the ATP. Examples of these states were described. We also investigated in detail trapped states only appearing for Cayley trees of orders $k = 5 + 4m$. Overall, there is no general analytical procedure for determination of trapped states in non-percolated quantum walks, but with our results for percolated walks we were able to find interesting effects also there.

A natural place to look for actual systems which could exhibit dynamics similar

to those investigated in the present work is in the field of macro-molecules. Such systems are just at the right level where on one hand quantum coherences are still possible and on the other hand complex structures appear. Further, these structures formed by atoms connected by chemical bonds are perfect for representation by graphs. Clearly, the carbon nanotube structures used in the work are directly motivated by the actual carbon nanotubes occurring in nature. Nevertheless, particularly in biological systems, much more sophisticated structures than those investigated here can be found. As coherent excitation transport was observed in photosynthetic macro-molecules and can also play a role in some synthetic polymers, it is of relevance to tackle more complex structures. In this regard, our results can be directly applied for the study of any other planar 3-regularized graphs. Admittedly, many of the relevant structures will contain vertices of degree higher than three. For example already the square lattice has vertices of degree four or one might want to investigate aggregates of simple molecules with higher degree vertices at the junctions. Technically, the definitions for both standard and percolated walks can be used directly and also the procedures of the search for attractors can be reused for arbitrary graphs. Nevertheless, even for the reflecting Grover walk it must be proven that there are no additional non-p-attractors if we are to calculate the ATP from common eigenstates. (Or it must be disproven and in such case different approaches need to be developed.) A big step forward in this regard and a convenient followup of this work would be identification of some general aspects of the graph, the coin or the shift operator which would guarantee this property. In either case, the construction of common eigenstates presented here can be used with some modification. Clearly, also different choices of the coin/shift operator can be investigated to search for other effects or to get a better idea of the range of scenarios in which the effects presented here can occur.

It is also possible to find structures playing the role of a sink in the world of macro-molecules. The photosynthetic reaction center acts as a sink for quantum transport absorbing the excitation whenever it enters. Some phenomena similar to trapping in quantum walks described in this work could both hinder and enhance transport of energy into the reaction center. On one hand, it could reduce the efficiency of transport by keeping the excitation away from the reaction center, but on the other hand, it could also keep the excitation in the vicinity of the center until the excitation is eventually absorbed. Another thinkable structure effectively acting as a sink on the molecular level could be some large structure (e.g. a very long chain of atoms) connected to our system of interest by a narrow link. Once traversing the link, the walker could effectively be lost from our system. In such cases the sink could be placed basically anywhere in the system of interest and so it is important to have tools at hand capable of determining the transport efficiency for arbitrary placements of the sink.

With respect to the percolation, it is notable that polymers can even exhibit dynamical changes of covalent bonds [57], so it is possible that the network of links allowing spreading of excitations in these systems undergo changes during transport. The observed changes are, nevertheless, typically on time scales much larger than those for which quantum coherence is preserved. In this regard it could be beneficial to focus more on utilizing the results for percolated walks to gain deeper insights in

the transport properties of non-percolated quantum walks. While percolated quantum walks represent a model of a significant interest and importance on its own, when concerning applications they should primarily contribute to the understanding of the big picture of quantum walks and quantum systems in general.

Appendix A

Fragments from the mathematical theory of graphs

A.1 Definitions of graphs

A.1.1 Simple undirected, directed and mixed graphs

An abstraction of networks of various kinds can be described by the mathematical theory of *graphs*. Depending on the nature of the network we want to describe, various types of graphs can be used and these graphs can have various distinct properties. Here we present fragments of the graph theory as an extension of the appendix of [38] based on the textbook [50].

A graph consists of a set of discrete nodes or *vertices* $v \in V$. We denote the number of vertices in a graph as $\#V$. These can represent arbitrary entities from cities over agents in communication networks all the way to energy levels in quantum systems.

Connections among vertices are represented by so called *edges*. Edges connect pairs of vertices or in some cases begin and terminate in the same vertex. Such edges are called *loops*. The two main kinds of edges are given by the directionality – *undirected edges* $e \in E$ represent a symmetrical connection and *directed edges* $e^{(d)} \in E^{(d)}$ have a given beginning vertex and an end vertex. Directed edges connecting two distinct vertices are also called *arcs*. We denote the numbers of undirected and directed edges as $\#E$ and $\#E^{(d)}$ respectively. Two vertices connected by an edge are said to be *adjacent*.

Here we assume all the sets of vertices and edges to be at most countably infinite. Moreover, most of the results in this work only address graphs with both the number of vertices and the number of edges finite.

We use the terms *undirected graphs* and *directed graphs* for graphs only having undirected and directed edges respectively. In this work we even use so called *mixed graphs* with some undirected and some directed edges.

Graphs can also have *parallel edges* – multiple edges connecting the same pair of

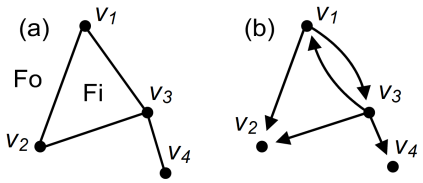

FIG. A.1. Planar representations of example graphs with four vertices $V = \{v_1, v_2, v_3, v_4\}$: (a) an undirected graph with undirected edges $E = \{\{v_1, v_2\}, \{v_2, v_3\}, \{v_3, v_1\}, \{v_3, v_4\}\}$ and (b) a directed graph with directed arcs $E^{(d)} = \{(v_1, v_2), (v_1, v_3), (v_3, v_1), (v_3, v_2), (v_3, v_4)\}$. Also the two faces (one standard inner face Fi and the outer face Fo) are labeled in (a).

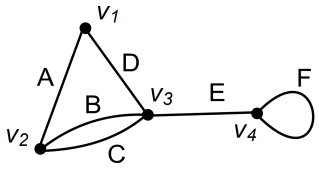

FIG. A.2. Example of a non-simple undirected graph with four vertices $V = \{v_1, v_2, v_3, v_4\}$, standard edges A, D, E, a loop F, and a pair of parallel edges B, C.

vertices (and in the same direction for directed edges). If there are no parallel edges and no loops in a graph, the graph is so called *simple*. The description of simple graphs truly is simple for the following reason: Undirected edges $e \in E$ are given by unordered pairs of vertices $e = \{v_1, v_2\} = \{v_2, v_1\}$, where $v_1, v_2 \in V$ and directed edges $e^{(d)} \in E^{(d)}$ are represented by ordered pairs $e^{(d)} = (v_1, v_2)$ for $v_1, v_2 \in V$. In contrast, for non-simple graphs edges have to be given distinct labels in general. An exception relevant for this work are directed graphs without parallel edges and with at most one loop in every vertex. Here the loop can be represented by the pair (v, v) for $v \in V$ and all the arcs are represented by pairs of vertices unambiguously. An example of a simple undirected graph is shown in FIG. A.1 (a) and an example of a simple directed graph in FIG. A.1 (b). An example of a non-simple graph is presented in FIG. A.2.

A.1.2 Degree of a vertex and regular graphs

Every vertex in a graph has a particular *degree*, which is the number of edges connected to that vertex. For example, the vertices v_1, v_2, v_3 and v_4 in FIG. A.1 (a) have degrees 2, 2, 3 and 1 respectively. In directed graphs we distinguish the *in-degree* (the number of edges ending in a vertex) and the *out-degree* (the number of edges beginning in a vertex). In this work we only work with directed graphs where the in-degree and out-degree is the same for every vertex, and so we simply use the term degree.

We denote the degree of a vertex $v \in V$ as $\mathrm{d}(v)$ and the maximal degree among vertices in a graph as Δ. If the degree of all vertices in a graph is the same number k, so $k = \Delta = \mathrm{d}(v)\ \forall v \in V$, the graph is said to be *regular* and in particular *k-regular*.

A.1.3 Planar embedding and planar graphs

The examples in FIG. A.1 are in fact not the graphs themselves but particular embeddings of the graphs into a plane. While graphs are abstract objects, their planar representation is often used to define them. Typically this does not cause problems. Nevertheless, caution is required since the embedding carries more information than the graph itself. It can be e.g. used to prevent ambiguity of labeling of vertices or edges. For example, at one point we use the planar embedding to fix the meaning of clock-wise and counter-clock-wise permutations of edges in vertices.

For any graph there exist an infinite amount of possible embeddings. On the other hand, it is often of interest if a graph is co called *planar* – it can be drawn into a plane without any crossing of edges. That is the case for both examples in FIG. A.1. An example of a non-planar graph is the so called complete bipartite graph $K_{3,3}$ shown in FIG. A.3.

Planar graphs can represent convex polyhedra like the cube or a dodecahedron. A planar embedding of the cube graph is shown in FIG A.8. From these the concept of *faces* is generalized to all planar graphs. Faces are defined as segments of the embedding plane bordered by edges which are not further separated by other edges. Somewhat less intuitive is the *outer face* - the rest of the plane outside of the graph. We denote the number of faces in a graph as $\#F$ (including the outer face). Examples of faces are shown in FIG. A.1 (a). In this work we will not need a definition of faces in directed or non-simple graphs.

For simple planar graphs a generalization of the Euler's polyhedron formula holds, which can be stated in terms of the graph theory as

$$\#V + \#F - \#E = 2, \tag{A.1}$$

where $\#V$ is the number of vertices, $\#F$ the number of faces (including the outer face) and $\#E$ the number of edges of the graph.

A.1.4 Coloring graphs

Some real-world problems can be transformed to the abstract problem of coloring vertices or edges of some graph. A direct example arises if we want to create a political map and ask, how many different colors are needed. Here the countries are vertices of a graph connected by edges between neighboring countries. The requirement is so that neighboring countries always have different color in the final map, therefore, we search for a coloring with different color for any adjacent vertices.

The example above used vertex-coloring of a graph. In this work we utilize the complementary task – an edge coloring of a graph, in our case coloring of undirected graphs. Here we search for a coloring of edges in which edges of the same color never meet in one vertex. For a graph in which the maximal degree of a vertex is Δ Vizing's theorem ensures the existence of a coloring by at most $\Delta + 1$ colors. An interesting question than is, whether for the given graph a coloring by Δ colors exists.

A.1.5 Walks and paths on graphs

Let us introduce some terminology for particular types of sequences of vertices and edges in graphs. Let us start with undirected graphs. The most general is a *graph walk*[1] which is an alternating sequence of vertices and edges beginning and ending by a vertex. Clearly, it is required that every vertex in a graph walk is followed by an edge connected to this vertex and also every edge is followed by a vertex that it leads to. For directed and mixed graphs the definition of a graph walk is analogous, just with the additional requirement of respecting the directionality of directed edges.

Further, there are some useful special cases. If the first and the last vertex of a graph walk coincide, the graph walk is *closed*. A closed graph walk where the first/last vertex is the only one repeating is called a *cycle*. A graph walk without any repeating vertices is called a *path*.

All kinds of graph walks can be *odd* or *even* depending on the number of edges covered, where repeating edges are counted multiple times.

We give some examples using the graph in FIG. A.2, because here we can denote the edges more easily than on the graphs in FIG A.1. The sequence (v_1, A, v_2, B, v_3) is an even path, so also an even graph walk. The sequence $(v_1, A, v_2, B, v_3, D, v_1)$ is an odd cycle, so also an odd closed graph walk. The sequence $(v_1, A, v_2, B, v_3, C, v_2, A, v_1)$ is an even closed graph walk but not a cycle. The sequence $(v_1, A, v_2, B, v_3, C, v_2)$ is jsut an odd graph walk. Finally, the sequences (v_1, E, v_3), (A, v_2, B) are not even graph walks.

Graphs used in this work are most often assumed to be *connected*. A graph is connected if and only if there exist a path from every vertex to every other vertex.

In this work we utilize a special kind of graph walks on mixed graphs. In particular, these mixed graphs have undirected edges and directed loops. We define a *capped graph walk*. (This specialized object is not a part of a standard graph theory.) A capped graph walk is a standard graph walk on vertices and undirected edges in a mixed graph, which is capped at the beginning and at the end by directed loops.

A.1.6 Some other types of graphs

A graph is *bipartite*, if its vertices can be split into two disjoint groups so that there are no intra-group edges in the graph. Equivalently, a graph is bipartite if and only if it has no odd cycles. An example of a bipartite graph is shown in FIG. A.3, but also e.g. the graphs of a cube in FIG. A.8 or a honeycomb lattice in FIG. A.10 are bipartite.

A connected graph is called a *tree*, if there are no cycles in the graph.

[1] Usually, in graph theory, this object is just called a *walk*. Here we use the tern *graph walk* for clarity, since the majority of the text using these terms deals with random and quantum walks.

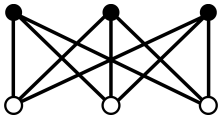

FIG. A.3. Planar representation of the complete bipartite graph $K_{3,3}$. The bipartition of the graph is depicted by the colors of vertices: black and white. As the graph is not planar, there will always be some crossing edges in its planar embedding.

FIG. A.4. Example of a finite line graph with $\#V = n = 5$ vertices.

A.1.7 3-regularized graphs

In Section 1.4 of the main text we define quantum walks on graphs. This definition is based on an undirected graph. Then we construct a directed graph with the same set of vertices by replacing every undirected edge with two directed edges in opposite directions. Further, we add some directed loops.

Our aim is to obtain a 3-regular directed graph so we add loops to vertices of degree lower than 3. We call graphs obtained in this manner *3-regularized*.

A.2 Example graphs

Here we describe some particular examples of graphs used in this work. To prepare these for our use, we typically display an undirected graph and then a 3-regularized mixed graph obtained by adding directed loop as described in section A.1.7.

A.2.1 Line (chain) graph

Probably the simplest non-trivial graph on which we can define dynamics given by either random or quantum walk is a *line graph*. (The term *chain* is probably more adequate, but line is used more in the literature.) Typically, the graph is represented with vertices aligned along a line with only the nearest neighbors being connected by an edge as illustrated in FIG. A.4.

A 3-regularized version of the line graph is obtained by adding one loop in every inner vertex and two loops in border vertices. This graph is used for so called lazy quantum walk [29] introduced in Section 3.3.3 and is illustrated in FIG. A.5.

The line graph can also be enclosed into a cycle, but we do not investigate these

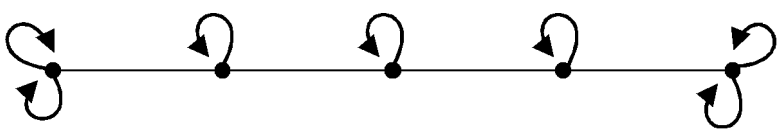

FIG. A.5. Example of a finite 3-regularized line graph with $\#V = n = 5$ vertices.

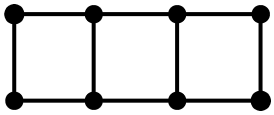

FIG. A.6. Example of a ladder graph of length $L = 3$.

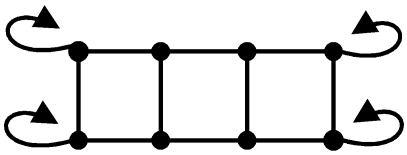

FIG. A.7. Example of a 3-regularized ladder graph of length $L = 3$.

graphs here.

A finite line graph is parameterized just by the number of vertices $\#V = n$ and it has $\#E = n - 1$ undirected edges.

A.2.2 Ladder graph

The *ladder* graph can be constructed by placing two line graphs in parallel and adding perpendicular edges as shown in FIG. A.6. As the inner vertices already have three neighbors, the 3-regularized version only has one loop in every vertex on each end of the ladder as seen in FIG. A.7.

The ladder is parameterized by the number of square faces denoted as its length $\#F = L$. Such graph has $\#V = 2L + 2$ and $\#E = 3L + 1$.

A.2.3 Planar 3-regular graphs representing convex polyhedra

Convex polyhedra can be represented as simple planar graphs. In FIG. A.8 we present a planar embedding of the cube graph. Note, how one of the faces of the cube forms the so called outer face – the rest of the plain.

The cube graph is already 3-regular, so there is no need for 3-regularization. The cube graph is also bipartite, which is indicated in FIG. A.8.

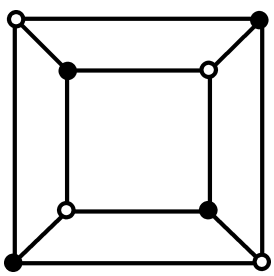

FIG. A.8. Planar embedding of the cube graph. A bipartition of the graph is indicated by black/white vertices.

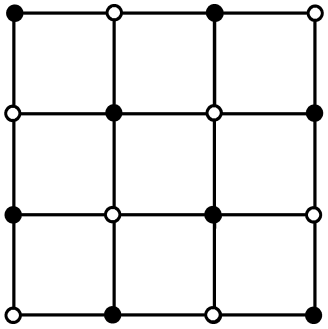

FIG. A.9. Example of a finite square lattice. A bipartition of the graph is indicated by black/white vertices.

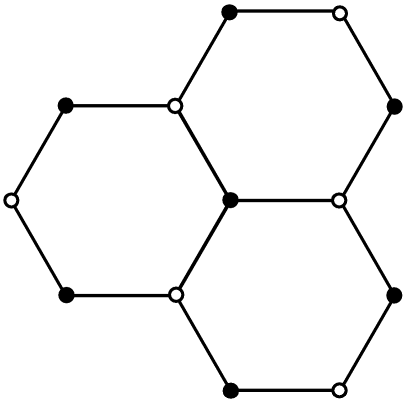

FIG. A.10. Example of a finite honeycomb lattice. A bipartition of the graph is indicated by black/white vertices.

The cube has $\#V = 8$, $\#E = 12$ and $\#F = 6$, which is in agreement with the Euler's formula (A.1).

A.2.4 Regular lattices

There are only three so called regular tessellations of the plane - only three possible regular polygons that are able to cover the whole plane without overlapping. Obviously, one of them results in the square lattice as shown in FIG. A.9.

The remaining two options are triangular and hexagonal or *honeycomb* lattices. (These are complements of each other if faces are understood as vertices.) An example of a small finite honeycomb lattice is shown in FIG. A.10 and an example of a finite triangular lattice in FIG. A.11.

The square and honeycomb lattices are bipartite, while the triangular lattice is not.

The square lattice has $\Delta = 4$ and the triangular $\Delta = 6$. Therefore, those can not be 3-regularized by adding edges and in this work we are particularly interested in the honeycomb lattice. The 3-regularized version of the graph in FIG. A.10 is presented in FIG. A.12.

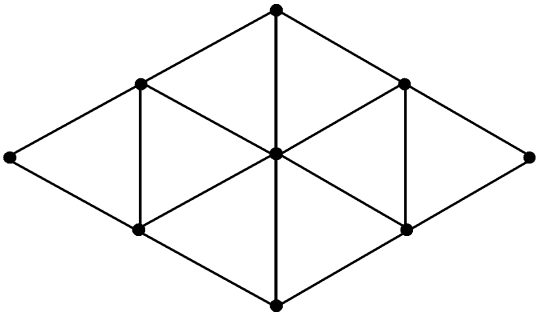

FIG. A.11. Example of a finite triangular lattice. This graph is not bipartite, since e.g. the neighbors of the central vertex are connected by edges.

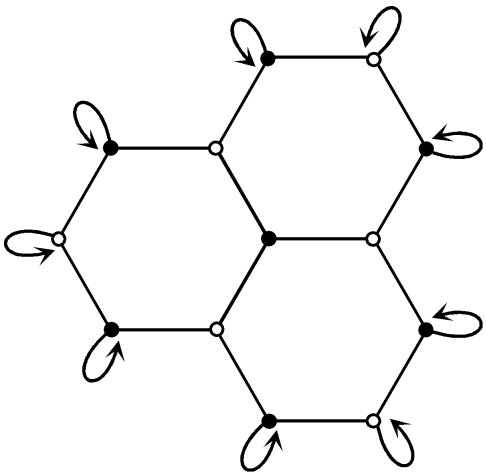

FIG. A.12. Example of a 3-regularized finite honeycomb lattice. A bipartition of the graph is indicated by black/white vertices.

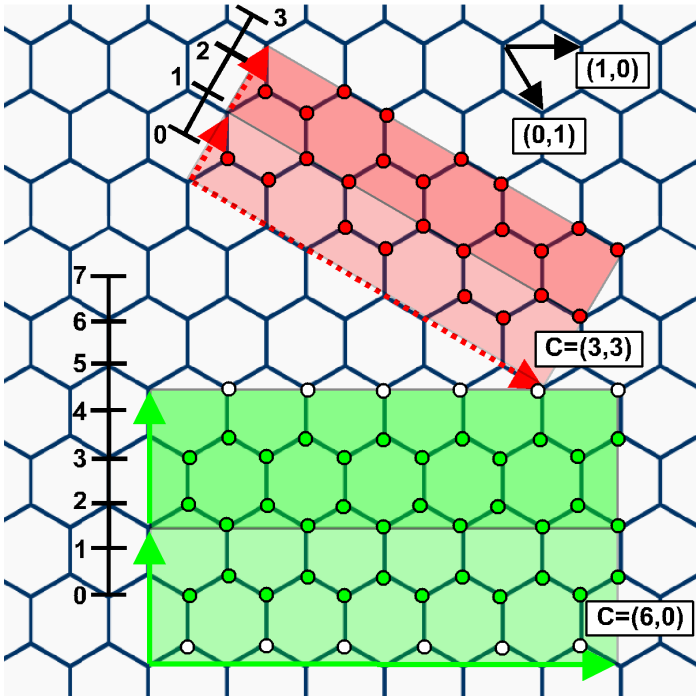

FIG. A.13. Explanation of the chirality of nanotubes. The figure shows the base vectors $(1,0)$ and $(0,1)$ (solid black arrows) in the non-orthogonal basis, the chirality vectors $(3,3)$ (dotted red arrow) and $(6,0)$ (solid green arrow) with two basal length segments each and scales showing the length of the tube measured as the multiple of the neighboring sites distance. The vertices laying on the arrows as well as the white vertices of degree one for $(n,0)$ chiralities are not included in the tube.

A.2.5 Carbon nanotube structures

Layers of the honeycomb lattice, which are naturally occurring as graphene, can be folded into tubular structures of carbon nanotubes. The actual existence of carbon nanotubes makes investigation of the corresponding graphs very relevant.

There are multiple ways in which a sheet of a honeycomb lattice can be folded into a tube. These are represented by the so called *chirality*, which is given by a pair of integers (m,n). In this work we only investigate two special cases: so called *zig-zag* tubes with chiralities $(n,0)$ and *armchair* tubes with chiralities (n,n). These integers define a vector in the non-orthogonal basis on the honeycomb lattice as shown in FIG. A.13. The chirality vector then defines the circumference and the orthogonal vector represents the axial direction of the tube.

For every chirality (m,n) there is a basal length segment, which is repeated in the axial direction of the tube. The length of this segment varies (rather non-trivially) with the chirality. The basal length segments are shown in FIG. A.13. To be able to compare zig-zag and armchair tubes in plots, we measure the length of the tube with the unit of the distance between neighboring sites instead of in the number of basal length segments. It is also notable that (n,n) tubes should be compared to $(2n,0)$ tubes, as those have the same number of vertices in the circumference. Examples of the $(3,3)$ and $(6,0)$ tubes are given in FIG. A.14.

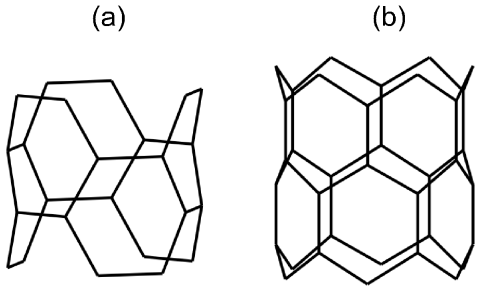

FIG. A.14. Examples of: (a) the $(3,3)$ armchair and (b) the $(6,0)$ zig-zag tubes both with two basal length segments.

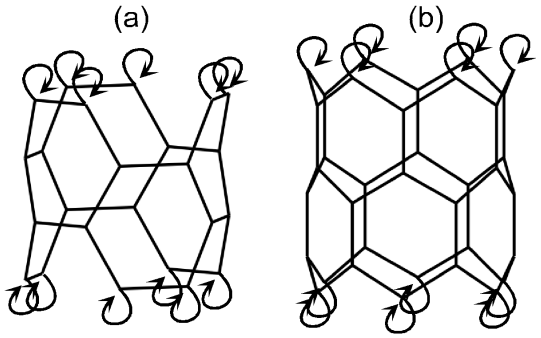

FIG. A.15. Examples of: (a) the $(3,3)$ armchair and (b) the $(6,0)$ zig-zag tubes both with two basal length segments after 3-regularization.

In the process of 3-regularization of tube graphs we just add loops in the vertices on both ends of the tube. In particular, there are $2n$ loops on each end of both (n,n) and $(2n,0)$ tubes. Examples are shown in FIG. A.15.

It is of importance that the graphs of carbon nanotube structures are planar. A planar embedding can be obtained by placing the tube orthogonally to the plane and extending e.g. its top end. An example for the $(6,0)$ tube from FIG. A.14 (b) is shown in FIG. A.16. Further, we also use the fact the inner face and the outer face have even number of edges. In particular, those have $4n$ edges in both (n,n) and $(2n,0)$ tubes, but the number is even also for all other chiralities. This is seen from ideas published in [49]: The tube is created by joining the beginning and the end of the chirality vector. Therefore, the inner and the outer face are given by a path connecting these two points in the honeycomb lattice. The chirality vector is composed from basal vectors, which both represent a path of length two. When we combine this with the fact that every modification of a path in the hexagonal lattice replaces some number k of edges with $6-k$ others, we see that the path always has even length.

A.2.6 Cayley trees

Cayley trees are very symmetrical trees constructed in the following way: a Cayley tree of order $k=0$ is just one vertex. Then we add certain number of vertices n, in our case $n=3$, and connect them to the first vertex to obtain a Cayley tree of the

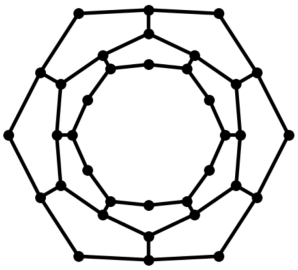

FIG. A.16. A planar embedding of the $(6, 0)$ tube from FIG. A.14 (b), which demonstrates its planarity.

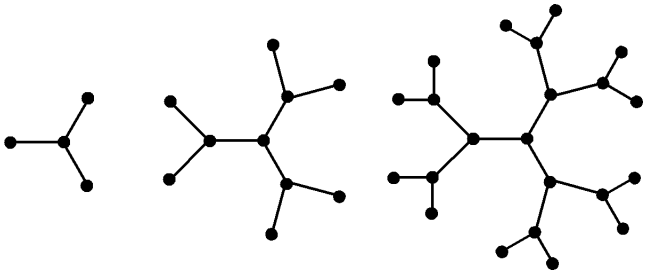

FIG. A.17. Examples of Cayley trees of orders $k = 1$, $k = 2$ and $k = 3$ respectively with $n = 3$.

order $k = 1$. The new vertices with degree one are called *leafs* of the graph. Next and for every other k we connect $n - 1$ new vertices, in our case two, to every leaf vertex. Examples for orders 1 to 3 are shown in FIG. A.17.

A 3-regularized version of a Cayley tree is simply obtained by adding $n - 1$ loops to very leaf vertex as demonstrated in FIG. A.18.

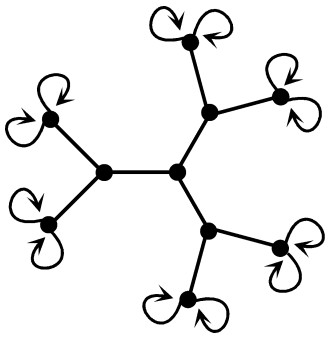

FIG. A.18. A 3-regularized Cayley tree of the order $k = 2$ with $n = 3$.

Literature

[1] B. D. Hughes. Random Walks and Random Environments, Vol. 1: Random Walks. *Oxford Univ. Press*, 1995.

[2] B. D. Hughes. Random Walks and Random Environments, Vol. 2: Random Environments. *Oxford Univ. Press*, 1995.

[3] G. H. Weiss and R J. Rubin. Random Walks: Theory and Selected Applications in Advances in Chemical Physics, Vol. **52**. 1982.

[4] L. Bachelier. Théorie de la spéculation, *Annales Scientifiques de l'École Normale Supérieure*, **3**(17), 1900.

[5] D. J. Higham and A. Taylor. The Sleekest Link Algorithm. *Mathematics Today*, **39**, 192-197, 2003.

[6] Y. Aharonov, L. Davidovich, and N. Zagury. Quantum random walks. *Phys. Rev. A*, **48**(2), 1687–1690, 1993.

[7] A. M. Childs *et al.*. Exponential algorithmic speedup by a quantum walk in Proc. 35th Annual STOC, ACM, NY. pp. 59–68, 2003.

[8] P. W. Anderson. Absence of diffusion in certain random lattices. *Phys. Rev.* **109**, 1492–1505, 1958.

[9] J. P. Keating, N. Linden, J. C. F. Matthews, and A. Winter. Localization and its consequences for quantum walk algorithms and quantum communication. *Phys. Rev. A* **76**, 012315, 2007.

[10] N. Inui, Y. Konishi, and N. Konno. Localization of two-dimensional quantum walks. *Phys. Rev. A* **69**, 052323, 2004.

[11] M. Štefaňák, I. Jex, and T. Kiss. Recurrence and Pólya Number of Quantum Walks. *Phys. Rev. Lett.* **100**(2), 020501, 2008.

[12] M. Štefaňák and S. Skoupý. Perfect state transfer by means of discrete-time quantum walk search algorithms on highly symmetric graphs. *Phys. Rev. A* **94**, 022301, 2016.

[13] N. Shenvi, J. Kempe, and K. B. Whaley. Quantum random-walk search algorithm. *Phys. Rev. A*, **67**, 052307, 2003.

[14] A. Childs. Universal Computation by Quantum Walk. *Phys. Rev. Lett.*, **102**, 180501, 2009.

[15] N. B. Lovett *et al.*. Universal quantum computation using the discrete-time quantum walk. *Phys. Rev. A*, **102**, 042330, 2010.

[16] P. W. Shor. Polynomial-Time Algorithms for Prime Factorization and Discrete Logarithms on a Quantum Computer. *SIAM Journal on Scientific and Statistical Computing*, **26**, 1484, 1997.

[17] A. M. Childs, D. Gosset, and Z. Webb. Universal Computation by Multiparticle Quantum Walk. *Science*, **339**(6121), pp. 791-794, 2013.

[18] M. Karski, L. Föster, J Choi, A. Steffen, W. Alt, D. Mechede and A. Widere. Quantum Walk in Position Space with Single Optically Trapped Atoms. *Science*, **325**, 5937, 2009.

[19] H. Schmitz, R. Matjeschk, C. Schneider, J. Glueckert, M. Enderlein, T. Huber and T. Schaetz. Quantum Walk of a Trapped Ion in Phase Space. *Phys. Rev. Lett.*, **103**, 090504, 2009.

[20] A. Schreiber, K. N. Cassemiro, V. Potoček, A. Gábris, P. J. Mosley, E. Andersson, I. Jex and C. Silberhorn. Photons Walking the Line: A Quantum Walk with Adjustable Coin Operations. *Phys. Rev. Lett.*, **104**, 050502, 2010.

[21] H. B. Perets *et al.*. Realization of quantum walks with negligible decoherence in waveguide lattices. *Phys. Rev. Lett.*, **100**, 170506, 2008.

[22] M. A. Broome *et al.*. Discrete single-photon quantum walks with tunable decoherence. *Phys. Rev. Lett.*, **104**, 153602, 2010.

[23] V. Kendon. Quantum walk computation, AIP Conference Proceedings, **1633**, 177, 2014.

[24] K. Pearson. The Problem of the Random Walk. *Nature*, **72**(294), 1905.

[25] M. Hillery, J. Bergou and E. Feldman. Quantum walks based on an interferometric analogy. *Phys. Rev. A*, **68**, 032314, 2003.

[26] M. Szegedy. Quantum Speed-Up of Markov Chain Based Algorithms in Proceedings of the 45th Symposium on Foundations of Computer Science (IEEE Computer Society, Washington, DC, 2004), pp. 32–41, 2004.

[27] B. Venancio and F. M. Andrade. Unveiling and exemplifying the unitary equivalence of discrete time quantum walk models. *Journal of Physics A Mathematical and Theoretical*, **46**(16), 165302, 2013.

[28] T.G. Wong. Equivalence of Szegedy's and coined quantum walks. *Quantum Inf. Process.*, **16**(9), 215, 2017.

[29] N. Inui, N. Konno, and E. Segawa. One-dimensional three-state quantum walk. *Phys. Rev. E* **72**, 056112, 2005.

[30] Ch. Moore and A. Russell, in Proc. of the 6th Intl. Workshop on Randomization and Approximation Techniques in Computer Science, 2002, edited by J. D.P. Rolim and S. Vadhan, (Cambridge, MA, USA, 2002), p. 164, 2002.

[31] K. Chisaki, M. Hamada, N. Konno, and E. Segawa. Limit Theorems for Discrete-Time Quantum Walks on Trees. *Interdisciplinary Information Sciences*, **15**, 423-429, 2009.

[32] N. Konno, N. Obata, and E. Segawa. Localization of the Grover Walks on Spidernets and Free Meixner Laws. *Commun. Math. Phys.*, **322**, 667-695, 2013.

[33] Ch. Lyu, L. Yu, and S. Wu. Localization in quantum walks on a honeycomb network. *Phys. Rev. A*, **92**, 052305, 2015.

[34] H. Bougroura, H. Aissaoui, N. Chancellor, and V. Kendon. Quantum-walk transport properties on graphene structures. *Phys. Rev A*, **94**, 062331, 2016.

[35] P. C. S. Lara, R. Portugal, and S. Boettcher. Quantum Walks on Sierpinski Gaskets. *International Journal of Quantum Information*, **11**(8), 1350069, 2012.

[36] S. E. Venegas-Andraca. Quantum walks: a comprehensive review. *Quantum Inf. Process.*, **11**, 1015-1106, 2012.

[37] M. Štefaňák, I. Bezděková, I. Jex, and M. Barnett. Stability of point spectrum for three-state quantum walks on a line. *Quantum Information and Computation*, **14**, 1213-1226, 2014.

[38] **J. Mareš, J. Novotný, and I. Jex. Percolated quantum walks with a general shift operator: From trapping to transport. *Phys. Rev. A*, 99, 042129, 2019.**

[39] V. Kendon. Decoherence in quantum walks – a review. *Math. Struct. Comp. Sci.*, **17**(6), 1169–1220, 2007.

[40] G. R. Grimmet. Percolation. *Springer*, 1999.

[41] K. M. Golden. Percolation Models for Porous Media. In: Hornung U. (eds) Homogenization and Porous Media. *Interdisciplinary Applied Mathematics*, vol 6. Springer, New York, NY, 1997.

[42] B. Kollár, T. Kiss, J. Novotný, and I. Jex. Asymptotic dynamics of coined quantum walks on percolation graphs. *Phys. Rev. Lett.*, **108**, 230505, 2012.

[43] B. Kollár, J. Novotný, T. Kiss and I. Jex. Percolation induced effects in 2D coined quantum walks: analytic asymptotic solutions. *New J. Phys.*, **16**, 023002, 2014.

[44] B. Kollár *et. al.*. Complete classification of trapping coins for quantum walks on the 2D square lattice. `https://arxiv.org/abs/2002.08070`.

[45] J. Novotný, G. Alber and I. Jex. Asymptotic evolution of random unitary operations. *Central Eur. J. Phys.*, **8**, 1001-1014, 2010.

[46] A. Ambainis, J. Kempe, and A. Rivosh, in *Proceedings of the Sixteenth Annual ACM-SIAM Symposium on Discrete Algorithms, SODA, 2005* (Society for Industrial and Applied Mathematics, Philadelphia, PA, USA, 2005) p. 1099, 2005.

[47] G. S. Engel *et al.*. Evidence for wavelike energy transfer through quantum coherence in photosynthetic systems. *Nature*, **446**(782), 2007.

[48] **J. Mareš, J. Novotný, M. Štefaňák, and I. Jex. Counterintuitive role of geometry in transport by quantum walks. *Phys. Rev. A*, 101, 032113, 2020.**

[49] **J. Mareš, J. Novotný, and I. Jex. Quantum walk transport on carbon nanotube structures. *Phys. Lett. A*, 384(15), 126302, 2020.**

[50] J.A. Bondy and U.S.R. Murty. Graduate Texts in Mathematics series, Graph Theory, 1st edition, *Springer-Verlag London*, 2008.

[51] J. Mareš. Quantum walks on percolated graphs. Master's thesis, FNSPE CTU in Prague, 2014.

[52] A. Patel, K. S. Raghunathan, and P. Rungta. Quantum Random Walks do not need a Coin Toss. *Phys. Rev. A*, **71**, 032347, 2005.

[53] F. M. Andrade, M. G. E. da Luz. Equivalence between discrete quantum walk models in arbitrary topologies. *Phys. Rev. A*, **80**, 052301 2009.

[54] G. Leung, P. Knott, J. Bailey, and V. Kendon. Coined quantum walks on percolation graphs. *New J. Phys.*, **12**, 123018, 2010.

[55] J. Blank, P. Exner, and M. Havlíček. Lineární operátory v kvantové fyzice. *Karolinum*, Prague, 1993.

[56] M. Štefaňák, J. Novotný, and I. Jex. Percolation assisted excitation transport in discrete-time quantum walks. *New J. Phys.*, **18**(2), 023040, 2016.

[57] F. García and M. Smulders. Dynamic Covalent Polymers. *Journal of Polymer Science Part A: Polymer Chemistry*, **54**, 3551-3577, 2016.